Master's thesis

NTNU
Norwegian University of Science and Technology
Faculty of Natural Sciences
Department of Materials Science and Engineering

Kristin Grue Asheim

Distinguishing bainitic and martensitic microstructures in high strength steels using advanced characterization methods

Master's thesis in MTMT
Supervisor: Ida Westermann
June 2020

NTNU
Kunnskap for en bedre verden

Kristin Grue Asheim

Distinguishing bainitic and martensitic microstructures in high strength steels using advanced characterization methods

Master's thesis in MTMT
Supervisor: Ida Westermann
June 2020

Norwegian University of Science and Technology
Faculty of Natural Sciences
Department of Materials Science and Engineering

NTNU
Norwegian University of
Science and Technology

Acknowledgements

I would like to thank my supervisor Associate Professor Ida Westermann for her guidance through my master thesis. I would like to thank her for her positivity and support, and for giving me regularly plausible feedback that helped me make this work as efficient as I wanted. Even through the difficulties met with the Covid-19 pandemic, she managed to be there for me online and deliver the help I needed to finish my work.

I would also like to thank Staff Engineer Birgitte Sofie Karlsen for lab training for TEM sample preparation, Senior Engineer Sergey Khromov and Senior Engineer Yingda Yu for SEM/EBSD training and giving me advice during the laboratory work where also Professor Jarle Hjelen was of big assistance. A huge thank you is directed to Staff Engineer Berit Vinje Kramer which really took her time to help me out with getting the material and chemicals I needed for my last weeks at the lab, and providing me with assistance at short notices.

I would like to thank PhD Candidate Håkon Wiik Ånes for being very helpful with his time and supervision during the use of EMsoft for EBSD pattern indexing. He introduced me to and taught me how to use the indexing software, and provided instructions when technical problems occurred. The use of EMsoft could not have been done without his assistance and guidance.

Thank you to Erlend Sølvberg from Kverneland Group, Cato Dybdahl and Morten Onsøien for helping me acquire steel alloys to work with that were in their interest, and for helping me answering questions about the alloys, heat treatments and analyzing procedures.

Ruben Bjørge at SINTEF helped me with doing the TEM analysis for my work when the pandemic prevented me from being able to get the training and supervision I would have needed to do the work myself, and I would like to greatly thank him for taking his time to do so.

I would like to thank the representatives for the TailorPro project (SINTEF); Morten Onsøien, Magnus Eriksson, Cato Dybdahl, Xiaobo Ren, Ruben Bjørge, Dirk Nolte and Bård Nyhus. They kept me on track with meetings and email-conversations and continuously encouraging me and my master work.

Lastly I have to thank my fiancé for his love and support and for making the work-from-home experience as bearable as possible for the both of us in a small apartment for two, even though him asking me to marry him was a little bit distracting in the middle of everything.

Abstract

In this work two steel alloys; 103Cr3/103C3 and 34CrNiMo6, were heat treated to pearlitic/ferritic, bainitic and martensitic structures for scanning electron microscope (SEM) analysis. Differentiating bainitic and martensitic structures in SEM has shown to be very difficult for an untrained eye because of the visual similarities in the structures, and often transmission electron microscopy (TEM) is the best solution to ensure which structure you have. The sample preparation for TEM is time-consuming and expects great precision and patience from the user, and therefore the purpose of this work has been to try out a SEM analysis procedure using electron backscatter diffraction (EBSD), the indexing software TSL OIM Data Collection for Hough indexing and EMsoft for dictionary indexing to differentiate bainite from martensite.

The challenge with EBSD analysis for the structures mentioned was that the difference in lattice parameters in bainite and martensite were small, and the phases were both indexed as ferrite using the traditional Hough indexing. With EMsoft the dictionary indexing was applied to the EBSD scans to index the possible phases present in the sample. Through EMsoft lattice parameters and atom positions for each phase were used to simulate all possible EBSD patterns for a given voltage range. These simulated patterns were then matched with the experimental patterns obtained in an EBSD scan to find the phase that fitted best.

While bainite has a body centered cubic structure with fixed lattice parameters, the lattice parameters of the martensite structure are dependent on the carbon content in the alloy. With an alloy containing a great amount of carbon (1.3 wt%), the differences in the lattice of bainite and martensite would in theory be big enough for EMsoft to index them separately and not confuse them with each other. The alloy with less carbon (0.36 wt%) was included in the work to see if the technique also worked for an alloy with lower carbon content if it showed to work for the high-carbon steel.

The martensite samples of both alloys were hardness tested and the martensite and bainite samples of both alloys were analyzed in TEM to ensure that the two structures were obtained. In the bainite samples tiny needle-formed carbides were found in the structure. No carbides were found in the TEM analysis of the martensite structures.

The two indexing softwares both gave similar results when indexing phases in the EBSD scans, showing the new EMsoft software to be just as good and reliable as the conventional TSL software. When EMsoft was used to index the bainite and martensite structure with ferrite and martensite phase, both the bainitic and martensitic structure was best indexed as ferrite. This was the result for both alloys, and showed that the procedure used on the experimental data obtained through this work was not able to differentiate bainite from martensite using EBSD in SEM.

Sammendrag

Gjennom dette arbeidet har to legeringer; 103Cr3/103C3 og 34CrNiMo6, blitt varmebehandlet til perlittisk/ferritisk, bainittisk og martensittisk struktur for å bli studert i SEM. Å skille mellom bainittiske og martensittiske strukturer i SEM har vist seg å være meget vanskelig da de visuelt ser veldig like ut, og vanligvis blir prøvene studert i TEM for å helt sikkert kunne avgjøre hvilken av de to strukturene man har. Prøvepreparering til TEM er tidkrevende og krever nøyaktighet og tålmodighet, og av den grunn har problemstillingen til denne masteroppgaven blitt å prøve ut en metode i SEM med bruk av EBSD og to ulike indekserisprogramvarer; TSL OIM Data Collection og EMsoft, for å skille martensitt fra bainitt.

Utfordringen med bruken av EBSD analyse er at de nevnte strukturene har relativt like gitterparametre, og ved bruk av den kommersielle Hough-indekseringen som TSL bruker blir begge strukturene indeksert med ferritt. EMsoft, som bruker dictionary indexing, tok i bruk gitterparametrene og atomposisjonene til atomene i enhetscellen til hver enkelt fase for å simulere alle mulige EBSD-mønstre for et gitt spenningsintervall. De simulerte mønstrene ble dermed sammenlignet med de eksperimentelle mønstrene i hver pixel i EBSD-skannen for å finne den fasen som passet best.

Bainitt har en BCC-struktur med faste gitterparametre, mens martensitt har en BCT-struktur hvor gitterparametrene avhenger av karboninnholdet i legeringen. Med en legering med høyt karboninnhold (1.3 wt% i dette arbeidet) burde forskjellen mellom gitterparametrene til bainitt og martensitt i teorien blitt stor nok til at EMsoft skulle klare å skille de fra hverandre i indekseringen. En legering med lavere karboninnhold (0.36 wt%) ble inkludert i masterarbeidet for å se om martensitt og bainitt med denne sammensetningen også kunne skilles i EMsoft hvis det viste seg å fungere for den første legeringen.

Martensittprøvene av begge legeringene ble hardhetstestet og martensitt- og bainittprøvene av begge legeringene ble studert i TEM for å forsikre at begge strukturene var blitt produsert gjennom varmebehandlingen. TEM-analysen av bainittprøvene fant nålformede karbider i strukturen, og slike karbider ble ikke funnet i martensittprøvene.

De to indekseringsprogrammene leverte lignende resultater når det gjaldt å finne hvor de ulike fasene befant seg i kartene av EBSD-skannen, noe som viste at EMsoft var en minst like troverdig indekseringsprogramvare som TSL. Når EMsoft ble brukt til å indeksere bainitt- og martensittstrukturen med ferritt- og martensittfasen ble begge strukturene indeksert best med ferritt. Det samme resultatet kom fram fra begge legeringene og viste at metoden brukt med de oppnådde eksperimentelle dataene ikke kunne brukes til å skille bainitt fra martensitt i ved hjelp av EBSD i SEM.

Table of contents

List of Figures

List of Tables

1 Introduction

This thesis was written and done in collaboration with the industrial partners Kverneland, Nøsted Kjetting, Ring Chairtech and Dokka Fasteners to the TailorPro project along with the R&D environment at SINTEF. The Project was established with the purpose of obtaining a better understanding of the interaction between different materials, their heat treatment and what relation they have to the damage resistance of the material. This thesis have been set to focus on the martensitic and bainitic structures of steel after their respective heat treatment.

Bainitic and martensitic steels are widely used in several designs requiring great hardness and strength. For the industry producing these structures it is important to know which of the microstructures they have achieved during the heat treatment, since the two microstructures look very similar in optical and electron microscopes, but do wary in their properties. The martensite is obtained by quenching steel from the austenite phase quickly to room temperature or lower. Bainite is obtained by quenching the austenite phase to a temperature just above M_S temperature where it is held until all austenite has transformed into bainite. The bainite is then cooled to room temperature. Even with close attendance during the process, one can not fully guarantee either of the microstructures without analyzing the material after the heat treatment.

Carbon atoms in the austenite phase behave differently during the heat treatment to martensite than in heat treatment to bainite. In the quenching of martensite, the transformation is so rapid that there is no diffusion of carbon, and the carbon atoms is locked in the lattice as interstitial impurities. This is what gives martensite the well known hardness. During the formation of bainite some diffusion of carbon is present, and while the bainitic ferrite forms into sheaves, carbide particles and cementite forms inside (lower bainite) or around (lower and upper bainite) the ferrite. The easiest way to differentiate the two microstructures is to analyze them in a transmission electron microscope (TEM) and find the carbide particles inside or around the bainitic ferrite which does not appear in martensite structure.

The bainite structure forms in a body centered cubic (BCC) lattice during the heat treatment, while martensite, because of the solid solution carbon in interstitial sites in the lattice, obtaines a body centered tetragonal (BCT) lattice. The lattice of bainite has a c/a ratio of 1 because of the cubic structure, but martensite has a c/a ratio that is higher than 1. The c/a ratio of martensite increases with the carbon content of the lattice, and as the carbon content increases, the lattice of martensite deviates more from the bainite lattice.

Even though TEM analysis is the best way to confirm the differences in the microstructures, the TEM sample preparation is a very time consuming process that requires great precision. This has been the motivation for trying a method for differentiating baintitic and matenistic structure in SEM for this thesis, which has a much easier sample preparation process. In this work the martensite and bainite samples has been analyzed in secondary electron microscope (SEM) with the purpose of trying out a method for characterizing martensite and bainite structure through electron backscatter diffraction (EBSD) analysis and indexing using a dictionary

indexing technique. This was done through a software called EMsoft and the use of the python program KikuchiPy. With this indexing it was possible to focus on the lattice differences between the bainite and the martensite structure.

2 Theory

This chapter explains heat treatment procedures for obtaining ferritic, martensitic and bainitic structure with the help of phase diagrams and transformation diagrams, lattice parameters of the different phases mentioned through the work, hardness testing and the methods used during SEM and TEM analysis. The SEM analysis consists of secondary electron imaging, Electron Dispersive Spectroscopy (EDS) and Electron Backscatter Diffraction (EBSD). The indexing of EBSD has been done by Dictionary Indexing (DI) using the software EMsoft and compared to the more commercial Hough Indexing method done with the TSL OIM Data Collection software.

2.1 Phase transformations in hardening steel

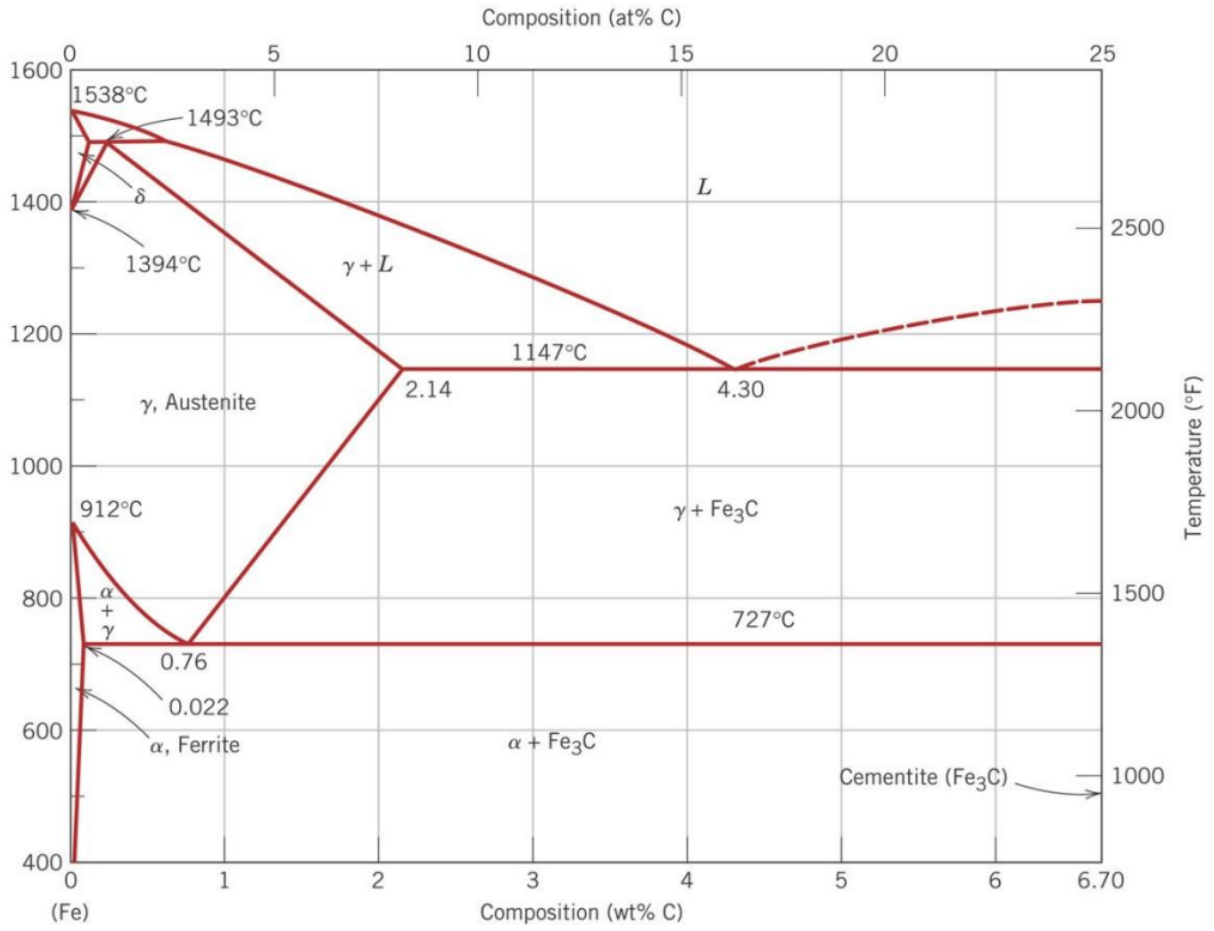

Figure 2.1: The Iron-Iron Carbide (Fe-Fe_3C) phase diagram. This diagram shows the equilibrium phases in steels and their transformation temperatures. The diagram is reprinted from Callister and Rethwisch (2015).

The Iron-Iron Carbide (Fe-Fe_3C) phase diagram in Figure 2.1 shows how different compositions of a steel will have different phase transformation temperatures. To obtain both martensite and bainite by quenching, the steel must be heated up to the temperature where austenite is formed first. With a composition containing 1.3 wt% C this temperature lies around 850°C, and for a composition of 0.36 wt% C this austenitizing temperature is somewhat higher.

2.1.1 Transformation diagrams

The transformation of martensite and bainite can not be described in a equilibrium phase diagram as showed in Figure 2.1 because they are unstable phases at room temperature (Bhadeshia and Honeycombe, 2017; Callister and Rethwisch, 2015). Transformation diagrams however shows the temperature and time dependence of different microstructures obtained when cooling a material, and the transformation to microstructures as martensite and bainite can be described by these diagrams. The transformation diagrams can be presented as an Isothermal Transformation diagram (ITT) or Continuous Cooling Transformation diagram (CCT).

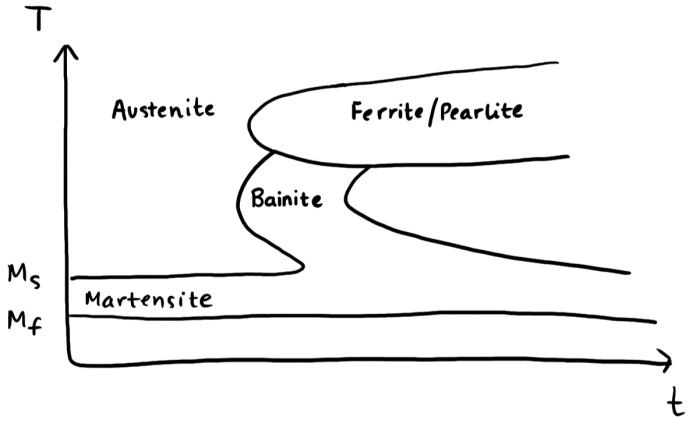

Figure 2.2: Illustration of a CCT diagram, showing how one can obtain martensite or bainite by rapidly cooling from austenite to prevent formation of ferrite or pearlite.

Figure 2.2 illustrates a CCT diagram that shows how one can obtain bainitic and martensitic microstructures. The transformation of martensite or bainite happens when the cooling from the austenite region is rapid enough to prevent the formation of ferrite or pearlite. These diagrams will differ from alloy to alloy since both the temperature and time dependence of the transformations changes with the alloy elements added. For example, the M_S temperature could be calculated with the formula given in Equation 2.1, where the addition of alloying elements lower the M_S temperature. Along with lowering the M_S and M_F temperatures, alloying elements also shift the noses of pearlite/ferrite and bainite to the right toward longer times (Callister and Rethwisch, 2015).

2.1.2 Formation of ferrite and pearlite

The stable steel phases at room temperature is ferrite (α-steel), cementite (Fe_3C) or a combined microstructure of the two, a structure called pearlite. What phases the austenitic steel (γ-steel) transforms into during cooling is determined by the chemical composition of the alloy. With a composition with less than 0.76 wt% C, proeutectoid ferrite will start to form on the austenite

grain boundaries in the two-phase region $\alpha + \gamma$ before the remaining austenite is transformed into pearlite below the eutectoid temperature (727 °C) (Figure 2.3a). With a composition with carbon between 0.76 - 2.14 wt% C, proeutectoid cementite will form in the two-phase region γ + Fe_3C before pearlite is formed from the remaining austenite below the eutectoid temperature (Figure 2.3c). When the composition is of 0.76 wt% C no proeutectoid phases are formed, and below 727 °C all austenite is transformed into pearlite (Figure 2.3b) (Callister and Rethwisch, 2015).

The pearlite microstructure consists of layers of ferrite and cementite. Since there is less solubility of carbon in ferrite with BCC structure than in austenite with FCC structure, the carbon diffuses away from the forming ferrite and into the adjacent austenite phase. The now carbon-rich austenite is then formed into cementite.

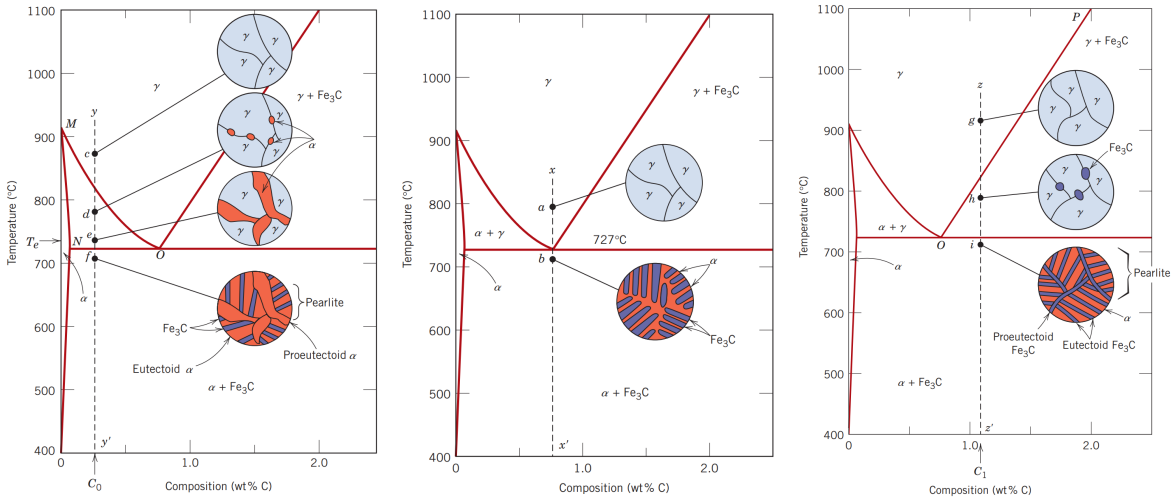

(a) The development of the microstructure transformation during cooling of a hypoeutectoid composition (less than 0.76 wt% C).

(b) The development of the microstructure transformation during cooling of an eutectoid composition (0.76 wt% C).

(c) The development of the microstructure transformation during cooling of a hypereutectoid composition (between 0.76 - 2.14 wt% C).

Figure 2.3: Phase diagrams focusing on the microstructure development of hypoeutectoid, eutectoid and hypereutectoid compositions. The images are collected from Callister and Rethwisch (2015).

2.1.3 Formation of martensite

Martensitic microstructure is obtained by quenching austenitic steel rapidly to room temperature (illustrated in Figure 2.4).

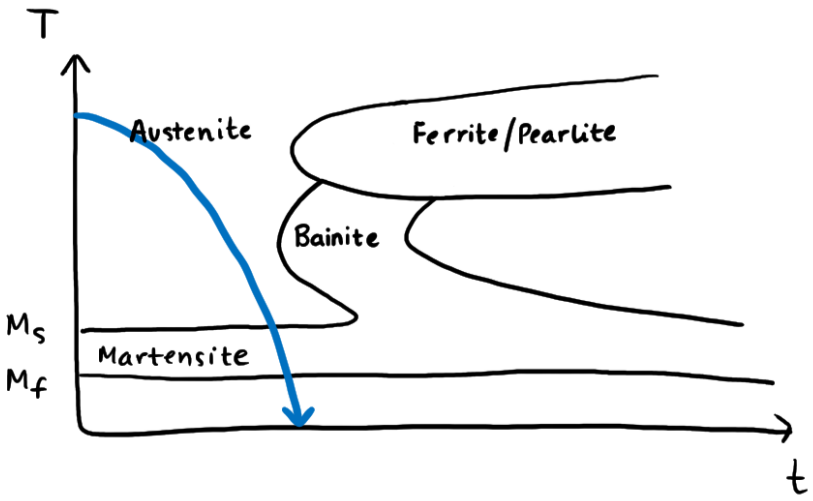

Figure 2.4: An illustration of a CCT diagram with a cooling rate that would provide martensitic structure.

The formation of the martensite structure begins first when the temperature reaches below the martensite start temperature M_S. Where this temperature lies is dependent on the chemical composition of the alloy, and is given by Equation 2.1 (Andrews, 1956). Bear in mind that this formula has an uncertainty of $\pm 20°C$ (Bhadeshia, 2015; Yang and Bhadeshia, 2007).

$$M_S(°C) = 539 - 423w_C - 30.4w_{Mn} - 17.7w_{Ni} - 12.1w_{Cr} - 7.5w_{Mo} \tag{2.1}$$

There is no temperature defined where all of the austenite is transformed into marteniste, but there is a martensite finish temperature M_F defined as where 95% austenite is transformed into martensite. This temperature is given by Equation 2.2 (Bhadeshia and Honeycombe, 2017).

$$M_F(°C) = M_S - 130 \tag{2.2}$$

w_i indicates the weight percent (wt%) of the different alloying elements in the alloy.

Equation 2.1 and 2.2 can only be applied to alloys with the minimum and maximum alloying element percentages as given in Table 2.1.

Table 2.1: Table presenting the minimum and maximum value of alloying element contents where Equation 2.1 and 2.2 are valid (Bhadeshia and Honeycombe, 2017).

	C	**Mn**	**Si**	**Ni**	**Cr**	**Mo**
Maximum (wt%)	0.11	0.20	0.11	0.00	0.00	0.00
Minimum (wt%)	0.55	1.67	1.74	5.04	3.34	1.00

For alloys containing more than 0.7 wt% C, the M_F is below room temperature, and with a quenching method using water at 20°C the martensite microstructure is likely to contain higher amounts of retained austenite after the heat treatment (Bhadeshia, 2015).

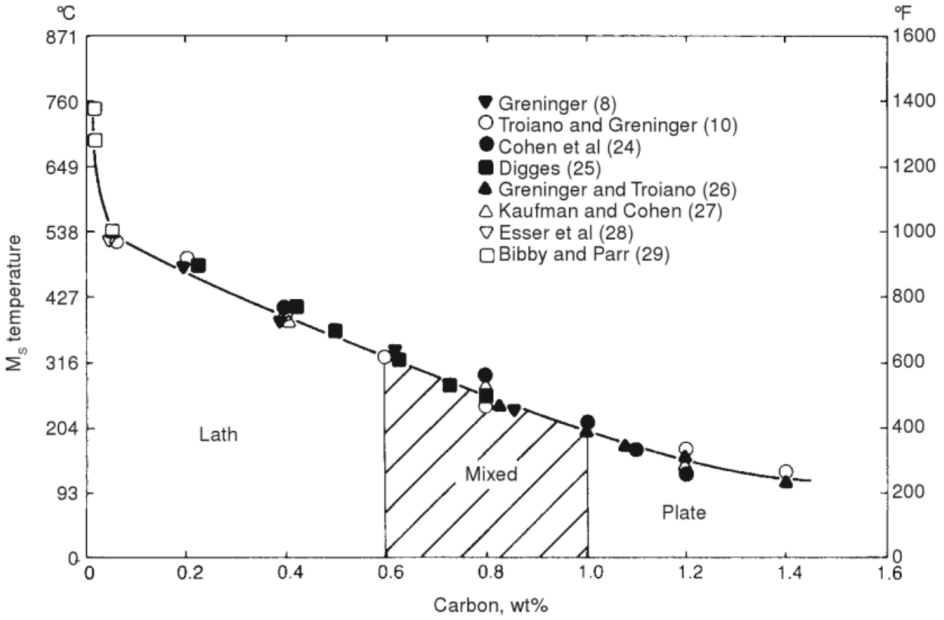

(a) The graph shows a relationship between the M_S temperature (°C) and the carbon content (wt%) in steels. The figure is collected from Krauss (2015). The investigations shown is related to the references in the main source of this graph; Marder (1967).

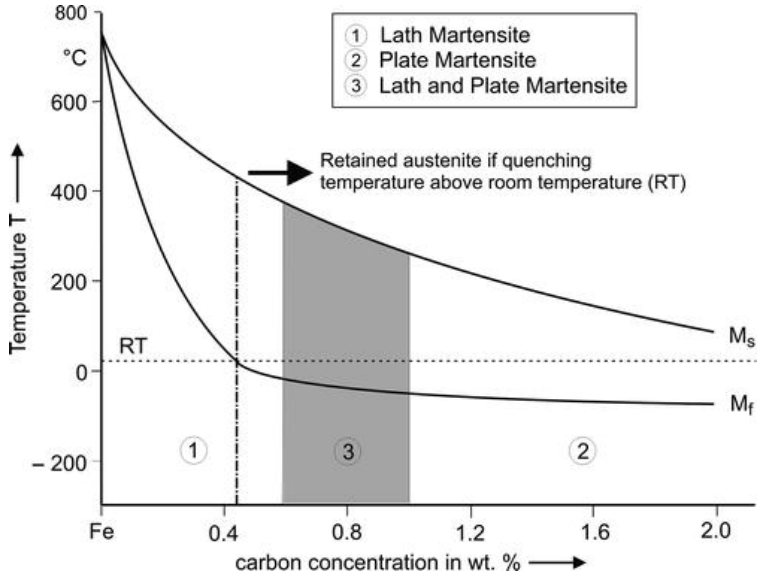

(b) This figure shows the relation that both M_S and M_F have to the carbon content in a steel alloy (Schwenk, 2014).

Figure 2.5: Two figures showing the relationship between the martensite start temperature and the carbon content in steels.

Figure 2.5 shows the relationship between the martensite start temperature M_S and the carbon content is steels, and could be used as a guideline for alloys with higher carbon content than 0.55 (max. wt % C, Table 2.1), where Equation 2.1 is not valid.

The austenite to martensite transformation is displacive, which means that the deformation is a shear deformation where the austenite FCC structure is physically deformed into the martensitic BCT structure. This is illustrated in Figure 2.6. Characteristic for the martensite formation is that there is no diffusion of carbon, and the carbon atoms remains as interstitial impurities in the BCT structure. The more carbon the alloy contains, the bigger the tetragonality of the BCT lattice (Bhadeshia and Honeycombe, 2017; Krauss, 2015). No carbon means that the martensite structure has no tetragonality and instead obtains a BCC structure (Ryde, 2006).

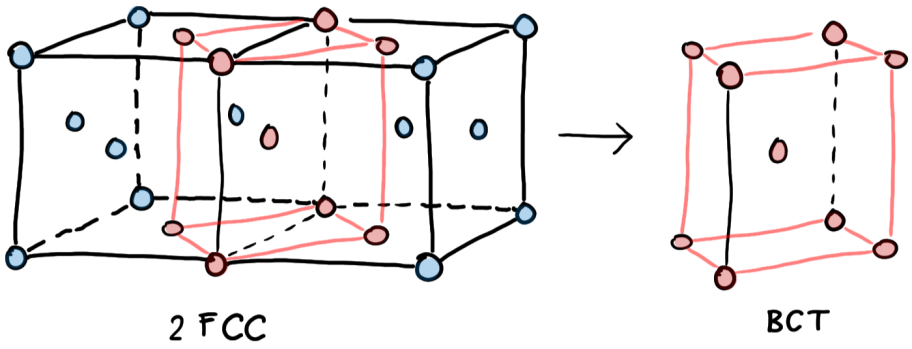

Figure 2.6: Illustration of the austenite to martensite deformation.

2.1.4 Formation of bainite

Bainite is formed at higher temperatures than martensite, and is also formed when the cooling is too rapid to transform austenite into ferrite/pearlite (Figure 2.7). The steel is quenched to a temperature just above the martensite start temperature and held there until the bainite transformation is finished. Then the steel is cooled down to room temperature. The transformation from austenite to bainite is also a displacive transformation, but unlike martensite, some carbon diffusion is present.

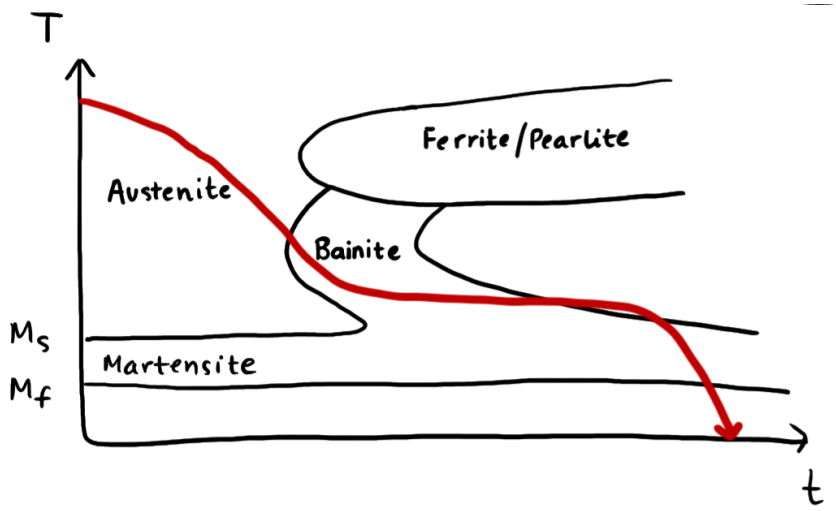

Figure 2.7: An illustration of a CCT diagram with a cooling process that would provide bainitic structure.

The bainitic structure can be divided into upper and lower bainite. Upper bainite forms at temperatures between 550-400 °C, while lower bainite forms between 400-250°C (Bhadeshia and Honeycombe, 2017). The structures are very alike, but differs in how carbon is diffused and where the carbon-rich cementite phase is precipitated.

Upper bainite forms in two stages. First bainitic ferrite formes on the austenite grain boundaries. This ferrite contains little carbon (<0.02 wt% (Bhadeshia and Honeycombe, 2017)), and the sorrounding austenite will therefore be carbon-rich. From this carbon-rich austenite, cementite is formed between plates of bainitic ferrite.

Lower bainite is formed in the same way as upper bainite, except that cementite particles also formes inside the ferrite plates. The cementite particles inside the needles appear to precipitate from supersaturated ferrite. These particles can also be other carbides that cementite (Fe_3C), depending on the chemical composition of the alloy (Bhadeshia and Honeycombe, 2017).

2.1.5 Formation of alloying element carbides in steel

If only transformation from austenite to ferrite and carbide during slow cooling is considered, alloying elements in a steel can be divided into three categories according to Bhadeshia and Honeycombe (2017):

1. elements that only enters the ferrite phase in solid solution;
2. elements that form stable carbides, but also can be found in solid solution in ferrite;
3. elements that only enters the carbide phase.

Ni, Cu, P and Si belongs to the first category as their solubility in cementite is very low. In the second category, the majority of the alloying elements in steel are placed. Typical of these elements are Mn, Cr, Mo, V, Ti, W and Nb, which is known as carbide formers. At low concentrations they can form in solid solution in both cementite and ferrite, but at higher concentrations they tend to form alloy carbides that is more thermodynamically stable than the cementite phase. In the third category, N is the most important element, and few other elements falls under this category.

As mentioned, most of the carbide forming elements in steel form alloy carbides that is more thermodynamically stable than cementite, which means, if the amount of carbide forming elements is high enough, they form in preference to cementite. During the tempering of martensite, alloy elements in cementite can form into alloy carbides when the temperature rises above about 500°C. Below this temperature the diffusion of the metallic elements is too slow to allow nucleation of the alloy carbides. The nucleation of these carbides can happen at pre-excisting cementite particles, where carbon is provided by the cementite which through this process will dissapear eventually (Bhadeshia and Honeycombe, 2017).

2.2 Structures of the steel phases

The phases mentioned in this thesis; austenite, ferrite, cementite, martensite and bainite, all have different lattice structures. These structures and all information related to them is essential for the indexing of EBSD patterns using both Hough Indexing and Dictionary Indexing. The carbon present in austenite, ferrite, cementite and martensite is located in interstitial sites.

2.2.1 The austenite structure

Austenite, also known as γ-iron forms in a face centered cubic structure (FCC) which is illustrated in Figure 2.8. The lattice parameters are $a = b = c = 0.3595$nm (Wyckoff, 1964).

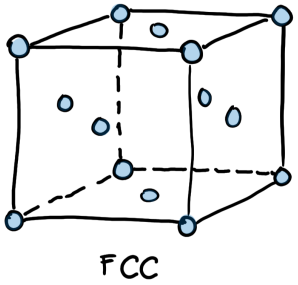

Figure 2.8: Illustration of the FCC structure that the austenite phase forms in.

2.2.2 The ferrite structure

Ferrite, also known as α-iron, forms in a body centered cubic structure (BCC) which is illustrated in Figure 2.9. The lattice parameters are $a = b = c = 0.28665$nm (Wyckoff, 1964).

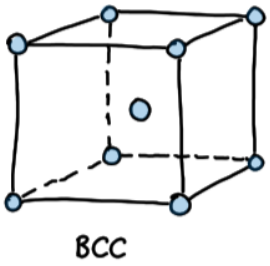

Figure 2.9: Illustration of the BCC structure the ferrite phase forms in.

2.2.3 The cementite structure

Cementite, the carbon-rich steel phase known as Fe_3C or θ-iron, forms in an orthorhombic structure with lattice parameters $a = 0.5092$nm, $b = 0.6741$nm and $c = 0.4527$nm (Fruchart et al., 1984).

2.2.4 The martensite structure

Martensite, also known as α'-iron, forms in a BCT structure shown in Figure 2.10 (Bhadeshia and Honeycombe, 2017).

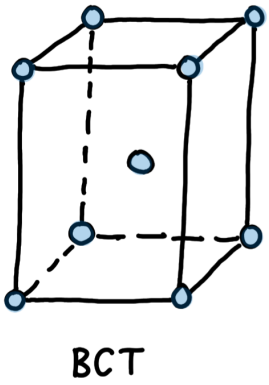

Figure 2.10: Illustration of the martensite BCT structure.

The tetragonality is dependent on the carbon content (wt% C) in the alloy, and increases as the carbon content increases. The lattice parameters of the martensite structure alters from alloy to alloy, and can be calculated using Equation 2.3.

$$c/a = 1 + 0.045 w_C \tag{2.3}$$

Equation 2.3 is a linear relationship known as the Honda & Nishiyama model which was tested experimentally to fit well for alloys with carbon content higher than 0.6 wt% (Lobodyuk et al., 2019; Lu et al., 2017; Bhadeshia and Honeycombe, 2017). Lu et al. focused on alloys with less carbon than 0.6 wt%, and adressed how these steels did *not* follow Equation 2.3, but instead a modified version of Equation 2.3 that is represented by Equation 2.4.

$$c/a = 1 + 0.031 w_C \tag{2.4}$$

The lattice parameter c for the two alloys used in this work can be calculated by Equation 2.3 and Equation 2.4 with the following results:

Alloy 1 (with 1.3 wt% C):
Carbon content of 1.3 wt% gives a lattice parameter of $a = 0.28415$nm (Lobodyuk et al., 2017).

$$c = a(1 + 0.045 w_C) = 0.28415(1 + 0.045 \cdot 1.3) = 0.30077\text{nm}$$

Alloy 2 (34CrNiMo6): Carbon content of 0.36 wt% gives a lattice parameter of $a = 0.28556$nm (Lobodyuk et al., 2017).

$$c = a(1 + 0.031 w_C) = 0.28556(1 + 0.031 \cdot 0.36) = 0.28875\text{nm}$$

2.2.5 The bainite structure

As mentioned above, the bainite microstructure is a combination of bainitic ferrite and cementite. Since the structure mainly consist of ferrite, the BCC structure of the ferrite phase and its lattice parameters are used when indexing the EBSD patterns of the bainite samples.

2.3 Hardness of steel phases

Hardness testing of a material could be a perfect tool for phase identification for phases that differ in hardness. A great example is pearlitic VS. martensitic microstructure that can have a difference in hardness in the magnitude of 700 HV. Figure 2.11 shows relation between hardness (Vickers and Rockwell C) and carbon content (wt%), and can be used to determine carbon content of a given alloy out of a hardness test if the microstructure is known.

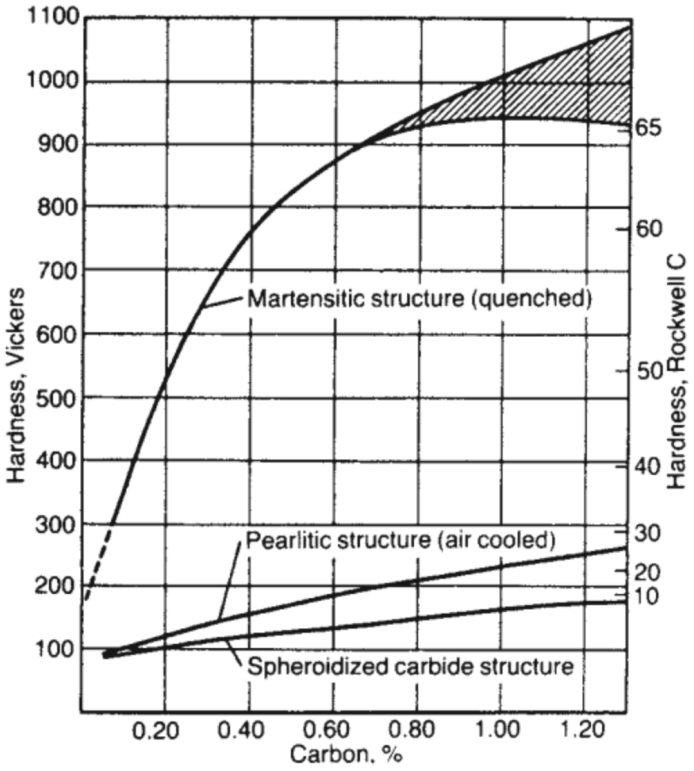

Figure 2.11: Vickers and Rockwell C hardness related to carbon content of some phases in steel (Krauss, 2015).

When carbon content exceeds 0.8 wt% the hardness of the martensitic structure drops. As the carbon content increases, the presence of retained austenite is higher after quenching than for lower carbon content. The hardness of austenite is much lower than martensite and the total hardness is reduced (Krauss, 1978).

Vickers hardness testing is done by pressing a diamond pyramid into the sample with a load (P) chosen by the user (illustrated in Figure 2.12). The two diameters (d_1 and d_2) of the indent is measured, and the hardness is calculated by Equation 2.5 below (Callister and Rethwisch, 2015).

$$HV = 1.854\frac{P}{d_1 d_2} \tag{2.5}$$

The load P is in kg and the diameters d_1 and d_2 uses mm as the unit of measurement.

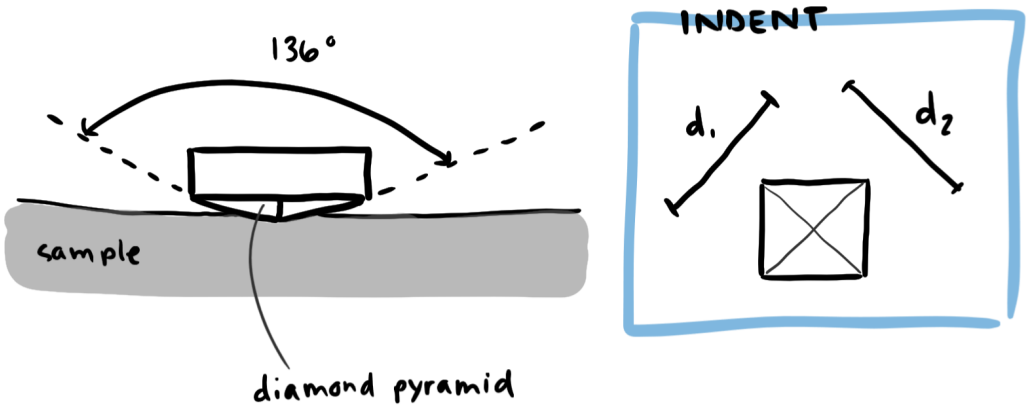

Figure 2.12: Illustration of Vickers hardness testing with description of indent geometry for calculating the HV hardess value.

2.4 Scanning Electron Microscope

The Scanning Electron Microscope (SEM) is a tool used for material characterization of both organic and inorganic materials, and offers a variety of methods for collecting data about the properties of the materials that are studied. SEM is most frequently used for topography analysis because of the ability to produce three-dimension like pictures of a surface, but can also be used to look at microstructures of a flat sample surface or to analyze a material both qualitatively and quantitatively.

During the analysis using a SEM the sample is illuminated by a electron beam. The beam hits the sample surface and electrons are emitted from the sample and can be detected by several detectors. The electrons emitted from the sample can be secondary electrons (SE), backscattered electrons (BSE) or characteristic radiation for the sample (used for EDS analysis). By choosing which detector to use to absorb the different emitted electrons, you choose what properties or details of the sample you want to study.

2.4.1 Secondary Electron Imaging

Secondary electrons (SE) are produced when an incident electron beam hits an electron in the outer shell of an atom. Through inelastic scattering an electron from the beam hits an electron in the outer shell. The electron that is hit is then ejected out of the sample - now known as a secondary electron. Figure 2.13 shows how the inelastic scattering works.

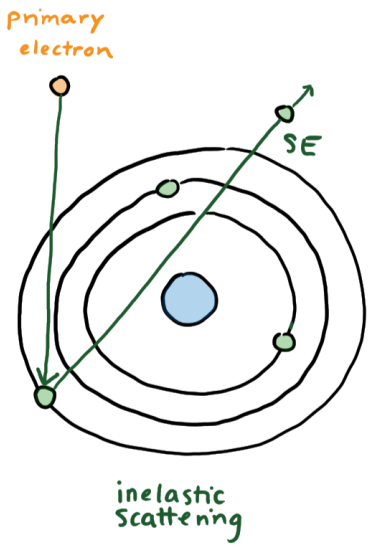

Figure 2.13: An illustration of inelastic scattering producing a secondary electron.

Secondary electrons can also originate from other backscattered electrons that interferes with electrons in the atom on their way out of the sample. To differentiate between the different SE they are referred to as SE_1 (produced by incident beam electrons) and SE_2 (produced by BSE) (Goldstein et al., 2002).

2.4.2 Backscattered Electron Imaging

Backscattered electrons (BSE) are electrons that are sent into the specimen, circle the nucleus of the atoms in the material and comes out of the sample without further interaction through elastic scattering (Figure 2.14). The amount of BSE depends on the nucleus size, which will differ between different elements. Increased size in nucleus causes a higher number of BSE, which can be very useful for obtaining a contrast between phases with different chemical composition.

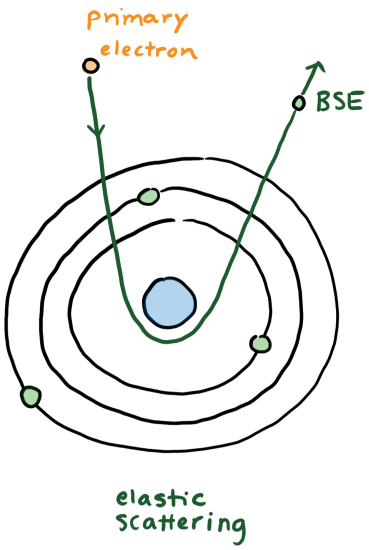

Figure 2.14: An illustration of elastic scattering producing a backscattered electron.

BSE imaging is as mentioned used to obtain contrast between phases with different chemical compositions (Z-contrast) or with different orientations (O-contrast or diffraction contrast). Heavier atoms (higher atom number Z) will produce more BSE, and the areas with high Z will be lighter than areas with low Z in the image.

Table 2.2: Common elements in a steel alloy and their atomic number (Z).

Elements	Atomic number (Z)
C	6
Si	14
Cr	24
Mn	25
Fe	26
Ni	28

2.4.3 Energy Dispersive Spectroscopy

Energy Dispersive Spectroscopy (EDS) is a method that takes use of the characteristic X-rays a sample will emit when incident beam electrons interact with electrons in the atoms of the sample. The emitted X-rays is produced when electrons that are excited by incoming electrons relax to its original energy level (Figure 2.15). This is a result of restoring the energy balance of each individual atom. The electron that is excited to a higher energy level absorbs energy from the incoming beam. When it relaxes back to its original energy level, the remaining energy of that electron leaves the sample as a photon or as auger electrons. This method can be used to analyze a material qualitatively and quantitatively.

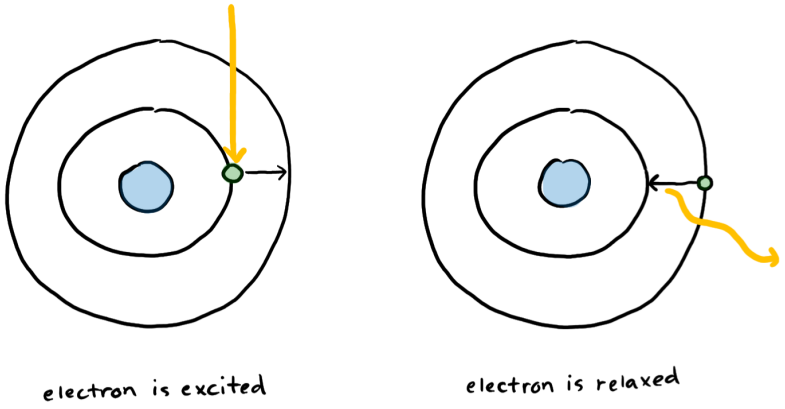

Figure 2.15: An illustration showing the excitation and relaxation of an electron, generating an X-ray.

The emitted photons are described as K-, L- or M-radiation indexed with α, β or γ depending on which energy level the electron is relaxed back to.

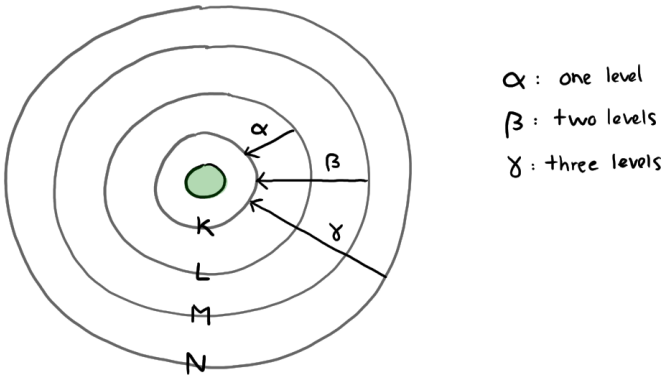

Figure 2.16: An illustration describing how the electron can relax, generating different types of radiation.

As showed in Figure 2.16, an electron relaxed from a L-orbital to K-orbital will generate K_α-radiation, M- to K-orbital will generate K_β-radiation and relaxation from a N- to K-orbital will generate K_γ-radiation. The electrons are excited to discrete levels, and when it is relaxed back to its original energy level, the X-ray generated will have energy that is characteristic to the energy gaps of the energy levels for that specific element. The wavelength of the generated photons will therefore be characteristic for different element atoms. The EDS detector in the SEM collects these photons and returns information on what elements the sample consist of. The energy of each photon is related to the atomic number (Z) through Moseley's law (Equation 2.6)

$$E = a \cdot (Z - \sigma)^2 \tag{2.6}$$

where a and σ are constants related to the type of radiation, Z is atomic number and E is the energy of the generated photon. For K_α-radiation σ = 1 and $a = 2.4692 \cdot 10^{15} Hz$ (Equation 2.7) (Singh, 2019).

$$a = \frac{3}{4} cR = \frac{3}{4} \cdot 2.9979 \cdot 10^8 m/s \cdot 1.0974 \cdot 10^7 m^{-1} = 2.4692 \cdot 10^{15} s^{-1} \tag{2.7}$$

The result of an EDS analysis is an EDS spectra, which is number of photons mapped against energy. These spectra can be used to perform a point or map scan.

When doing a EDS scan it is important that the accelerating voltage (EHT) used in the SEM is higher than two times the excitation energy of the elements you want to detect. If the chemical composition of the sample is known, the element with the highest excitation energy decides what acceleration voltage to use. The excitation energies of an element is divided into K_α-, L_α- and M_α-energy, but the K_α-energy is the one used for choosing the accelerating voltage. Some of these energies are shown in Table 2.3.

Table 2.3: X-ray energies for elements in the alloy. Extracted from Bruker Periodic Table of Elements and X-ray Energies (Bruker, 2015).

Elements	K_α (keV)	L_α (keV)
Fe	6.405	0.705
C	0.277	
Si	1.740	
Mn	5.900	0.637
Cr	5.415	0.572
Ni	7.480	0.849

It is important to also consider the emission depth of the X-rays during an EDS analysis. This depth is dependent on the density of the material and the acceleration voltage used on the sample and when analyzing small particles, a small emission depth would be beneficial so the X-rays gathered only comes from the particle, and not the volume beneath it too. If the purpose of the EDS analysis is to study particles with lower excitation energies that the matrix, a lower excitation energy could be considered to reduce the emission depth.

2.4.4 Electron Backscatter Diffraction

Electron Backscatter Diffraction (EBSD) makes it possible to study the texture of the grains in a material, to find grain size distribution, phase identification and phase distribution of a sample. Each grain will have the same structure consisting of unit cells with the same orientation, and the planes in these unit cells will diffract incoming light in a specific way. Another grain with a different orientation will diffract the light differently, and this information is used to differentiate the grains in the microstructure. Some phases in steel have different lattice structures (austenite with FCC structure, ferrite with BCC structure and cementite with an orthorhombic structure) and can be differentiated from each other since they will diffract light differently and produce individual EBSD patterns.

The EBSD patterns are obtained in a SEM by illuminating a sample tilted to about 70°, which is illustrated by Figure 2.17. The electrons from the incident beam that hits the sample are diffracted and form cones of intensity above the sample. We get two cones per atom plane because both the front and the back of each plane causes diffraction. These cones intercept the imaging plane and we see them as two nearly straight lines separated by an angle of 2θ where θ is the angle where Bragg reflection occurs. The cones generated from the sample interferes with a phosphor screen and creates the straight lines, called *Kikuchi lines*, that results in a diffraction pattern (Goldstein et al., 2002).

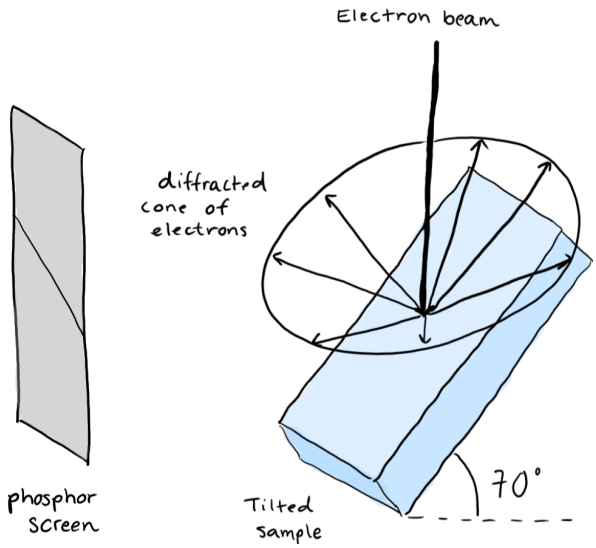

Figure 2.17: Illustration of the experimental arrangement within a SEM to obtain EBSD patterns.

2.4.5 Indexing EBSD patterns

The lines that are formed from the intensity cones intercept each other in symmetric points and forms EBSD patterns. These patters are characteristic for a given structure and is directly related to the lattice of that structure. The symmetric points, called zone axes, are related to a specific crystallographic direction in a crystal, while the lines in the pattern represent the different planes in the same crystal. The distance between parallel lines in the pattern is related to the Bragg angle θ_B. The bigger the distance, the higher the angle.

$$2sin\theta_B = \frac{n\lambda}{d} \tag{2.8}$$

Bragg's law given in Equation 2.8 shows that a higher bragg angle means smaller distance between planes in the lattice, d (Goldstein et al., 2002).

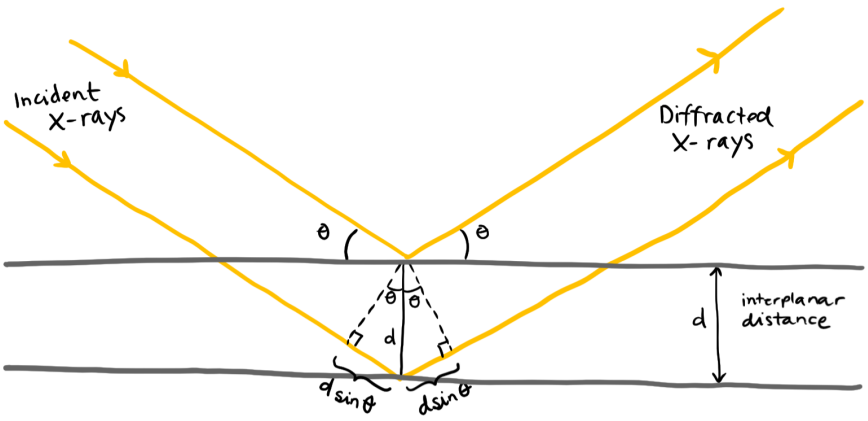

Figure 2.18: Illustration used to derive and understand Bragg's law.

Softwares used for indexing EBSD patterns are dependent on knowing the lattice parameters, space group and atomic positions of the different phase structures. Since martensite is dependent on carbon content and therefore has lattice parameters that vary from alloy to alloy, most softwares does not have a structure file for the martensite phase. In programs as TSL OIM Data Collection the martensite sample is indexed with ferrite phase. Since the bainitic structure consists mostly of ferrite and some cementite, ferrite phase is used for indexing the bainitic structure. With the TSL software, martensitic and bainitic structures can not be separated from each other during the indexing of the EBSD patterns.

In this work, two softwares for indexing EBSD patterns are used; TSL and EMsoft. In EMsoft structure files for the different phases is produced, including structure files for martensite dependent on the carbon content of the alloy.

TSL software - Hough Indexing

The TSL software takes the NORDIF pattern file obtained in the EBSD scan as an input, and uses a Hough transformation on the information in the pattern file to detect the position of the Kikuchi bands in the EBSD patterns. This Hough transformation is given by Equation 2.9.

$$\rho = x\cos\theta + y\sin\theta \tag{2.9}$$

The Kikuchi bands are represented by ρ and is turned into a point in Hough space by the Hough Transformation. When the position of the bands are found, angles between the lines can be calculated. The crystal orientation of the grains in the sample can be calculated from the Kikuchi band positions, and each Kikuchi band is related to the Miller indices of the plane sending out the corresponding diffraction pattern (Wang et al., 2018).

The information gained from the scan is matched to phases chosen for indexing from the TSL database, and returns a confidence index (CI) for each matching. For a good match, this CI value should be as close as 1 as possible.

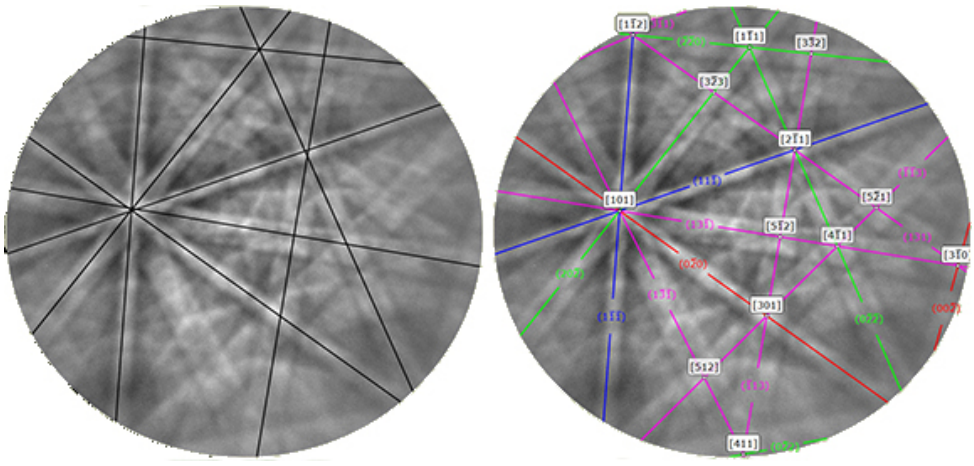

Figure 2.19: The left figure shows the lines collected from the Hough Transformation, and the right shows an indexing solution based on the Hough Transformation. `https://edaxblog.com/2017/01/31/the-hough-transform-an-amazing-tool/`

EMsoft - Dictionary Indexing

The EMsoft software uses Dictionary Indexing for analysing EBSD patterns, which is said to index EBSD scans with high amounts of noise better than Hough Indexing. Before the indexing can be done, a few programs needs to be run. A Monte Carlo simulation must be run and master patterns must be collected from the Monte Carlo simulation. This is done separately for each singe phase. The simulated master pattern for a give phase is matched against the patterns in the pattern file (.dat) obtained using the NORDIF software.

Creating structure files

The Monte Carlo simulation program needs a structure file as an input, and this structure file (.xtal) collects information given by the user of space groups, lattice parameters and atomic positions of the atoms in each basis of the different crystal lattices in a given phase.

Table 2.4: Atom positions and occupation of the phases used for indexing the EBSD patterns (Jackson et al., 2019; Wyckoff, 1964; Fruchart et al., 1984).

Austenite							
Site	**Element**	**Wyckoff**	**X**	**Y**	**Z**	**Occupation**	**B$_{iso}$**
1	Fe	4a	0.0000	0.0000	0.0000	1	0.005

Ferrite							
Site	**Element**	**Wyckoff**	**X**	**Y**	**Z**	**Occupation**	**B$_{iso}$**
1	Fe	2a	0.0000	0.0000	0.0000	1	0.005

Cementite							
Site	**Element**	**Wyckoff**	**X**	**Y**	**Z**	**Occupation**	**B$_{iso}$**
1	C	4c	0.8770	0.2500	0.4440	1	0.0207
2	Fe	4c	0.0367	0.2500	0.8402	1	0.0036
3	Fe	8d	0.1816	0.0666	0.3374	1	0.0028

Martensite							
Site	**Element**	**Wyckoff**	**X**	**Y**	**Z**	**Occupation**	**B$_{iso}$**
1	Fe	2a	0.0000	0.0000	0.0000	1	0.005

The parameters of the martensite lattice is dependent on the carbon content (wt%), and the lattice parameters listed in Table 2.5 are calculated for the carbon content in the two different alloys used in this work. Because of a significant amount of cementite in the first alloy, the carbon content in the martensite structure is reduced. Because of this a martensite with carbon content of 1.16 wt% is added, which is explained in Appendix A. Table 2.4 and 2.5 shows the parameters used for creating the structure files for the phases chosen to study for the samples in this work.

Table 2.5: Lattice parameters needed for creating a structure file in EMsoft.

Phase	Lattice	a (nm)	b (nm)	c (nm)	Space group
Austenite	FCC	0.35950	0.35950	0.35950	225 (Fm3m)
Ferrite	BCC	0.28665	0.28665	0.28665	229 (Im3m)
Cementite	Orthorhombic	0.50920	0.67410	0.45270	62 (Pnma)
Martensite (1.3 wt %)	BCT	0.28415	0.28415	0.30077	107 (I4/mm)
Martensite (1.16 wt%)	BCT	0.28510	0.28510	0.30000	107 (I4/mm)
Martensite (0.36 wt %)	BCT	0.28556	0.28556	0.28875	107 (I4/mm)

Simulating the master patterns

A Monte Carlo simulation is run through EMsoft to collect the information of the energy, the exit depth and distribution of the backscattered electrons (BSEs) for a given incident beam energy. The effect of electrons with energies from the incident beam energy (20keV in this work) down to 5keV are summed. The Monte Carlo simulation has shown to work well for energies above 5keV, and the lower value is chosen because of this (Jackson et al., 2019). The final master patterns represents all possible diffracted patterns for exit energies that range from 20-5keV and the grain orientation in every pixel of the scan (Chen et al., 2015).

The master pattern program run through EMsoft stores master patterns as square Lambert projections (decribed in (Roşca, 2010; Callahan and De Graef, 2013)) and stereographic projections. The latter is presented in Figure 2.20 where the southern/northern hemisphere of the spherical projections for the relevant phases for this work is shown.

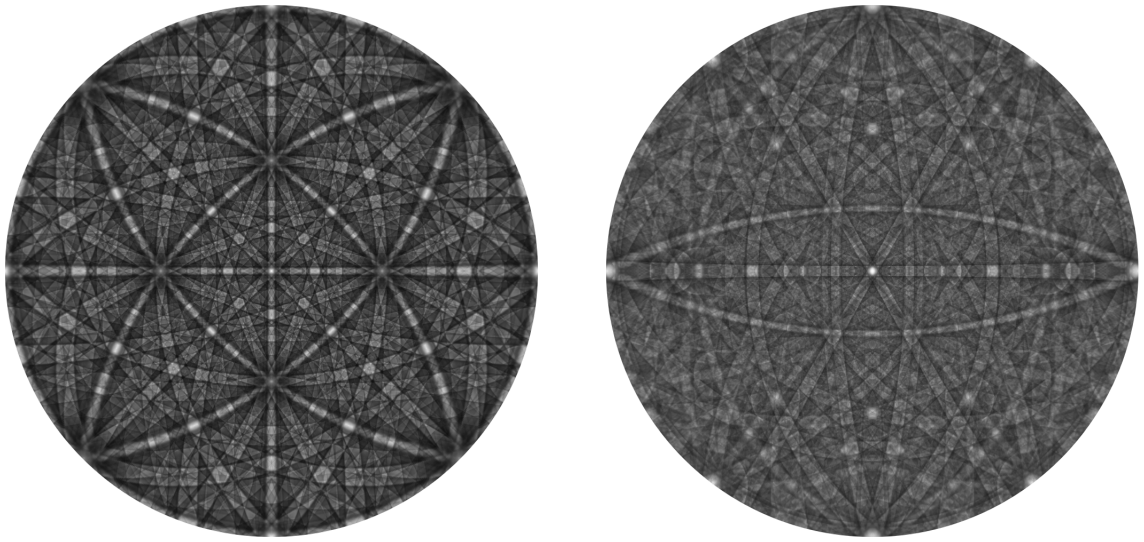

(a) Simulated master pattern for austenite. Max intensity is 2.60.

(b) Simulated master pattern for cementite. Max intensity is 1.07.

Figure 2.20: The simulated master patterns for austenite, cementite, ferrite and martensite for the 20 kV energy bin. The master patterns are produced though the EMEBSDmaster EMsoft program.

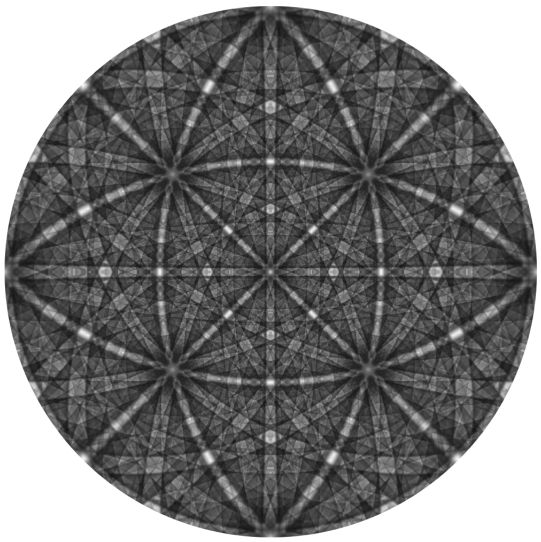

(c) Simulated master pattern for ferrite. Max intensity is 2.30.

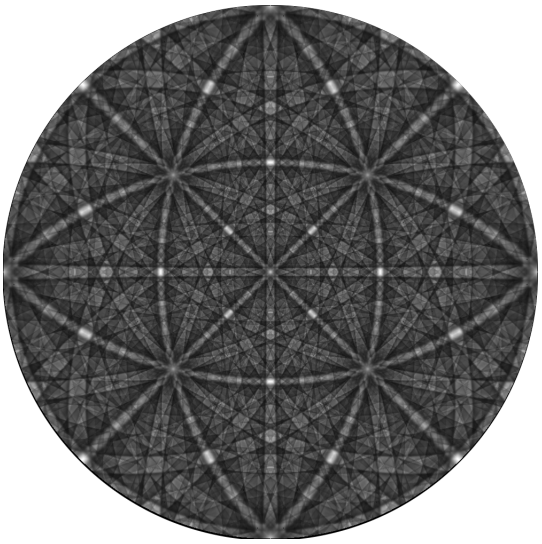

(d) Simulated master pattern for martensite containing 0.36 w% C. Max intensity is 2.66.

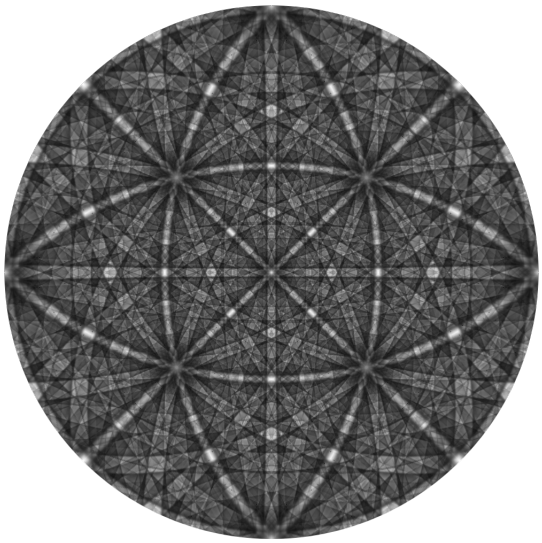

(e) Simulated master pattern for martensite containing 1.16 w% C. Max intensity is 2.26.

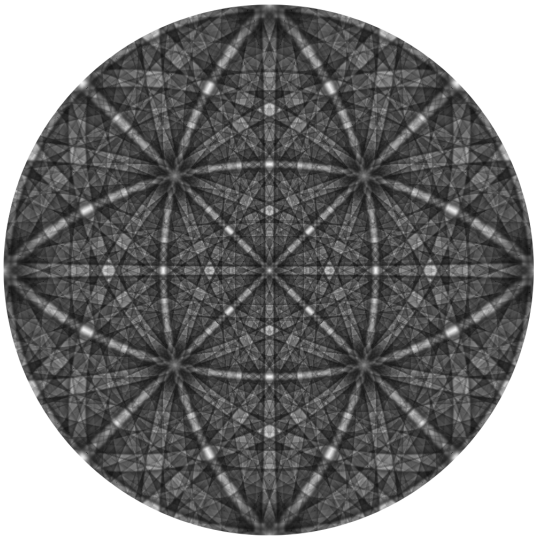

(f) Simulated master pattern for martensite containing 1.3 w% C. Max intensity is 2.27.

Figure 2.20: The simulated master patterns for austenite, cementite, ferrite and martensite for the 20 kV energy bin. The master patterns are produced though the EMEBSDmaster EMsoft program. (cont.)

Dictionary Indexing (DI)

To be able to run the indexing program in EMsoft it requires a pattern center (dependent on detector) and the distance from the sample to detector as some input values. When running an EBSD scan with NORDIF software, the user is asked to choose 5 reference patterns. With the use of TSL Data Collection, the pattern center coordinates (x*, y*, z*) for these patterns can be found. Since EMsoft only requires one value, the coordinates from the five patterns are converted to new values; x_{pc}, y_{pc} and L, and these values for the five patterns are then averaged. The conversion from EDAX/TSL to EMsoft is shown in Equation 2.10 below (Jackson et al., 2019).

$$\begin{aligned} x_{pc} &= -N_x^s(x^* - 1/2) \\ y_{pc} &= N_x^s y^* - N_y^s/2 \\ L &= N_x^s \delta z^* \end{aligned} \tag{2.10}$$

δ is the detector pixel size, and N_x^s and N_y^s the detector dimensions in pixels (before binning).

Running the indexing program in EMsoft generates a dictionary of simulated diffraction patterns. These patterns are tuned to the setup parameters of the experiment and to the crystal symmetry groups of the sample.

Each experimental pattern collected through the EBSD scan is compared to all the simulated patterns in the dictionary produced in EMsoft. An inner product of the best matching patterns for each pixel is computed, and only the highest values of the inner products are stored for each pixel. The set of inner products for each pixel are analyzed to determine which orientation and phase that is the most probable for each experimental pattern in the EBSD scan (Ram and De Graef, 2018).

2.4.6 Maps obtained from indexing an EBSD scan

OS = orientation similarity map is a map that best shows the different microstructural components (grains, phases, grain boundaries, etc.). The intensity in each pixel shows how many of the top N matches that specific pixel has in common with its nearest neighbors. The N value is chosen during the indexing with EMsoft. Neighbouring pixels inside a grain normally have very similar top matches, so the OSM value between these pixels will be high - and result in light areas in the map. When a pixel inside a grain is neighbour to a pixel inside a grain boundary, the top matches lists for these pixels would be quite different, and therefor produce a low OSM value. A low value corresponds to darker colors in the map (De Graef, 2019).

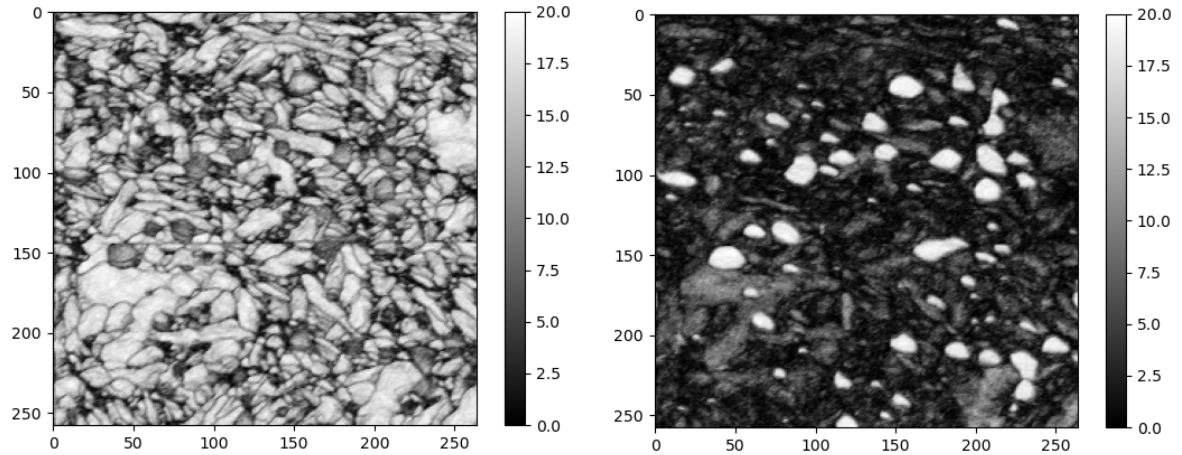

(a) OS map of a martensite sample indexed with ferrite.

(b) OS map of a martensite sample indexed with cementite.

Figure 2.21: Orientation Similarity (OS) maps of a martensite sample indexed with ferrite and cementite phase. The information is produced from EMsoft while the maps are provided by KikuchiPy (Ånes and Bergh, 2020) through Python.

ADP = Average dot product maps separates grain/phase boundaries from grain matrix. The dot products computed for each pixel is compared to the values of adjacent pixels. The pixels on or near a grain/phase boundary will have an average dot-product that in general is lower than for the pixels inside a grain. On the ADP map a low average dot product value corresponds to darker colors (Marquardt et al., 2017).

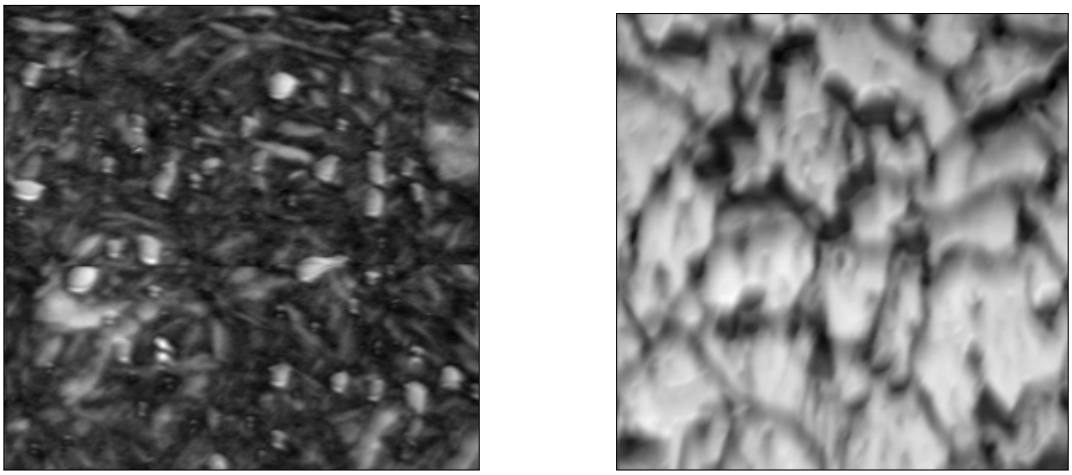

(a) ADP map of a martensite sample, produced in EMsoft.

(b) ADP map of a pearlite sample, produced in EMsoft.

Figure 2.22: Average Dot Product (ADP) maps of a martensite and pearlite sample.

CI = confidence index map is a map showing the value of the dot products by being light where the value is high (good match) and dark where the values are low (poor or no match).

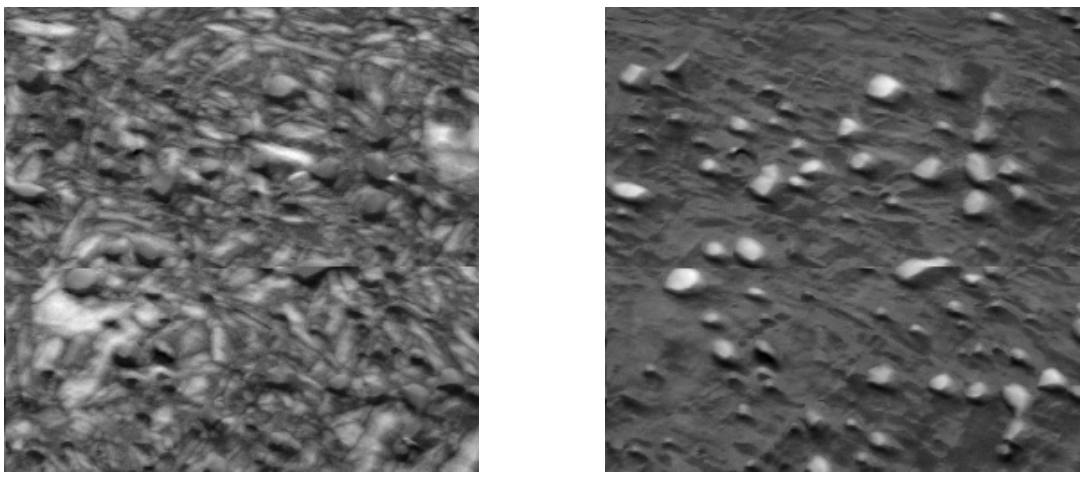

(a) CI map of a martensite sample indexed with ferrite phase in EMsoft.

(b) CI map of a martensite sample indexed with cementite phase in EMsoft.

Figure 2.23: CI maps of a martensite sample indexed with ferrite and cementite phase separately. The maps are light where the phase matches good with the experimental patterns, and dark where it does not.

IQ = image quality map is defined different for Hough Indexing and Dictionary Indexing. For Hough Indexing the maps show how well the patterns can be indexed with the Hough transform approach. For The Dictionary Indexing, these maps shows where the patterns are most ”sharp” (Marquardt et al., 2017). All in all, both versions of the map visually tells us the quality of the experimental EBSD patterns from our scan. Light areas represent areas with good patterns, and dark areas shows areas with poorer pattern quality (often grain boundaries). These maps are not related to the different phases used during indexing.

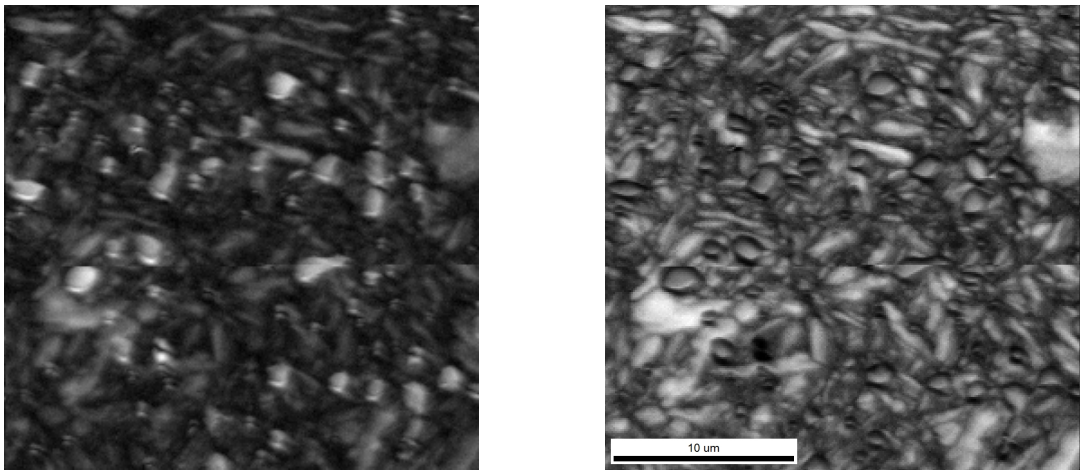

(a) IQ map of a martensite sample, provided by EMsoft.

(b) IQ map of a martensite sample, provided by TSL OIM Data Collection.

Figure 2.24: IQ maps of a martensite sample provided by EMsoft and TSL OIM Data Collection separately. The maps are light where the experimental patterns is of good quality, and dark where they are of poor quality.

2.5 Transmission Electron Microscope

Transmission Electron Microscope (TEM) is used to study microstructures of materials down to atomic level, and are able to construct images of much higher resolution and detail than in a SEM.

The sample in a TEM analysis needs to be down to 5-100 nm thin because the electron beam needs to travel through the sample to produce an image in TEM (Kittel, 2004). This means that the sample preparation is much more advanced and time-consuming than for SEM analysis. Ion-beam etching and electropolishing can be used to obtain a thinner sample in the center. Similarly to SEM, the sample should have electrical conductivity to avoid charging in the image. Because of great abberations in the optical lenses, very small apertures of the order of 10–25 mrad are needed to obtain a resolution of 0.1-0.3nm (Kohl and Reimer, 2008).

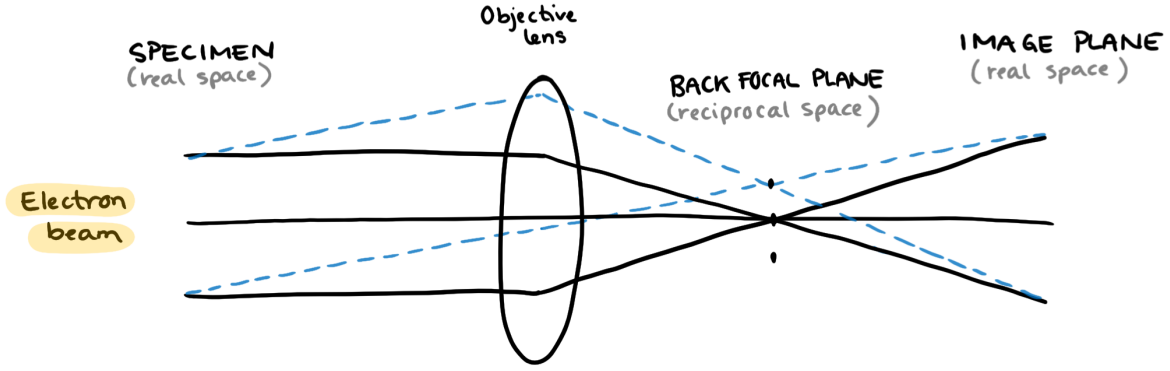

Figure 2.25: Ray diagram with an objective lens showing how the TEM works in prinsiple. The figure is reproduced from Bendersky and Gayle (2001).

Figure 2.25 shows a ray diagram with an objective lens describing how the incident beam in a TEM is used to obtain both information in real space as an electron microscope image or in reciprocal space as diffraction patterns. We can obtain this information from the same region just by adjusting the objectives in the microscope and inserting different apertures (Bendersky and Gayle, 2001).

2.5.1 Imaging modes: Bright field and dark field

Different images with focus of different details can be obtained by taking use of the specimens ability to diffract the incident electron beam. The electrons can transmit right through the sample without any diffraction (direct beam), or the electrons could be diffracted (scattered electrons). This is illustrated in Figure 2.26.

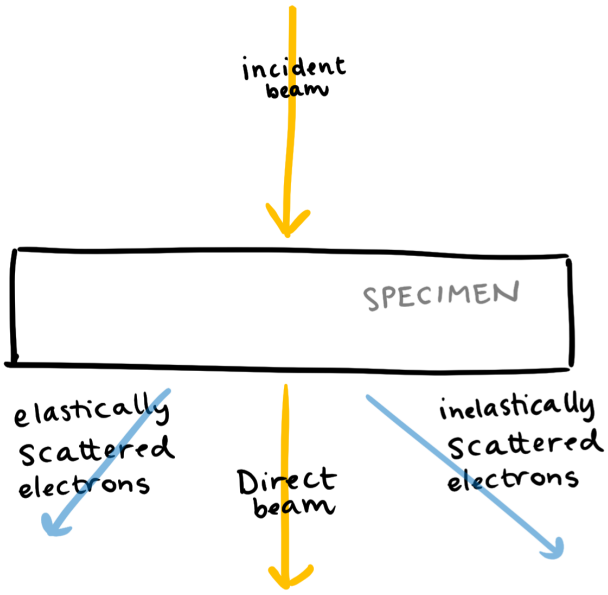

Figure 2.26: Illustration of the diffraction of the electron beam going through a TEM sample.

Bright field (BF) imaging mode lets the transmitted beam through the aperture while the diffracted beams are closed off. Areas in the sample that diffract the electrons strongly will appear dark in the image. This imaging mode is often used to construct an image with atomic mass contrast, since heavier atoms will diffract electrons more strongly (Spence, 2013).

Dark field (DF) imaging mode is obtained by changing the aperture to only let one diffracted beam through. In contrast to BF imaging mode, areas that do not diffract any light (where the electron beam goes right through the sample) will in DF appear dark. The DF imaging mode is great for studying crystal defects or for imaging crystallographic phases (Buseck et al., 1989).

Both imaging modes are illustrated in Figure 2.27.

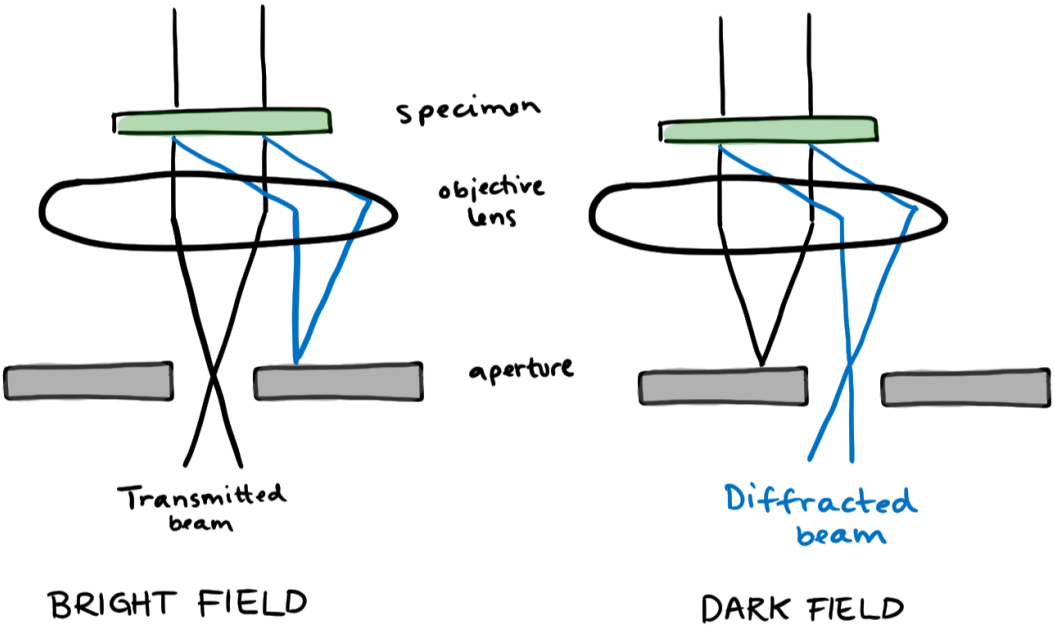

Figure 2.27: The illustration shows how one can obtain bright field and dark field mode by shifting the aperture to let trough either the transmitted beam, or a diffracted beam.

2.5.2 Scanning Precession Electron Diffraction

Similarly to the EBSD technique in SEM, Scanning Precession Electron Diffraction (SPED) is a technique in TEM that collect diffraction patterns from the sample. A finely focused electron probe is scanned across the sample, and at each probe position a PED pattern is collected. This pattern consist of kikuchi bands, identical to the ones constructing the EBSD patterns in SEM (Barnard et al., 2017; Rauch and Véron, 2014). The PED patterns are indexed in the same way as EBSD patterns, and orientation maps, strain maps and phase maps could be collected.

3 Materials and experimental methods

In this chapter the two steel alloys used in this work are presented as delivered, and the chemical composition of both alloys is shown. The rest of the chapter presents the different procedures done through this work which are heat treatment to obtain different steel phases, sample preparation, hardness testing, settings used for SEM analysis and explanation of all work done with the EBSD indexing software EMsoft.

3.1 Samples as delivered

Alloy 1: 103Cr3/103C3

The first steel used in this work was delivered as Figure 3.1 shows. The original microstructure of the steel was heat treated to martensite, but with aging the delivered sample was assumed to have been tempered and that areas of cementite and ferrite had been formed.

Figure 3.1: The steel as delivered, Alloy 1: 103Cr3/103C3. Full length about 50 cm.

A sample of the first alloy was sent to SINTEF Norlab for chemical analysis to find the chemical composition of the steel alloy. The result is presented in Table 3.1.

Table 3.1: The chemical composition of the 103Cr3/103C3 alloy given in wt%.

Alloy elements	C	Mn	Cr	P	S
103Cr3/103C3	1.3	0.27	0.74	0.016	0.011

Alloy 2: 34CrNiMo6

This alloy was said to be delivered as a steel with ferritic microstructure. The geometry and dimensions of the steel is presented in Figure 3.2. It was delivered with charge number and chemical composition which is given in Table 3.2.

(a) Full length: 40cm.

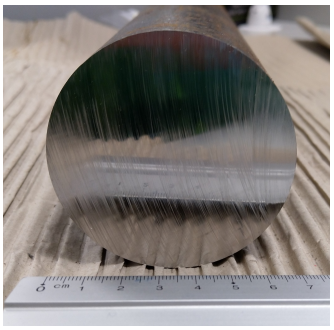

(b) Cross section: 6cm diameter.

Figure 3.2: The steel as delivered, Alloy 2: 34CrNiMo6.

Table 3.2: The chemical composition of the 34CrNiMo6 alloy given in wt%.

Alloy elements	C	Si	Mn	Cr	Mo	Ni
34CrNiMo6	0.36	0.21	0.61	1.58	0.21	1.47

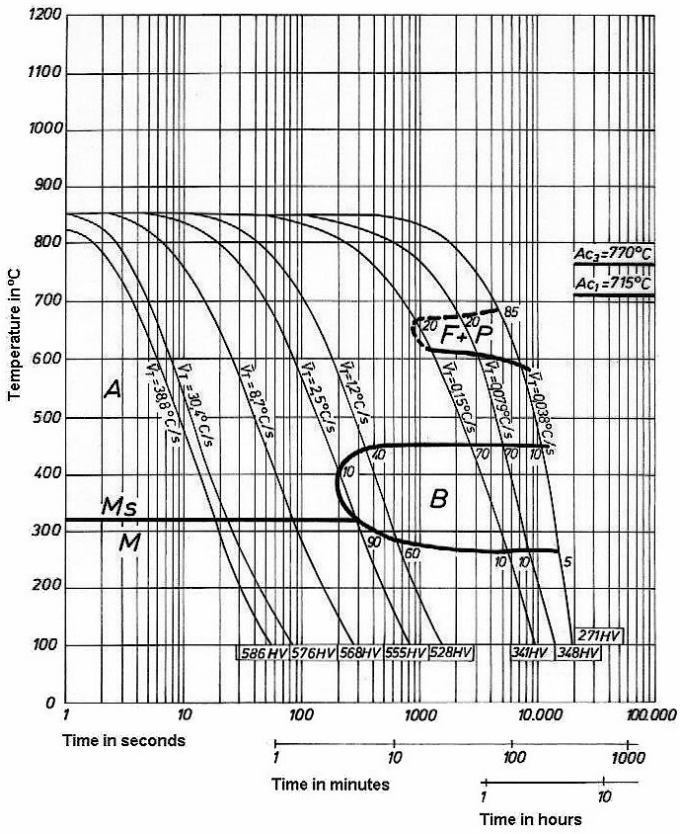

Figure 3.3: A CCT diagram showing transformation temperature related to cooling rate for the alloy containing 0.36 wt% C. The diagram is collected from `https://steelselector.sij.si/steels/VCNMO150.html`.

The CCT diagram for this alloy is presented in Figure 3.3, which gives a M_S temperature around 320 °C.

3.2 Heat treatment

The samples cut from both of the alloys were all heat treated differently to obtain three different types of microstructures. The hardening procedures performed was direct hardening, slow cooling and austempering. The temperature for the austenitizing temperature was decided from a Fe-Fe_3C phase diagram similar to Figure 2.1 for a composition with approximately 1 wt% C to be about 860 °C and for a composition with 0.36 wt% C to be about 890 °C. For the austempering process to obtain bainite, the M_S temperature was needed so the temperature of the salt baths could set a bit above that value.

Alloy containing 0.36 wt% C:

M_S was with the help of the chemical composition and Equation 2.1 calculated to be 320.9 °C. The calculated value was checked against the CCT diagram for this alloy in Figure 3.3, which shows that this was a reasonable value.

Alloy containing 1.3 wt% C:

For the alloy containing 1.3 wt% C the alloying elements exceeded the max. value for Equation 2.1 which was presented in Table 2.1, and therefore M_S could not be calculated the same way as for the alloy containing 0.36 wt% C. The M_S temperature was instead decided by comparing the carbon content of the alloy with the graphs in Figure 2.5, and chosen to be between 300°F $\approx$ 150 °C and 220 °C.

Table 3.3: The heat treatment done to obtain ferritic/pearlitic, martensitic and bainitic microstructure.

Desired microstructure	Autenizing temperature	Austenizing time	Cooling
Alloy 1: 103Cr3/103C3			
Pearlite	860 °C	30 min	Slowly in oven until it reached about 40 °C (for over 20h).
Martensite	860 °C	30 min	water (about 25 °C)
Bainite	860 °C	30 min	Salt bath at 280°C in 20 min before air cooling to room temperature.
Alloy 2: 34CrNiMo6			
Ferrite	890 °C	30 min	Slowly in oven until it reached about 40 °C (for over 20h).
Martensite	890 °C	30 min	water (about 25 °C)
Bainite	890 °C	30 min	Salt bath at 350°C in 20 min before air cooling to room temperature.

Making samples for investigation
For both alloys a sample of the steel was cut out without further heat treatment to investigate the alloy with its microstructure and properties as delivered. For each alloy samples of size 0.5-1 cm^3 was cut and heat treated to ferritic/pearlitic, martensitic and bainitic microstructure as Table 3.3 describes.

3.3 Sample preparation

3.3.1 SEM preparation

After heat treatment, all samples was mounted in epoxy for grinding and polishing. The procedure is described in Table 3.4 below.

Table 3.4: Grinding and polishing procedure for high strength alloy steels.

Grinding

Step	Surface	Abrasive type	Lubricant	Speed (rpm)	Direction	Force (N/sample)	Time (min)
1	SiC foil 220	-	Water	300	Same as blade	20	2
2	MD-Largo	DiaPro Allegro/Largo 9 μm	-	150	Same as blade	30	5

Polishing

Step	Surface	Abrasive type	Lubricant	Speed (rpm)	Direction	Force (N/sample)	Time (min)
3	MD-Dac	DiaPro Dac 3 μm	-	150	Same as blade	25	4
4	MD-Nap	DiaPro Nap B 1 μm	-	150	Same as blade	20	1

The first step of polishing was done with *Struers RotoPol-31/RotoForce-4* and step 2-4 was done with *Struers TegraPol-31/TegraForce-5*. After step 4 of polishing (Table 3.4) the samples was further polished in *VibroMet* 2 using *MasterMet 2* for 19-20 hours.

As the last step of preparation for EBSD analysis, two polishing methods was used; plasma cleaning and ion polishing. For the plasma cleaning a *Fischione 1020 Plasma Cleaner* was used for a total of 10 minutes per sample. For the ion polishing a *Hitachi IM-3000 Ion Mill* was used with the following settings:

Mode: 2
Ion beam current: 110-125 μm
Gas flow: 0.08 cm^3/min
Tilt angle: 75 °
Acc. voltage: 5kV
Time: 30 min

3.3.2 Etching for optical light microscopy

Some of the samples were studied in optical light microscopy (OM). The preparation of these samples followed the same routine as for preparation for SEM, but without the final steps from vibration polishing and further on. Instead the samples were etched with Nital 2% etch for 30-40 seconds after polishing.

Nital 2% etch: 2 ml HNO_3 and 98 ml ethanol.

3.3.3 TEM preparation

For the preparation of samples for TEM analysis, a very thin film of the samples was needed to be made. Each sample was cut as thin as possible ($<$ 1 mm) before polishing. To begin with, the first side of the sample was polished with SiC foil paper from # 180 to # 2400. The polished side was mounted to a block of plexi glass with double sided tape so the sample could be ground thin and simultaneously polished on the other side of the sample (Figure 3.4).

Figure 3.4: The images show the manual polishing with SiC foil paper of the TEM samples.

When the sample was ground and polished to a thickness of approximately 80-100 μm, the block with the sample was cooled in aqueous nitrogen. After a few minutes the thin film could be peeled off the block using tweezers and the thin film was soaked in acetone so any of the glue from the tape would dissolve, obtaining a clean sample. Finally, small plates with diameter of 3 mm was cut out of the thin film (see Figure 3.6).

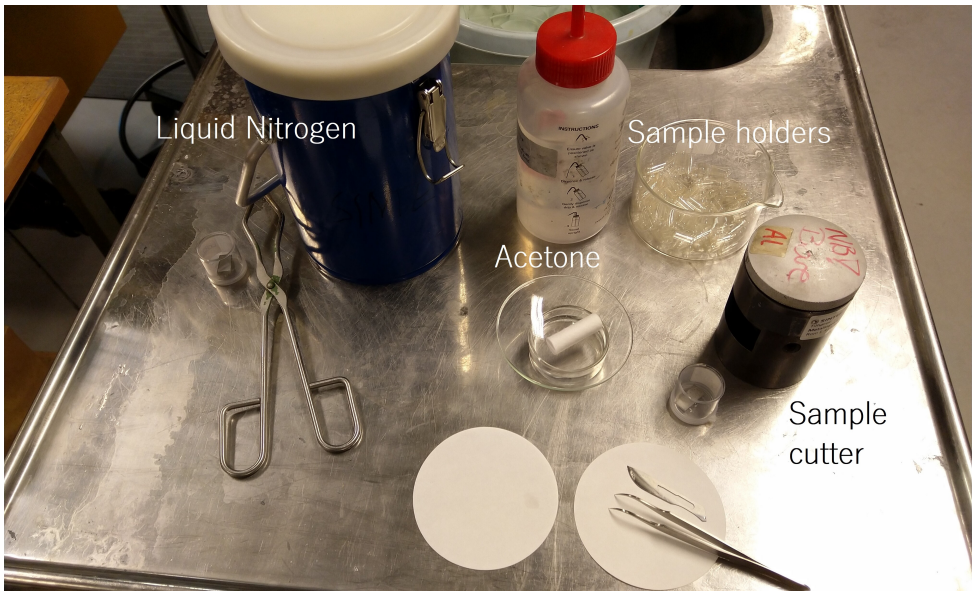

Figure 3.5: The image shows all parts of the sample preparation after polishing used to make TEM samples.

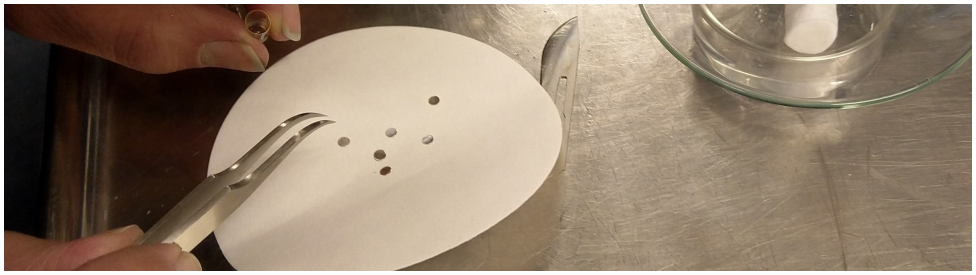

Figure 3.6: TEM samples after grinding and polishing. The samples were cut from the polished steel plate into samples with a diameter of 3 mm.

The samples was electropolished with TenuPol-5 using the Struers electrolyte A8. The polishing was done with voltage at 31.0V, room temperature (23 °C), pump flow rate at 15 and light act at 8. The time used for each sample varied from 1,5 - 5 minutes. After the polishing the samples was rinsed in ethanol before drying on filter paper.

Struers electrolyte A8: 50 ml perchloric acid and 950 ml Ethylene glycol monobutyl ether.

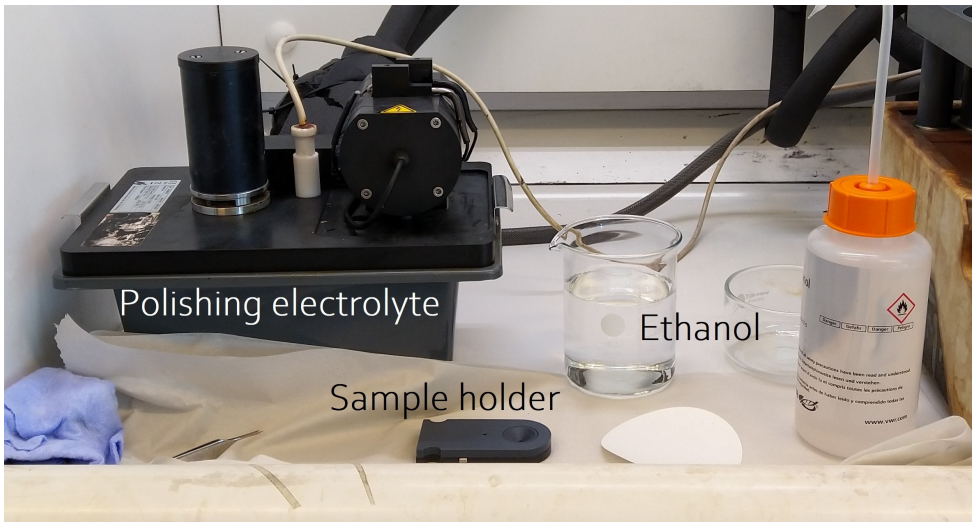

Figure 3.7: Setup for the electropolishing procedure of the TEM samples using TenuPol-5.

3.4 Hardness testing

The hardness testing was done with an InnovaTest manual hardness testing machine. For the martensite sample of alloy 1 (103Cr3/103C3) 10kg was applied for each indent for 15 seconds. For the martensite sample of alloy 2 (34CrNiMo6) 5kg was applies for 15 second on each indent.

3.5 TEM

All experimental work in TEM was done by Ruben Bjørge. Bright field images were taken with a JEOL JEM-2100 while HAADF SPED scans were done with a JEOL JEM-2100F.

3.6 SEM

The SEM anaysis for this thesis was all done on a Zeiss Ultra FESEM. The microscope settings used are given in Table 3.5.

Table 3.5: Settings used for EDS and EBSD analysis of all samples.

	Acc. Voltage	**Aperture**	**Working distance**	**Tilt angle**
EDS	15 kV	60 μm	10 mm	0
EBSD	20 kV	300 μm + High Current mode	25-26 mm	70 °

The EBSD scan settings used varied from sample to sample and was dependent on the desired resolution of the scan. The magnification was chosen by what would give big enough grains for the indexing maps to be good. For the pearlite and ferrite samples a magnification of 400-500x was used. For the martensite and bainite samples a magnification of 1000x was used.

Table 3.6: Table showing two examples of acquisition and calibration settings used for one pearlite and one martensite EBSD scan.

	Pearlite		Martensite	
	Acquisition	**Calibration**	**Acquisition**	**Calibration**
Averaging	2/4	5	4	4
Frame rate	130 fps	60 fps	70 fps	70 fps
Resolution	240x240 px	240x240 px	240x240 px	240x240 px
Exposure time	7642 μs	16616 μs	14235 μs	14235 μs
Gain	5	1	5	2
Step size	0.1 μm		0.1 μm	

The specific settings used for each scan are presented along with the results of each scan in chapter 4 .

3.7 EBSD indexing

For the indexing of the EBSD scans, two softwares was used. TSL OIM Data Collection 7 was used to index the EBSD patterns with the Hough Indexing technique, and EMsoft was used for the Dictionary Indexing technique.

TSL OIM Data Collection 7
The software uses the pattern.dat-file collected by NORDIF 3 during the EBSD scan as an input file, and through the software the user chooses the desired phases to index the scans with from the library. For the first alloy austenite, ferrite, cementite and $Cr_{23}C_6$ was chosen and the indexing phases, and several indexing rounds was done with the different phases as follows to study the different results:

austenite - ferrite - cementite - $Cr_{23}C_6$,
austenite - ferrite - $Cr_{23}C_6$,
austenite - ferrite - cementite, and
austenite - ferrite.

For Alloy 2 only austenite, ferrite and cementite was included in the indexing.

EMsoft
The EMsoft software also take the pattern.dat NORDIF file as an input, but before that step, a few other programs had to be run first. Each phase the scan was going to be indexed with needed a structure file and a master pattern file before the indexing itself could be done.

The structure file was produced by running the EMsoft program `EMmkxtal` and the file produced contained information about space group, lattice parameters, atom positions and number of atoms in the unit cell and what type of atoms the unit cell consists of.

To obtain the master pattern file for a phase, two EMsoft programs needed to be run. First, a Monte Carlo simulation was run with the EMsoft program `EMMCOpenCL` which collected information about the acceleration voltage used during the scan, and stored knowledge of the

energy, depth, and directional distributions of the backscattered electrons for that given incident electron beam energy and for the specific sample tilt (which in all experiments of this work was set to be 70 °). This program used the structure (.xtal) file as input. After the Monte Carlo simulation the EMsoft program `EMEBSDmaster` had to be run. With this program, the file produced by `EMMCOpenCL` was taken as input. The program systematically simulated patterns for each energy bin from 5 keV to 20keV, and produced a master pattern for that given phase. All the information collected during the run of this program was stored in the same file used as an input.

Before the indexing step could be run, the pattern file obtained through NORDIF needed to be background corrected to get more distinct EBSD patterns. This was done by subtracting the static background from the scan with KikuchiPy, a program run in Python (Ånes and Bergh, 2020). Figure 3.8 shows the same pattern before and after doing a static background correction.

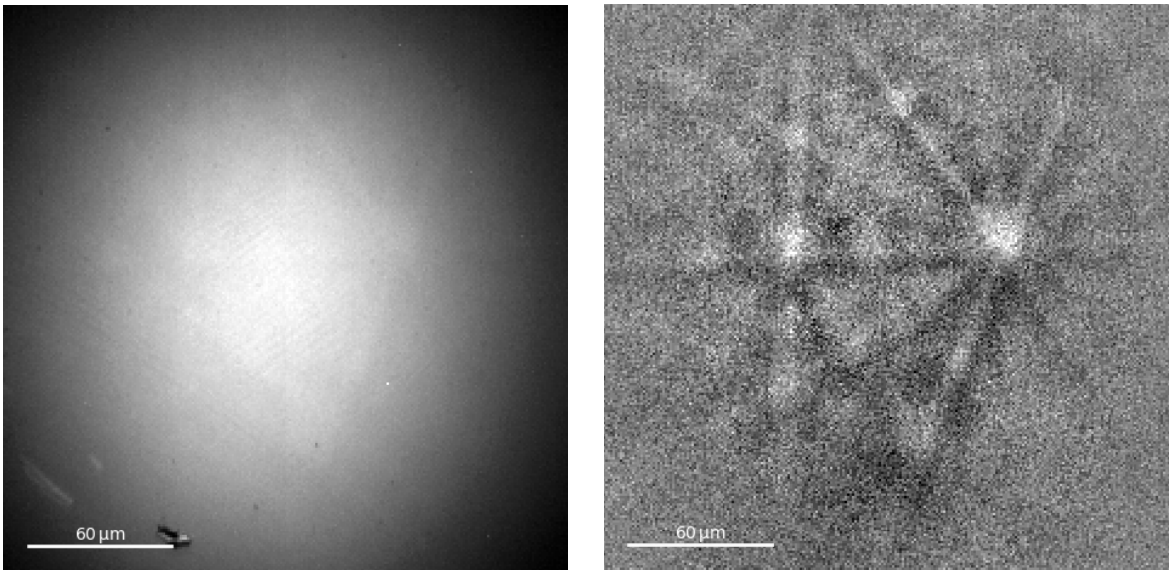

(a) EBSD pattern from one pixel in a martensite sample scan before the static background correction.

(b) EBSD pattern from one pixel in a martensite sample scan after the static background correction.

Figure 3.8: The same pixel of an EBSD scan is showed before and after the static background correction done with KikuchiPy. The pattern is diffracted from a martensite sample.

Finally the indexing EMsoft program `EMEBSDDI` could be run. This program took in the file produced in `EMMCOpenCL` (and supplied in `EMEBSDmaster`) and the pattern.dat NORDIF file as inputs, along with information about number of pixels in the scan, detector geometry, scan step size and resolution of the scan.

All of these five steps were needed to be done for all the phases the scan was going to be indexed with, for every EBSD scan. This whole process is described in detail in the Hands-On Tutorial provided by M. A. Jackson, E. Pascal and M. De Graef in `https://link.springer.com/content/pdf/10.1007/s40192-019-00137-4.pdf`.

4 Results

This chapter presents the results of OM and SEM analysis of the as-delivered steel structures, hardness testing of the martensite samples, EDS SEM analysis of Alloy 1, and both TSL and EMsoft indexing of all the samples. Lastly a TEM analysis of the bainite and martensite sample from both the alloys are presented.

4.1 Investigation of the as-delivered structures of the two alloys

Samples of both alloys was made for investigation of the microstructure of the steels as delivered before samples that were heat treated were studied. The samples were polished and etched for optical light microscopy, and then polished further for SEM analysis where secondary electron images was taken of both of the samples. The results are presented below.

4.1.1 Optical light microscopy (OM)

Alloy 1: 103Cr3/103C3
The original structure was investigated using optical light microscopy (OM) to get an overview of ferrite or cementite in the martensite matrix formed over time.

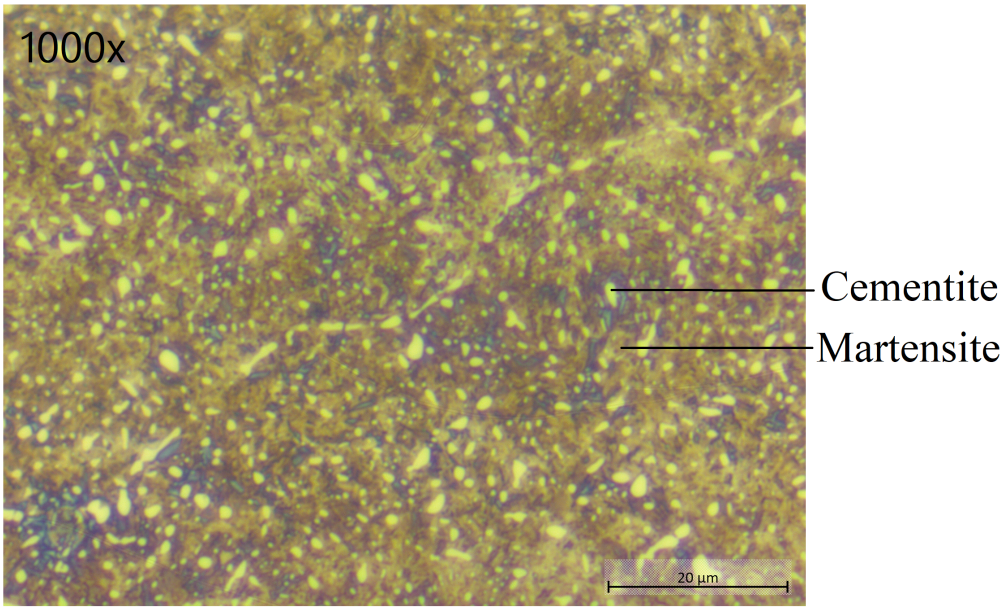

Figure 4.1: Original structure of Alloy 1 etched with 2% Nital for 40 seconds. The brown colored areas are the etched martensite, while the ferrite/cementite particles are the light unetched areas. The light particles seems to be lined up along grain boundaries.

The bright areas that are not etched are ferrite/cementite, while the brown areas are martensite. The somewhat spheroidized lighter particles have diameters up to 2 μm, and the longer non-spherical particles has lengths up to 6 μm.

Alloy 2: 34CrNiMo6

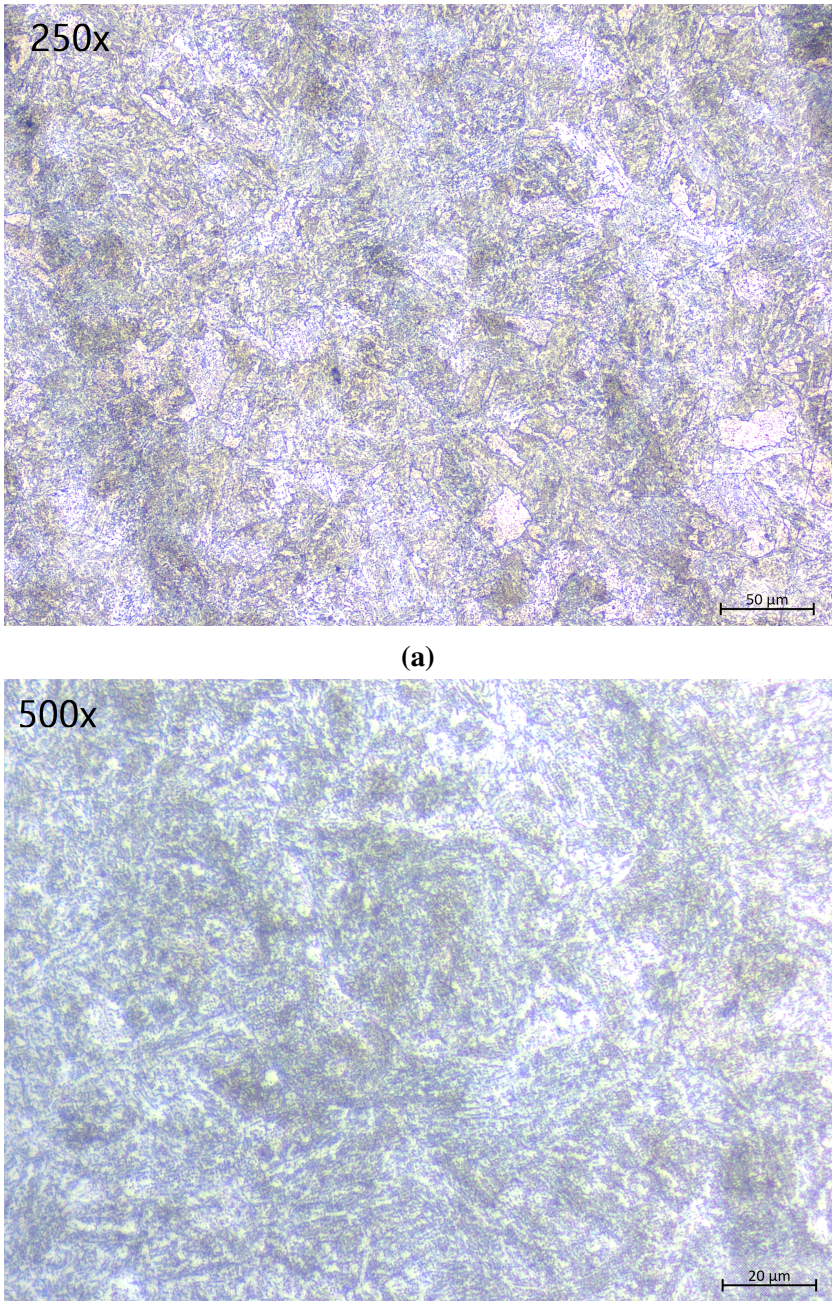

Figure 4.2: Original structure of Alloy 2. Etched with 2% Nital for 30-40 seconds.

In contrast to the sample of Alloy 1, the etching of the original structure of Alloy 2 did not result in a brown-colored sample surface typical for martensitic structure. The image in Figure 4.2a might look more red than the image in Figure 4.2b, but this is only because of a change in white balance. The magnification of the samples from the two alloys are not the same so they

can not directly be compared, but for this alloy no particles made big contrast to the matrix after etching in the same way as for Alloy 1.

4.1.2 Secondary electron (SE) imaging in SEM

After the OM investigation of the etched sample surfaces, the samples were re-polished for SEM analysis.

Alloy 1: 103Cr3/103C/3
Figure 4.3 shows SE images of the original martensitic structure, and spherical particles of size up to 2 μm was found throughout the whole sample surface.

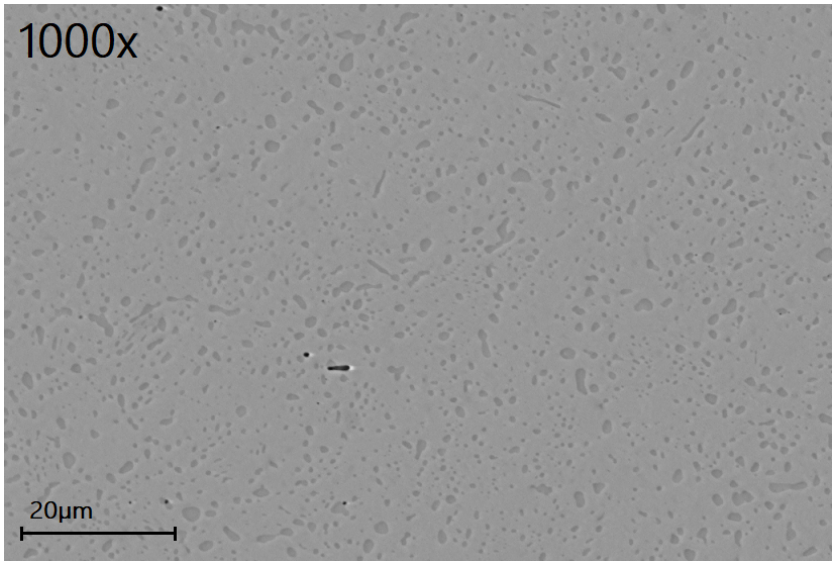

(a)

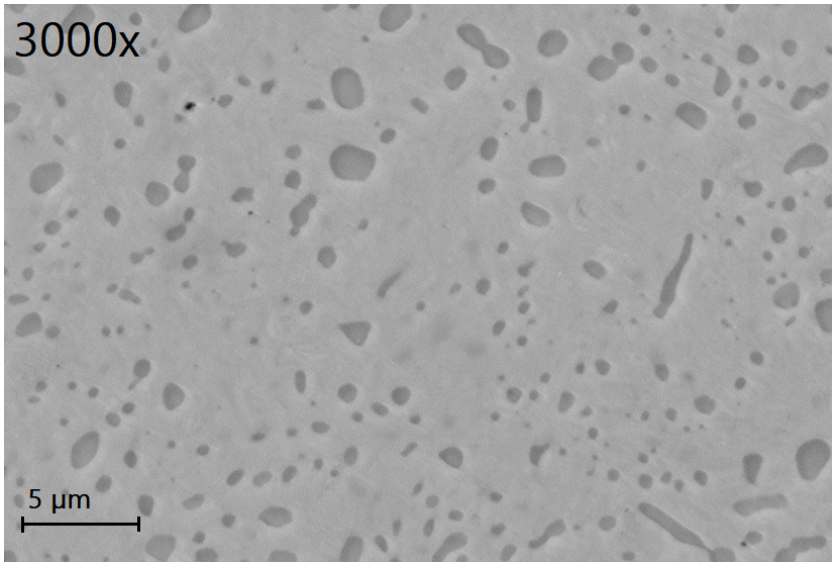

(b)

Figure 4.3: SE images of the original structure of Alloy 1 showing cementite particles in a martensitic matrix.

Alloy 2: 34CrNiMo6
Figure 4.4 Shows a SE image of the original structure of Alloy 2 before heat treatment done in this work. In comparison to Alloy 1, no clear particles/areas of possible cementite were visible.

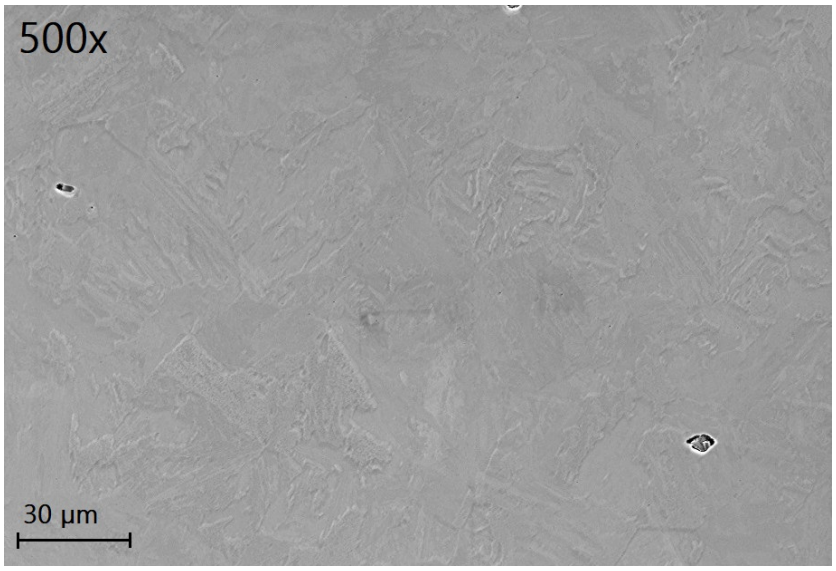

(a)

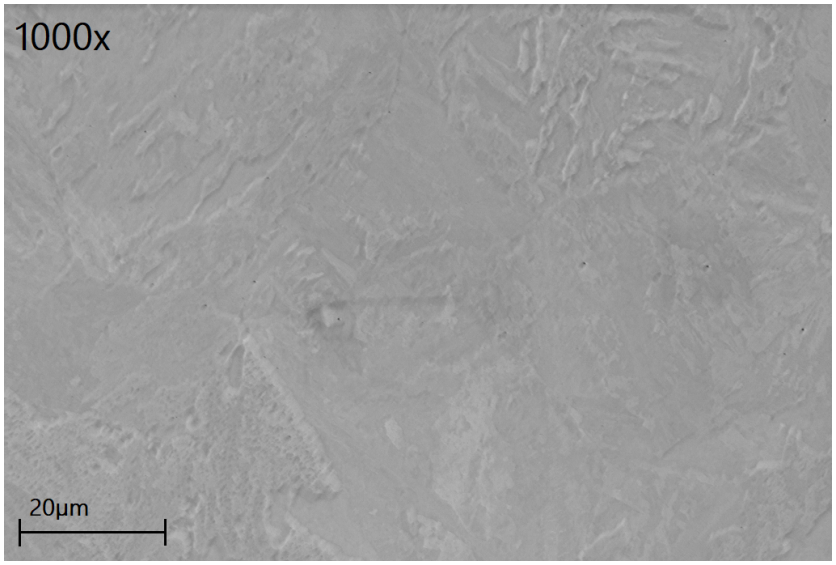

(b)

Figure 4.4: SE images of the original structure of Alloy 2.

4.2 Hardness testing

The martensite sample of both alloys were hardness tested to help decide if the right microstructure was produced during the heat treatment. 16 indents was done throughout the surface of both samples to get an overall understanding of the hardness of the sample.

4.2.1 Alloy 1: 103Cr3/103C3

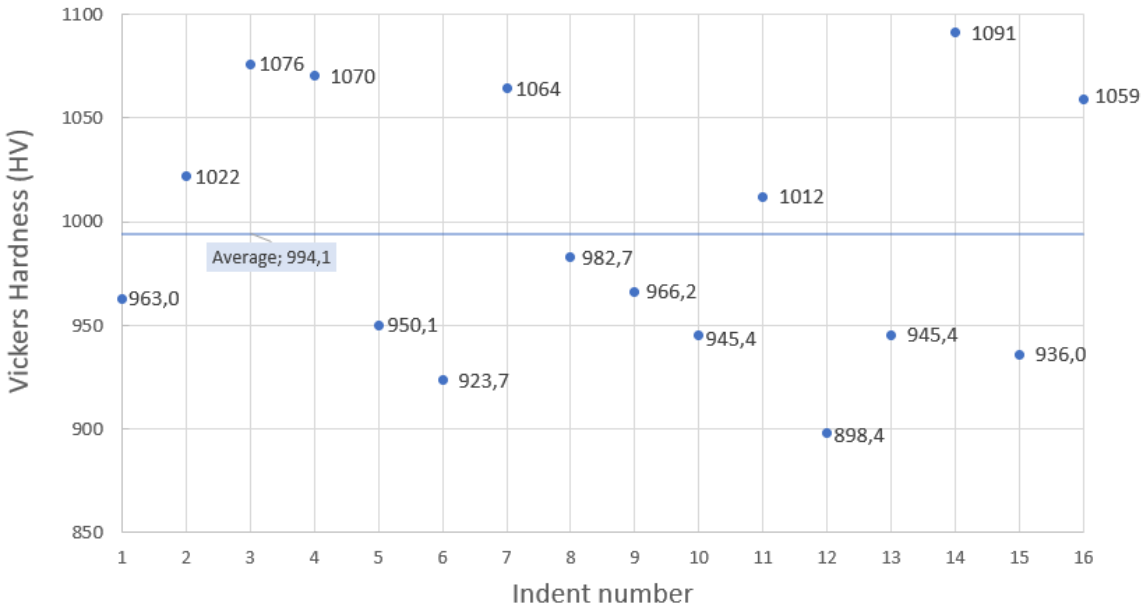

Figure 4.5: Vickers hardness testing of the martensite sample of Alloy 1. 10kg was applied for 15 seconds for each indent.

16 indents was performed spread out on the sample surface of the martensite sample. Figure 4.5 shows how the hardness ranged from 898,4 to 1091. The average hardness value was calculated to be 994,1.

4.2.2 Alloy 2: 34CrNiMo6

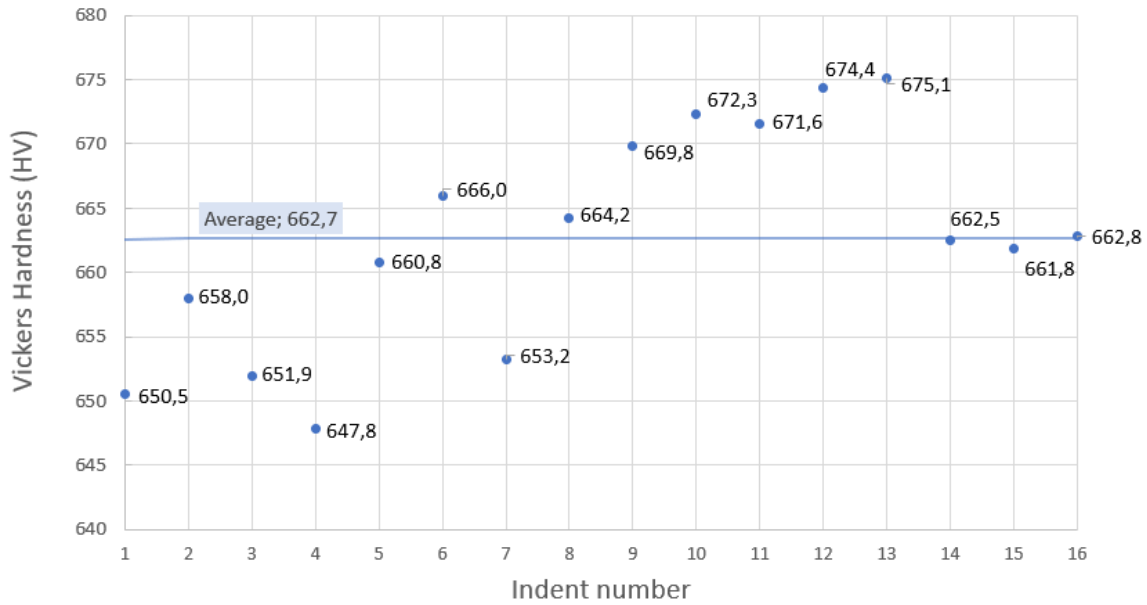

Figure 4.6: Vickers hardness testing of the martensite sample of Alloy 2. 5kg was applied for 15 seconds for each indent.

16 indents was performed across the surface of the martensite sample. Figure 4.6 shows the values of the Vickers hardness calculated from the indents, varying from 647,8 to 675,1. The average hardness value of these indents was 662,7.

4.3 EDS analysis of Alloy 1

In the SE and OM images of all the samples of the Alloy 1 dark areas could be seen. To begin with they were assumed to be pores, and a new round of polishing was done. The areas did not disappear however, and therefore an EDS scan was executed on one of the samples. The pearlite sample of Alloy 1 was the first sample analyzed in SEM, and therefore the EDS scan was done of this sample. The EDS map scans are presented below.

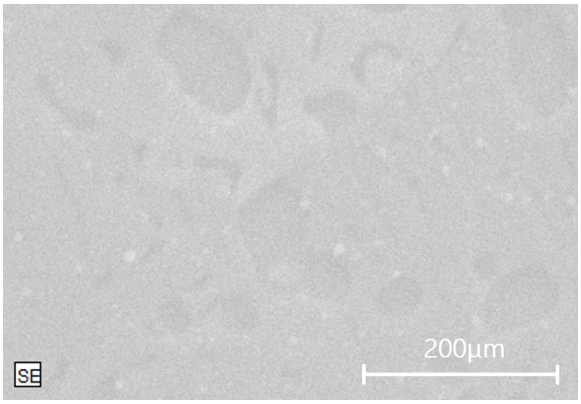

(a) SE image showing the area studied in an EDS map scan.

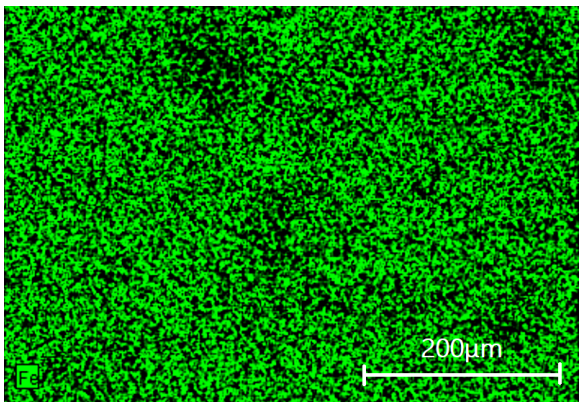

(b) EDS map of element Fe.

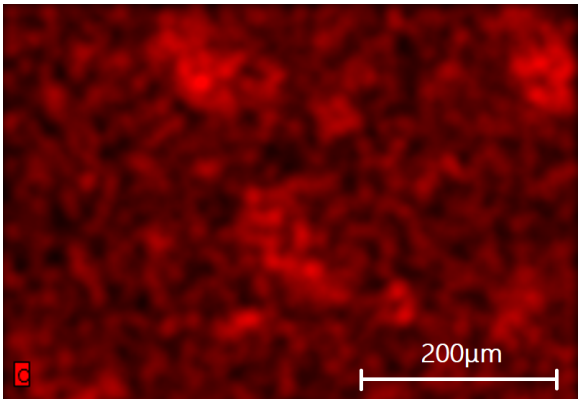

(c) EDS map of element C.

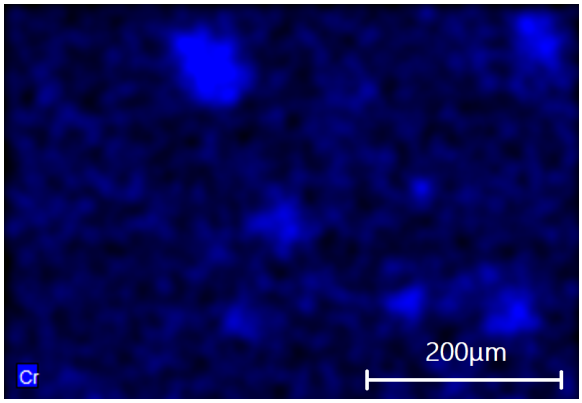

(d) EDS map of element Cr.

Figure 4.7: EDS scan done of the ferrite sample. The EDS map scans shows distribution of Fe, C and Cr in the area presented in the SE image in 4.7a.

Figure 4.7 shows that the dark areas in the SE image has less iron and more carbon and chromium than the adjacent areas. It is likely to think that these areas consist of chromium carbide, cementite or chromium enriched cementite in the ferrite matrix.

4.4 Indexing the EBSD scans of Alloy 1: 103Cr3/103C3

4.4.1 Pearlite sample

The EBSD scan of the pearlite sample was done with magnification 400x, working distance 26.0 mm and step size 0.1 μm. The acquisition and calibration settings were as follows:

Acquisition settings
Frame rate: 130 fps
Resolution: 240x240 px
Exposure time: 7642 μs
Gain: 5

Calibration settings
Frame rate: 60 fps
Resolution: 240x240 px
Exposure time: 16616 μs
Gain: 1

TSL indexing of the pearlite sample

The sample was indexed with austenite (γ), ferrite (α), cementite (θ) and $Cr_{23}C_6$ phase, with the following combinations; γ, α and θ, γ, α and $Cr_{23}C_6$, and lastly γ, α, θ and $Cr_{23}C_6$. While tuning the reference patterns in TSL OIM Data Collection the ferrite and $Cr_{23}C_6$ phase showed to have very similar pattern geometries, and to differentiate the two phases showed to be difficult for both the naked eye and the software. This resulted in messy indexings, which is easiest seen in the Auto Grain maps. The results are presented below.

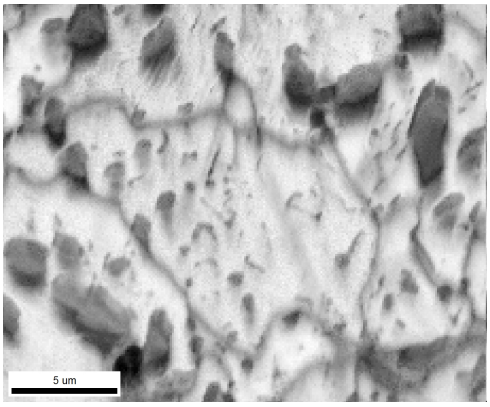

Figure 4.8: Alloy 1. Image Quality (IQ) map of the pearlite sample indexed with TSL.

The IQ map in Figure 4.8 shows the quality of the EBSD scan of the pearlite sample. The dark areas represents areas with poorer kikuchi patterns, while light areas represents good patterns. The map of this scan has large light areas, showing the result of an EBSD scan with good and easily indexed kikuchi patterns.

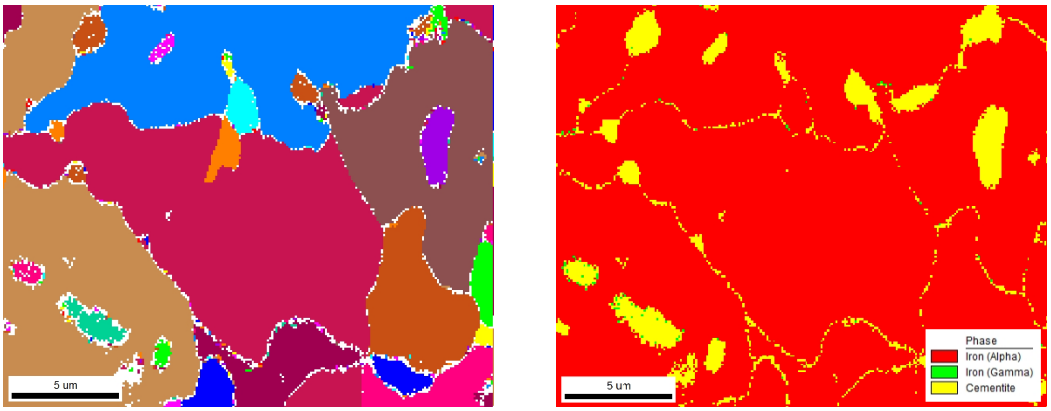

(a) Grain map of the pearlite sample indexed with the α, γ and θ phase.

(b) Phase map of the pearlite sample indexed with the α (red), γ (green) and θ (yellow) phase.

Figure 4.9: Alloy 1. TSL indexing of the pearlite sample using the α, γ and θ phase.

Figure 4.9 and Figure 4.10 shows the same EBSD scan, only they are indexed with different phases using the TSL OIM Data Collection software. Both are indexed with austenite and ferrite, but the first is also indexed with cementite, while the other is indexed with a chromium carbide phase. The indexing with the cementite phases gives a result with less noice and mis-indexing, while the indexing with the chromium carbide phase has problems differentiating the ferrite phase (red) from the chromium carbide (blue) phase.

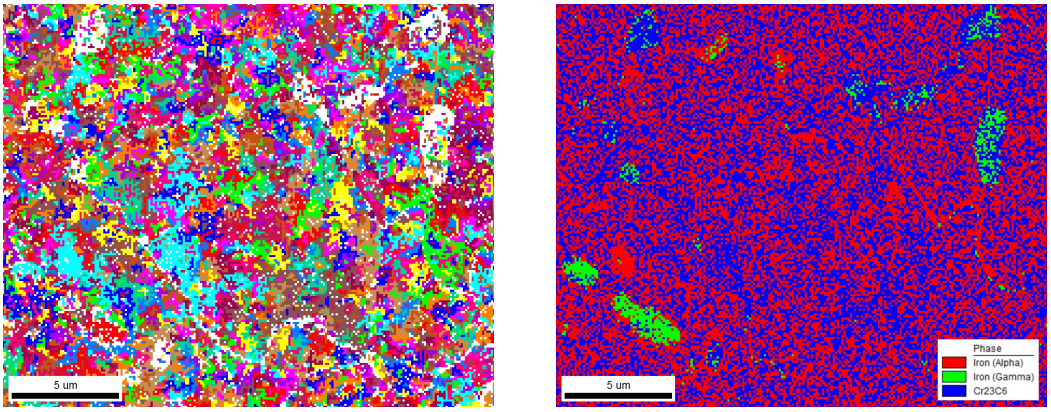

(a) Grain map of the pearlite sample indexed with the α, γ and $Cr_{23}C_6$ phase.

(b) Phase map of the pearlite sample indexed with the α (red), γ (green) and $Cr_{23}C_6$ (blue) phase.

Figure 4.10: Alloy 1. TSL indexing of the pearlite sample using the α, γ and $Cr_{23}C_6$ phase.

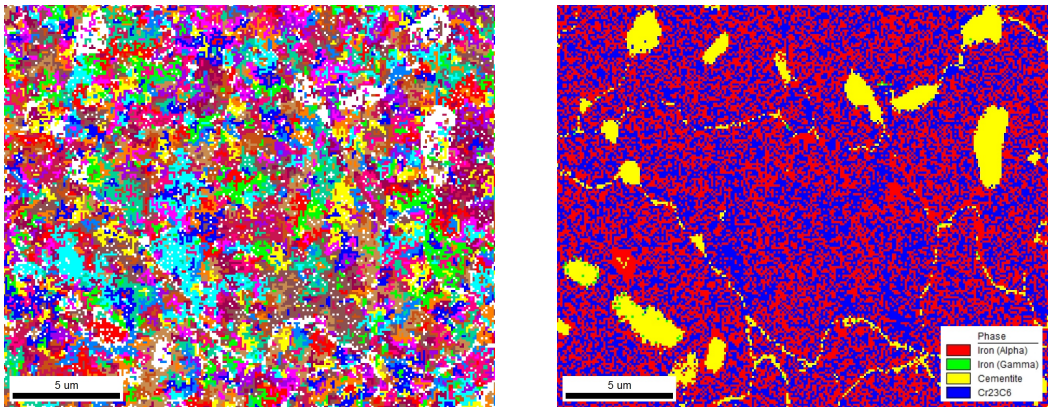

(a) Grain map of the pearlite sample indexed with the α, γ, θ and $Cr_{23}C_6$ phase.

(b) Phase map of the pearlite sample indexed with the α (red), γ (green), θ (yellow) and $Cr_{23}C_6$ (blue) phase.

Figure 4.11: Alloy 1. The pearlite sample indexed with the TSL software using all four phases.

Figure 4.11 presents an indexing done with all four phases, which shows how the dark areas visible in the IQ map (Figure 4.8) are best indexed as cementite (*yellow* in the phase maps). In an indexing of the pearlite sample done without the cementite phase, these areas are poorly indexed and the software tries to index them as austenite or chromium carbide (Figure 4.10b). Once cementite is added as an indexing phase, these areas are clearly indexed as cementite. When the chromium carbide phase is added, the grain maps in Figure 4.10a and 4.11a shows that the software has trouble finding the same grains as in Figure 4.9a which results in messy maps.

The IQ map in Figure 4.8 and the phase maps in Figure 4.9b and 4.11b shows cementite particles of size ranging from 1-4 μm. The scan is taken from a relatively small area and the ferrite grains in the scan are quite large, making it difficult to get a overview of the average grain size. The grain in the middle of the scan has a width of about 12 μm.

Table 4.1: Alloy 1. Phase fractions obtained from the phase maps through the different rounds of indexing in TSL of the pearlite sample. α = ferrite, γ = austenite, θ = cementite, $Cr_{23}C_6$ = chromium carbide.

Indexing phases	**Fraction α**	**Fraction γ**	**Fraction θ**	**Fraction $Cr_{23}C_6$**
α, γ, θ	0.918	0.002	0.080	-
$\alpha, \gamma, Cr_{23}C_6$	0.479	0.023	-	0.498
$\alpha, \gamma, \theta, Cr_{23}C_6$	0.453	0.002	0.077	0.468

In Table 4.1 the phase fractions obtained trough the different indexing rounds with the TSL software using Hough indexing are presented. For both the indexing rounds done with cementite (θ), the values of austenite (γ) and cementite stays somewhat the same. For both the indexing rounds with $Cr_{23}C_6$, the fraction of ferrite (α) is greatly reduced. This can be seen from the phase maps presented in Figure 4.10b and 4.11b where $Cr_{23}C_6$ in blue have indexed well with patterns that in the indexing round without $Cr_{23}C_6$ was indexed as ferrite.

EMsoft indexing of the pearlite sample

Because of the amount of noise in the indexing when the chromium carbide phase was included, this phase was excluded during the indexing with EMsoft. Each scan was indexed with cementite (θ), austenite (γ), ferrite (α) and martensite (α') phase separately.

Image Quality (IQ) and Average Dot Product (ADP) maps are presented below along with Confidence Index (CI) maps and Orientation Similarity (OS) maps in Figure 4.13 and 4.14. The OS maps are presented along with its corresponding colorbar showing the intensity of the different areas. Some of the maps will look more or less the same, but the intensity could be different. The colorbar was added so the results could be compared.

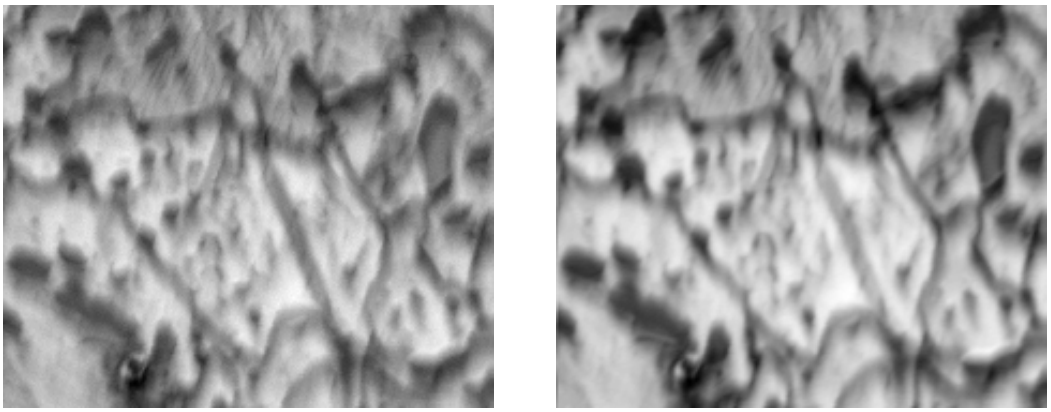

(a) Image Quality Map of the pearlite sample indexed with EMsoft.

(b) Average Dot Product Map of the pearlite sample indexed with EMsoft.

Figure 4.12: Alloy 1. IQ and ADP maps obtained through indexing with EMsoft.

Figure 4.12 shows the IQ and ADP maps of the pearlite sample indexed with EMsoft. These maps show where the EBSD scan has good kikuchi patterns by being light in these areas, and darker in areas where the patterns are of poorer quality. The EBSD scan of the pearlite sample has very light IQ and ADP maps, meaning that the scan is of good quality.

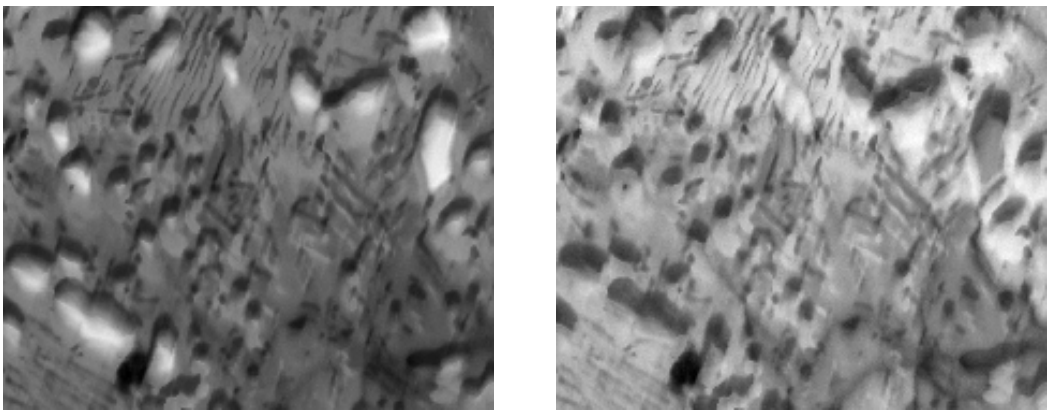

(a) Confidence Index Map of the pearlite sample indexed with the cementite (θ) phase.

(b) Confidence Index Map of the pearlite sample indexed with the austenite (γ) phase.

Figure 4.13: Alloy 1. CI maps from the EMsoft indexing of the pearlite sample using the θ,γ, α and α' phase.

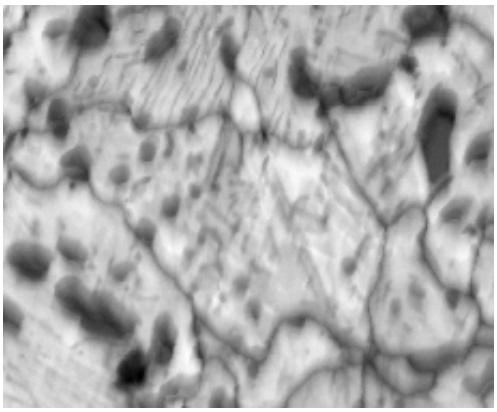

(c) Confidence Index Map of the pearlite sample indexed with the ferrite (α) phase.

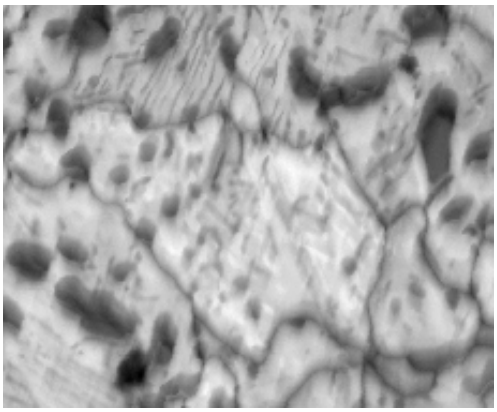

(d) Confidence Index Map of the pearlite sample indexed with the martensite (α') phase.

Figure 4.13: Alloy 1. CI maps from the EMsoft indexing of the pearlite sample using the θ,γ, α and α' phase. (cont.)

Figure 4.13 shows Confidence Index (CI) maps of the pearlite sample indexed with the cementite, austenite, ferrite and martensite (1.3 wt% C) phase through EMsoft. These maps are light where the software is positive that the simulated and the experimental patterns have a good match, and dark when they do not match well. Figure 4.13a shows that the cementite phase matches good with the same particles indexed as cementite in TSL, and clearly matches poorly with the ferrite matrix. The indexing with austenite in Figure 4.13b shows no clear particles matched well with the phase, but the matrix does not match as poor as for the cementite indexing. The ferrite and martensite indexing in Figure 4.13c and 4.13d matches very well with the matrix, and matched poorly in the cementite particles.

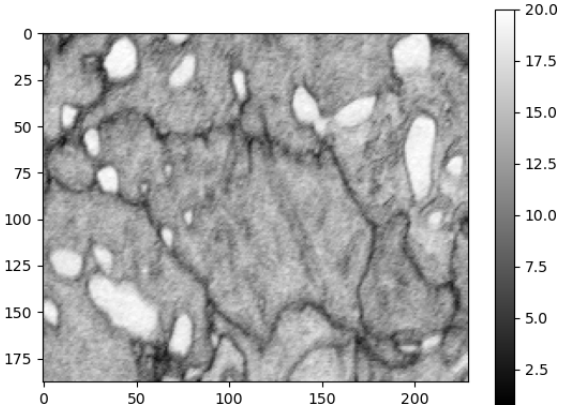

(a) Orientation Similarity Map of the pearlite sample indexed with the cementite (θ) phase. The indexing has an OSM mean value of 12.73.

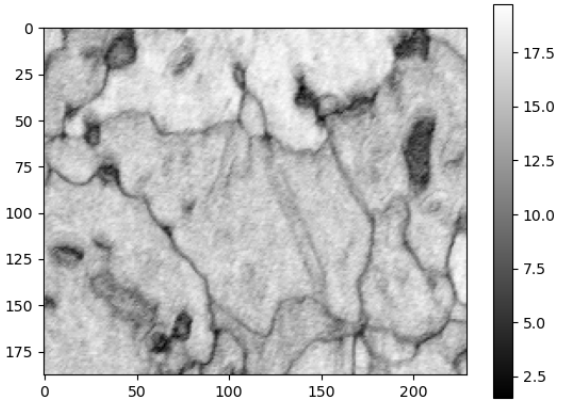

(b) Orientation Similarity Map of the pearlite sample indexed with the austenite (γ) phase. The indexing has an OSM mean value of 14.69.

Figure 4.14: Alloy 1. OSM maps from the EMsoft indexing of the pearlite sample using the θ, γ, α and α' phase.

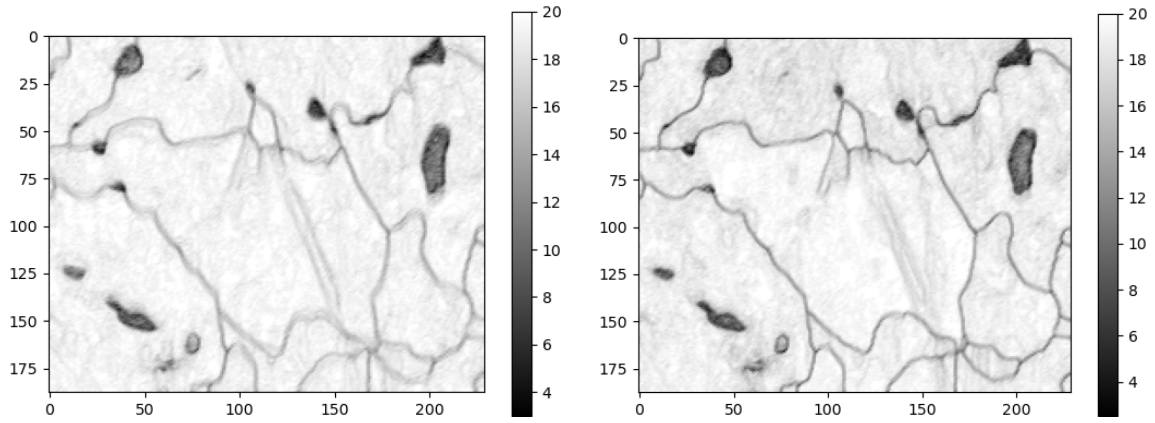

(c) Orientation Similarity Map of the pearlite sample indexed with the ferrite (α) phase. The indexing has an OSM mean value of 18.52.

(d) Orientation Similarity Map of the pearlite sample indexed with the martensite (1.3 wt%C) (α') phase. The indexing has an OSM mean value of 18.13.

Figure 4.14: Alloy 1. OSM maps from the EMsoft indexing of the pearlite sample using the θ, γ, α and α' phase. (cont.

Figure 4.14 shows OS maps of the pearlite sample indexed with the cementite, austenite, ferrite and martensite (1.3 wt% C) phase in EMsoft. In similarity to CI maps, light areas in OSM maps also represents the areas where the simulated patterns produced for each indexing phase in EMsoft matches good with the experimental patterns. OSM maps do however show more detail of the structure than the CI maps. Along with the CI maps in Figure 4.13, the small areas indexed as cementite with TSL also has a good match with cementite in the EMsoft indexing. From the colorbar added to each OS map, these areas have a high intensity when indexed with cementite, while the rest of the matrix has low intensity. In the maps for the other phases, these small areas has lower intensity than the matrix, which shows that the simulated patterns of the other phases matches poorly with the experimental there.

Table 4.2 presents the OSM mean and max intensity values for the maps presented in Figure 4.14. All phases has some areas with intensity at max (20.00), except austenite. The highest mean OSM intensity value is obtained through the indexing with ferrite, with a value of 18.52. Two different indexings with martensite were done, and the result of the second indexing is added to Table 4.2. The maps from this indexing and the explanation of why it was added is described in Appendix A.

Table 4.2: Alloy 1. The OSM max and mean values from the indexing done of the pearlite sample with EMsoft.

Indexing phase	θ	γ	α	α' **(1.3 %)**	α**' (1.16%)**
OSM max value	20.00	19.75	20.00	20.00	20.00
OSM mean value	12.73	14.69	18.52	18.13	18.18

4.4.2 Martensite sample

An EBSD scan of the martensite sample is presented below. The scan was done with magnification 1000x, working distance 26.0 mm and step size 0.1 μm. The acquisition and calibration settings were as follows:

Acquisition settings
Frame rate: 70 fps
Resolution: 240x240 px
Exposure time: 14235 μs
Gain: 4

Calibration settings
Frame rate: 70 fps
Resolution: 240x240 px
Exposure time: 14235 μs
Gain: 4

TSL indexing of the martensite sample

Similarly as for the pearlite sample, the martensite sample was indexed with austenite (γ), ferrite (α), cementite (θ) and chromium carbide ($Cr_{23}C_6$) phase, with the same combinations to compare the results. Figure 4.16 shows the indexing with α, γ and θ, while Figure 4.17 shows the indexing with α, γ and $Cr_{23}C_6$.

All maps presented below show a structure with smaller grains than the pearlite sample, and there is more areas with poorer patterns resulting in maps with more possible mis-indexed pixels. Particles indexed as cementite can be found with sizes around 2 μm, and areas indexed as austenite can be found with a length up to 2.5 μm and widths ranging from 0.25 to 1 μm.

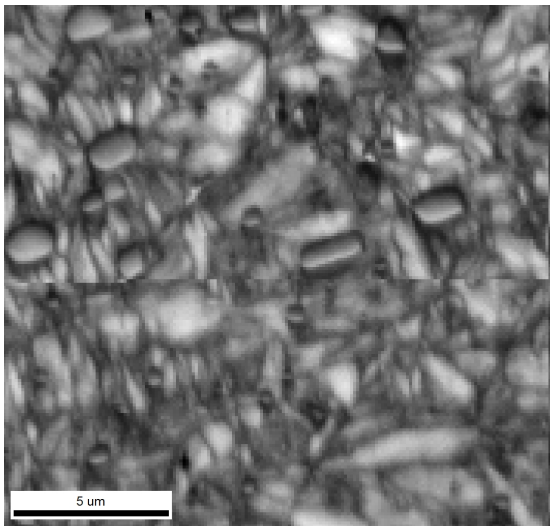

Figure 4.15: Alloy 1. Image Quality (IQ) map of the martensite sample indexed with TSL.

Figure 4.15 shows the Image Quality (IQ) map of the martensite sample indexed in TSL. If the EBSD patterns are good and easily to read the map presents these areas with a light color. Dark areas in the map represents areas with poorer patterns, and these areas are often grain boundaries. This results in a map that often shows the grains in the structure, and in this image the martensite needle-like structure can be seen.

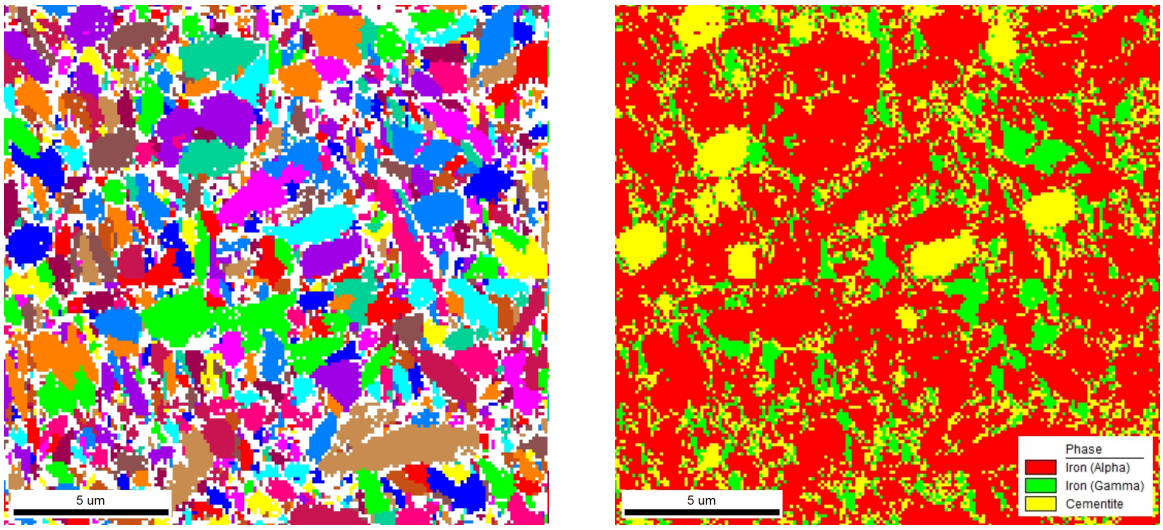

(a) Grain map of the martensite sample indexed with the α, γ and θ phase.

(b) Phase map of the martensite sample indexed with the α (red), γ (green) and θ (yellow) phase.

Figure 4.16: Alloy 1. TSL indexing of the martensite sample using the α, γ and θ phase.

Figure 4.16 shows the indexing done with the ferrite, austenite and cementite phase. A few distinct areas are indexed as cementite and they have a size of about 2 μm. In contrast to the pearlite sample, in the indexing of the martensite sample separate areas are indexed as austenite, and not only pixels at and around grain boundaries.

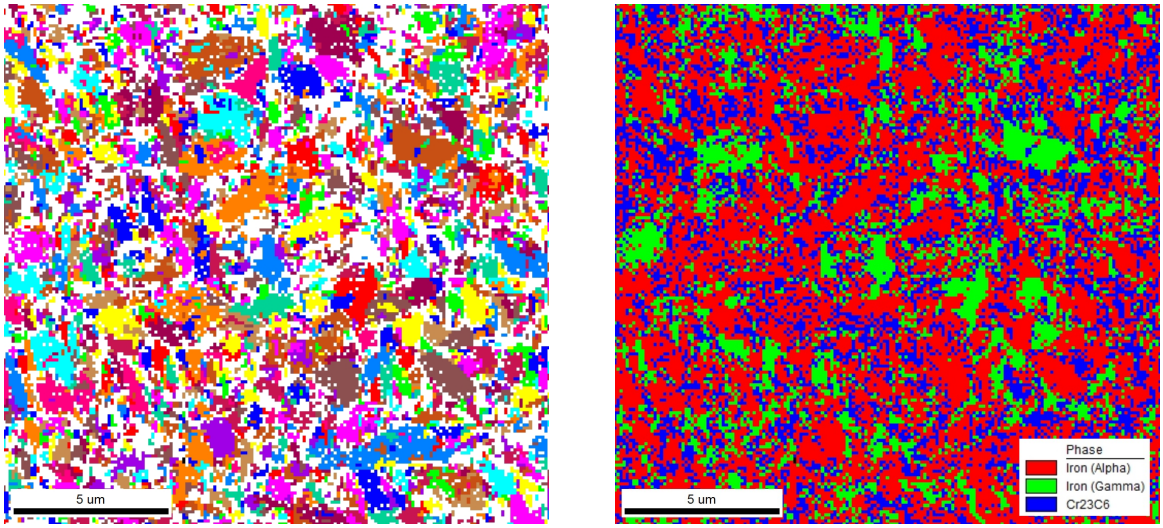

(a) Grain map of the martensite sample indexed with the α, γ and $Cr_{23}C_6$ phase.

(b) Phase map of the martensite sample indexed with the α (red), γ (green) and $Cr_{23}C_6$ (blue) phase.

Figure 4.17: Alloy 1. TSL indexing of the martensite sample using the α, γ and $Cr_{23}C_6$ phase.

Figure 4.17 shows the indexing when the chromium carbide phase is switched with the cementite phase. As for the pearlite sample, the chromium carbide indexes pixels that previously was indexed as ferrite, but this time the austenite seems to index more or less the same areas.

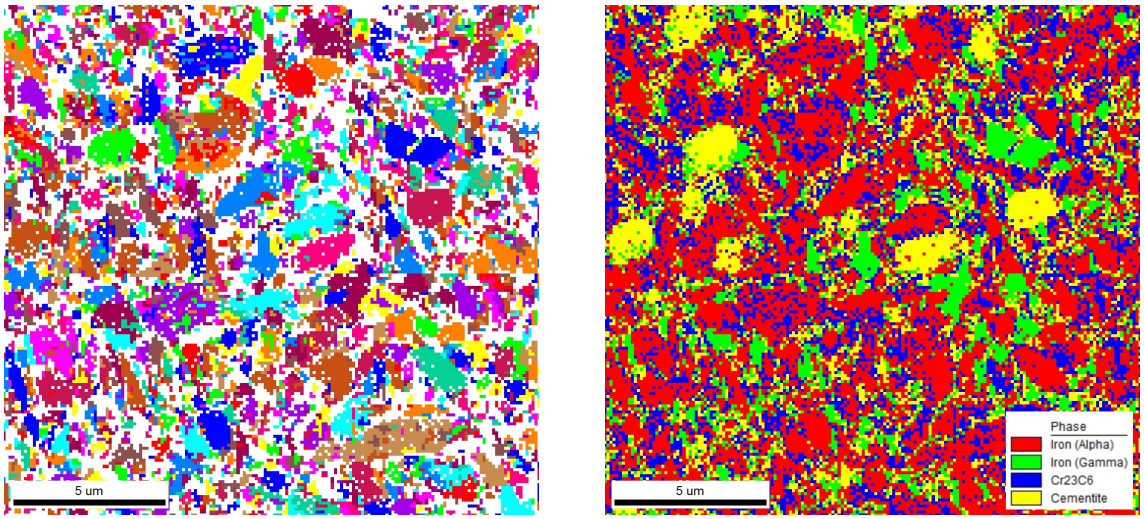

(a) Grain map of the martensite sample indexed with the α, γ, θ and $Cr_{23}C_6$ phase.

(b) Phase map of the martensite sample indexed with the α (red), γ (green), θ (yellow) and $Cr_{23}C_6$ (blue) phase.

Figure 4.18: Alloy 1. TSL indexing of the martensite sample showing grain and phase maps for the four indexing phases; α, γ, θ and $Cr_{23}C_6$.

Figure 4.18 shows the EBSD scan of the martensite sample indexed with all four phases. Again, the phase map for this indexing shows some areas that are unnoticeable in Figure 4.17b now clearly indexed as cementite.

Table 4.3: Alloy 1. Phase fractions obtained from the phase maps produced through the different rounds of indexing in TSL of the martensite phase.

Indexing phases	**Fraction α**	**Fraction γ**	**Fraction θ**	**Fraction $Cr_{23}C_6$**
α, γ, θ	0.673	0.131	0.196	-
$\alpha, \gamma, Cr_{23}C_6$	0.527	0.199	-	0.274
$\alpha, \gamma, \theta, Cr_{23}C_6$	0.462	0.138	0.176	0.225

Table 4.3 sums up the phase fractions of the different indexing rounds done of the EBSD scan of the martensite sample. The fractions are collected from the Auto Phase maps collected through TSL. Similarly as for the pearlite sample, the fraction of austenite and cementite stays somewhat constant in the indexing without the chromium carbide phase and when all phases are used in the indexing. When cementite is excluded, the fraction of austenite is increased and the ferrite fraction is reduced.

EMsoft indexing of the martensite sample

As for the pearlite sample, $Cr_{23}C_6$ was not used as an indexing phase because of the amount of noise obtained through the indexing with TSL. The martensite sample was indexed with ferrite (α), austenite (γ), cementite (θ) and martensite (α') phase, separatedly. Image Quality (IQ), Average Dot Product (ADP), Confidence Index (CI) and Orientation Similarity OS) maps of the sample for the different phases are presented below.

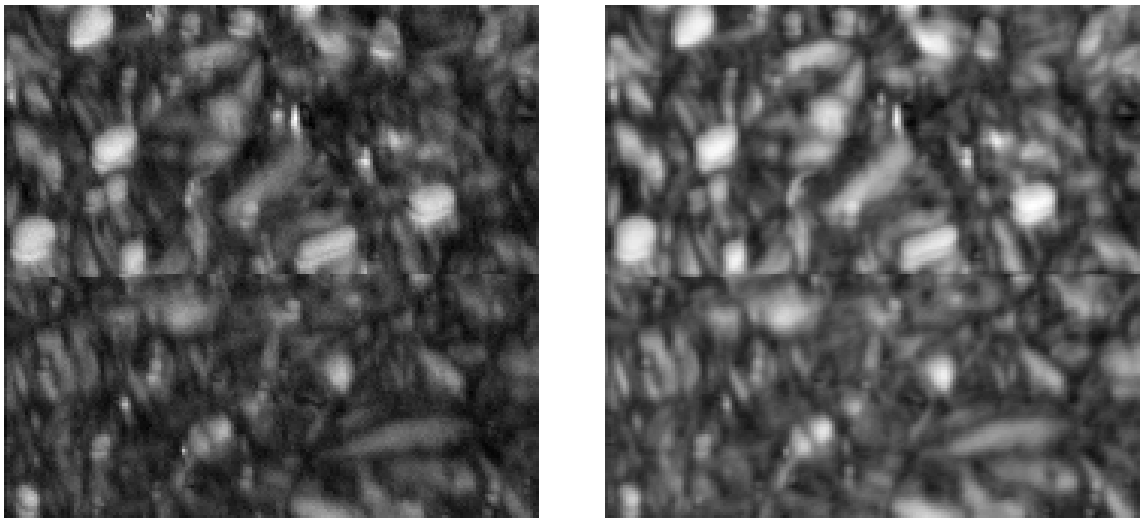

(a) Image Quality (IQ) map of the martensite sample obtained by EMsoft.

(b) Average Dot Product (ADP) map of the martensite sample, obtained through EMsoft.

Figure 4.19: Alloy 1. IQ and ADP map of the martensite sample obtained through the indexing with EMsoft.

Figure 4.19 shows the IQ and ADP maps obtained of the martensite sample from the indexing with EMsoft. Both the maps show the quality of the EBSD patterns; being light where they are good and easily indexed, and dark where they are not. The EBSD patterns of the martensite sample is clearly of poorer quality than for the pearlite sample. The images also shows the martensitic needle structure, just as the IQ map obtained through TSL does.

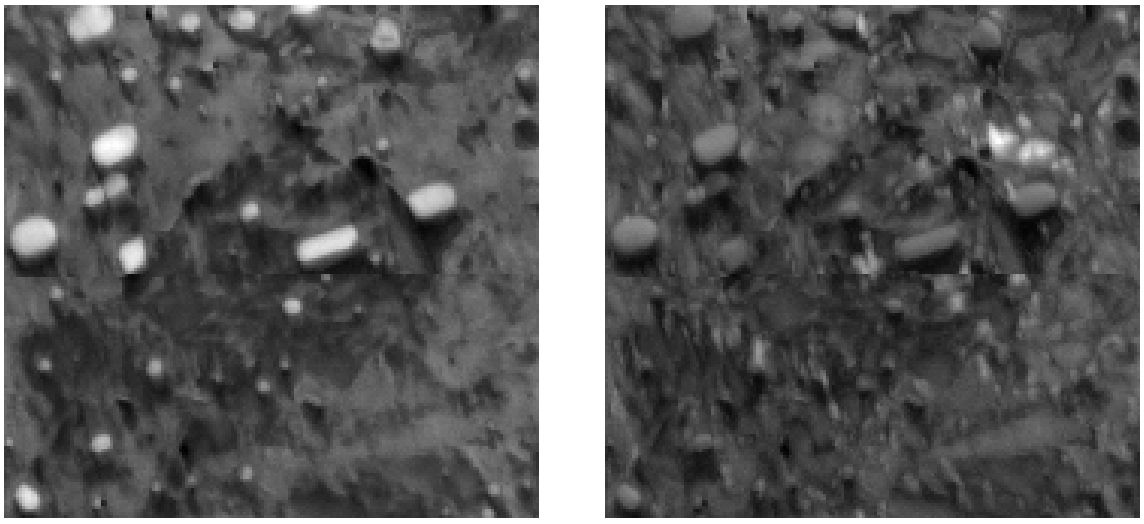

(a) Confidence Index Map of the martensite sample indexed with the cementite (θ) phase.

(b) Confidence Index Map of the martensite sample indexed with the austenite (γ) phase.

Figure 4.20: Alloy 1. EMsoft indexing of the martensite sample using the θ,γ, α and α' phase. Here the Confidence Index (CI) maps are presented for each phase.

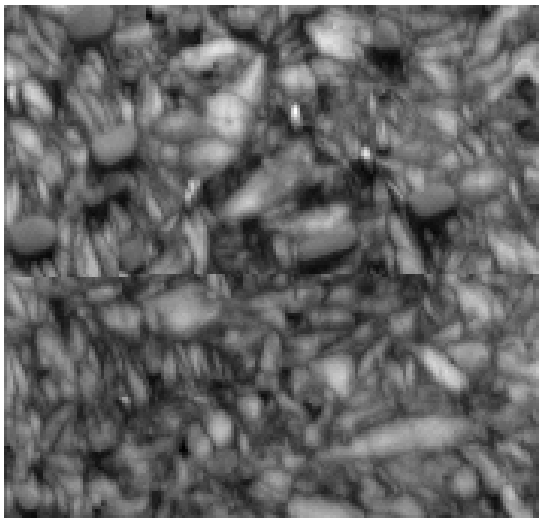

(c) Confidence Index Map of the martensite sample indexed with the ferrite (α) phase.

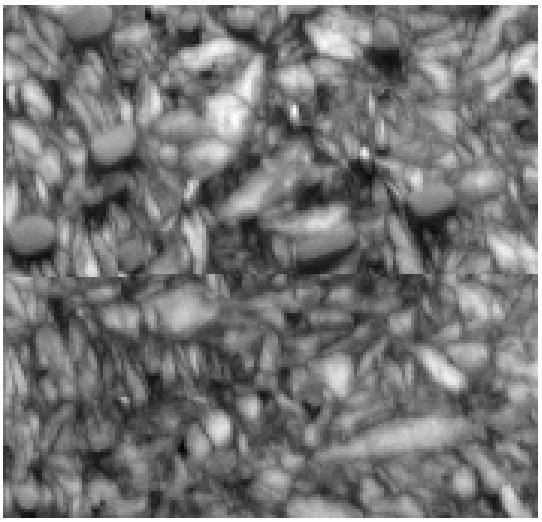

(d) Confidence Index Map of the martensite sample indexed with the martensite (α') phase.

Figure 4.20: Alloy 1. EMsoft indexing of the martensite sample using the θ,γ, α and α' phase. Here the Confidence Index (CI) maps are presented for each phase. (cont.)

Figure 4.20 shows CI maps of the martensite EBSD scan indexed with cementite, austenite, ferrite and martensite (1.3 wt%) phase. Light areas represent where the simulated patterns for the different indexing phases matched well with the experimental pattern, and therefore the different maps varies in where the light areas are. The indexing with the cementite phase matches very well with the cementite particles in Figure 4.20a, presented by the white dots across the maps. The indexing with austenite in Figure 4.20b matches overall poorly with the patterns in the EBSD scan, apart from one area in the upper right corner of the map which also is indexed as austenite in TSL. As for the pearlite sample, the indexing with ferrite and martensite in Figure 4.20c and 4.20d matches the best with the matrix.

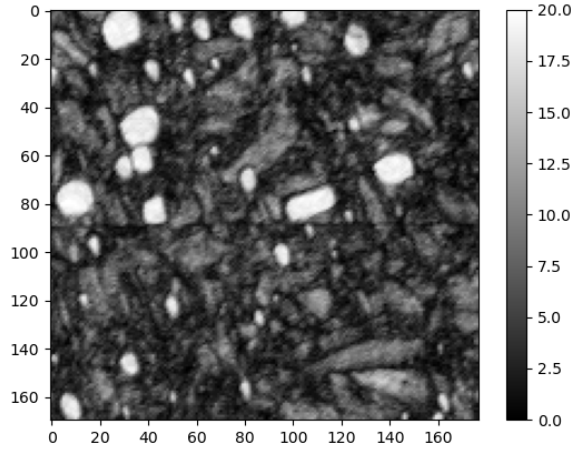

(a) Orientation Similarity Map of the martensite sample indexed with the cementite (θ) phase. The indexing has an OSM mean value of 5.86.

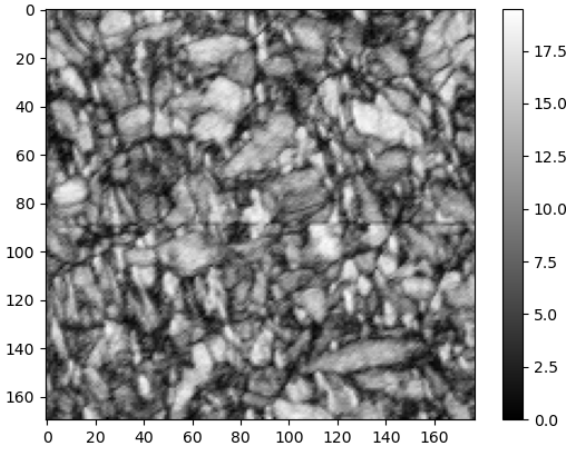

(b) Orientation Similarity Map of the martensite sample indexed with the austenite (γ) phase. The indexing has an OSM mean value of 9.28.

Figure 4.21: Alloy 1. EMsoft indexing of the martensite sample using the θ, γ, α and α' phase. Here the Orientation Similarity (OS) maps are presented for each phase.

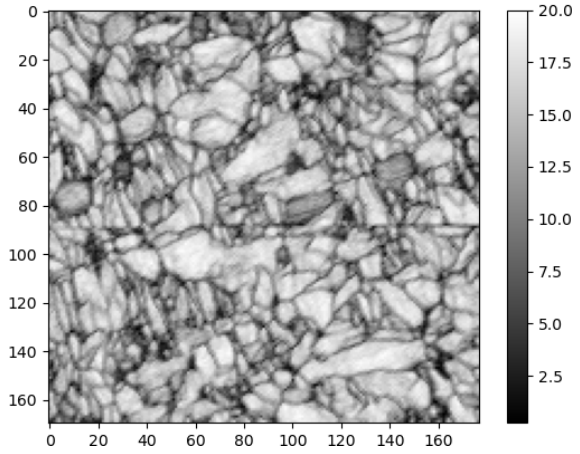

(c) Orientation Similarity Map of the martensite sample indexed with the ferrite (α) phase. The indexing has an OSM mean value of 12.77.

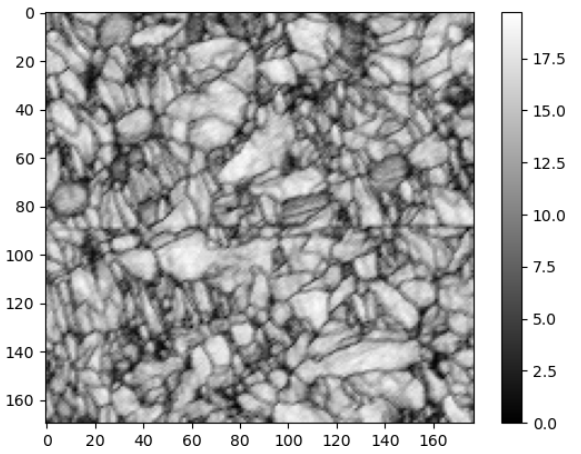

(d) Orientation Similarity Map of the martensite sample indexed with the martensite (1.3 wt%C) (α') phase. The indexing has an OSM mean value of 11.51.

Figure 4.21: Alloy 1. EMsoft indexing of the martensite sample using the θ, γ, α and α' phase. Here the Orientation Similarity (OS) maps are presented for each phase. (cont.)

Figure 4.21 shows the OS maps obtained of the martensite EBSD scan through EMsoft. These maps also present areas of good match with the indexing phase as light, but in contrast to CI maps also show the grains ans structure in great detail. Figure 4.20a and 4.21a both index the round areas appearing in contrast to the matrix as cementite.

Table 4.4: Alloy 1. The OSM max and mean values from the indexing done of the martensite sample with EMsoft.

Indexing phase	θ	γ	α	α' **(1.3 %)**	α**' (1.16%)**
OSM max value	20.0	19.50	20.00	19.75	20.00
OSM mean value	5.86	9.28	12.77	11.51	11.53

Table 4.4 shows the corresponding OSM mean and max value to the different OS maps presented in Figure 4.21. This shows that all phases have some areas with intensity at max (20.00), except austenite which has a max value of 19.50. From the OSM mean values ferrite has the highest at 12.77.

4.4.3 Bainite sample

An EBSD scan of the bainite sample is presented below. The scan was done with magnification 1000x, working distance 26.0 mm and step size 0.1 μm. The acquisition and calibration settings were as follows:

Acquisition settings
Frame rate: 60 fps
Resolution: 240x240 px
Exposure time: 16616 μs
Gain: 1

Calibration settings
Frame rate: 140 fps
Resolution: 160x160 px
Exposure time: 7092 μs
Gain: 1

Because of difficulties with the NORDIF software during the EBSD scan of this sample, the image size is smaller than the other samples which results in images of lower resolution. The scan still works for its purpose and is therefore included.

TSL indexing of the bainite sample

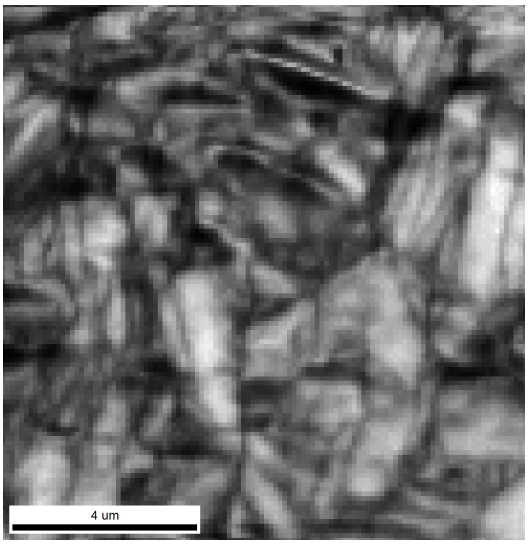

Figure 4.22: Alloy 1. Image Quality (IQ) map of the bainite sample indexed with TSL.

The IQ map in Figure 4.22 shows the quality of the EBSD scan of the bainite sample. The dark areas represents areas with poorer kikuchi patterns, while light areas represents good patterns. As for the martensite sample, this type of map can also be used to present the needle like structure of the bainite structure because the grain boundaries often stand out as dark areas in the map.

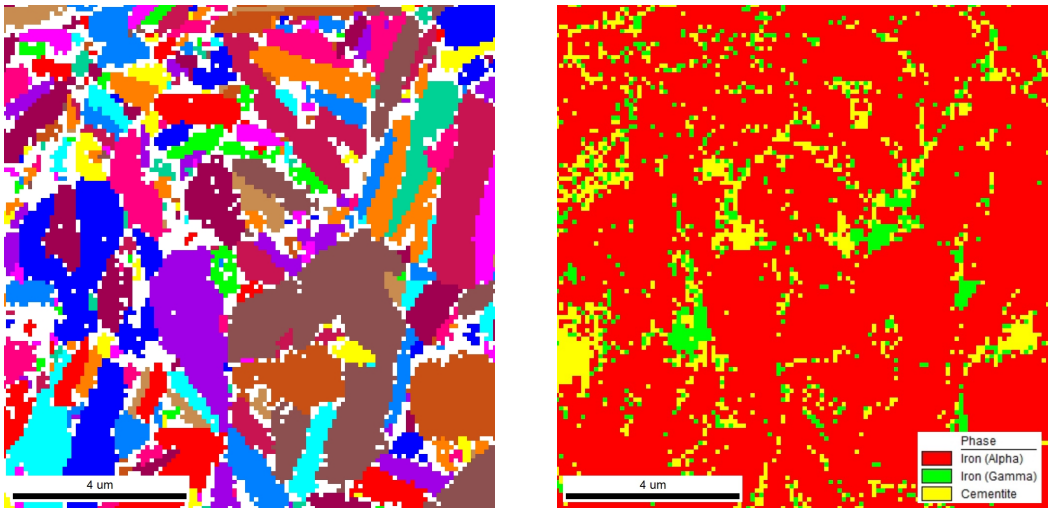

(a) Grain map of the bainite sample indexed with the α, γ and θ phase.

(b) Phase map of the bainite sample indexed with the α (red), γ (green) and θ (yellow) phase.

Figure 4.23: Alloy 1. TSL indexing of the bainite sample using the α, γ and θ phase.

Figure 4.23 shows the indexing of the bainite sample indexed with the ferrite (α), austenite (γ) and cementite (θ) phase. The sample is mainly indexed as ferrite which is the phase used for recognizing bainite structure in the EBSD analysis of this work. There is not much of white areas in the grain map which shows that most of the pixels in the scan have good enough kikuchi patterns to be indexed. In the phase map there are some areas indexed as cementite which is not just on grain boundaries or in the corresponding white areas in the grain map. There are also some areas where the indexing has found austenite. Since these areas are more than just a few pixels, it is likely to believe that the phase is present and not just the map giving a result of mis-indexing of pixels.

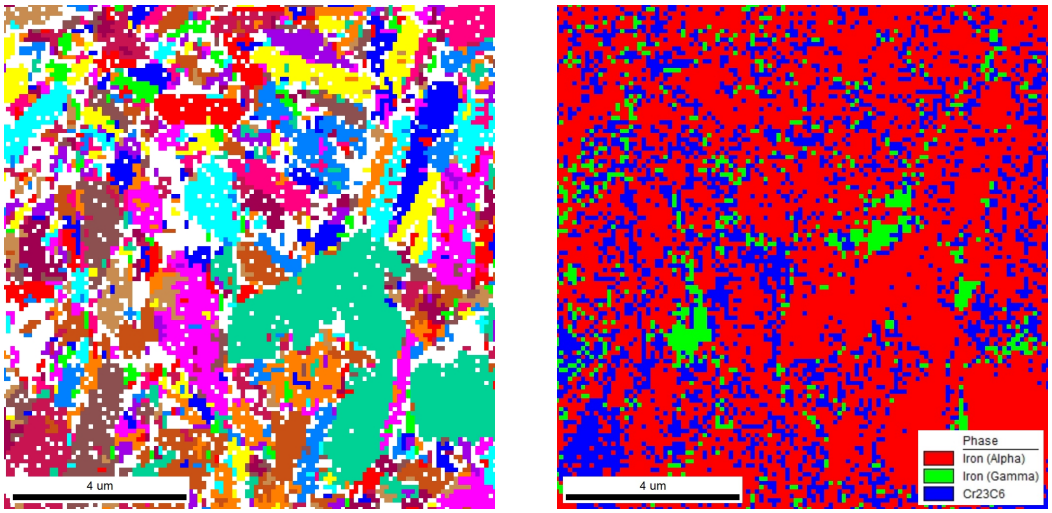

(a) Grain map of the bainite sample indexed with the α, γ and $Cr_{23}C_6$ phase.

(b) Phase map of the bainite sample indexed with the α (red), γ (green) and $Cr_{23}C_6$ (blue) phase.

Figure 4.24: Alloy 1. TSL indexing of the bainite sample using the α, γ and $Cr_{23}C_6$ phase.

Figure 4.24 shows the same scan now indexed with the α, γ and $Cr_{23}C_6$ phase. The areas of austenite indexed in Figure 4.23b are also indexed as austenite in Figure 4.24b. As for the ferrite and martensite sample, the indexing including $Cr_{23}C_6$ gives a messy result and it breaks apart the grains in the grain map in Figure 4.24a. The areas indexed as cementite in Figure 4.23b are in this indexing replaced by austenite and $Cr_{23}C_6$.

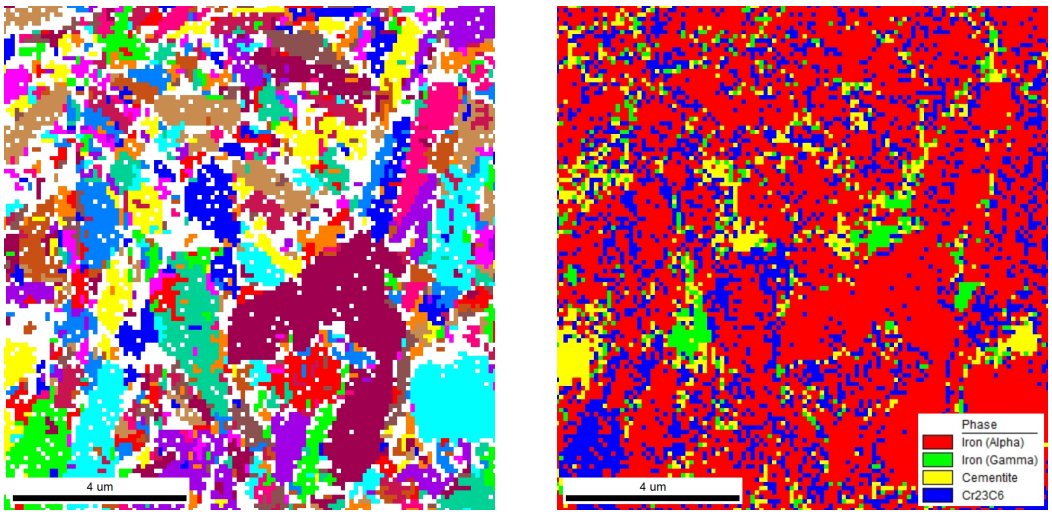

(a) Grain map of the bainite sample indexed with the α, γ, θ and $Cr_{23}C_6$ phase.

(b) Phase map of the bainite sample indexed with the α (red), γ (green), θ (yellow) and $Cr_{23}C_6$ (blue) phase.

Figure 4.25: Alloy 1. TSL indexing of the bainite sample using the α, γ, θ and $Cr_{23}C_6$ phase.

Figure 4.25 Shows the same EBSD scan now indexed with all four phases. The austenite grains are still the same as above, and cementite is also quite similar as the indexing in Figure 4.23.

Table 4.5 shows the phase fractions obtained from the phase maps of each indexing. Both austenite and cementite stays somewhat constant in all indexings, and it is therefore easily seen that the pixels indexed as $Cr_{23}C_6$ was previously indexed as ferrite.

Table 4.5: Alloy 1. Phase fractions obtained from the phase maps produced through the different rounds of indexing in TSL of the bainite sample. α = ferrite, γ = austenite, θ = cementite, $Cr_{23}C_6$ = chromium carbide.

Indexing phases	**Fraction α**	**Fraction γ**	**Fraction θ**	**Fraction $Cr_{23}C_6$**
α, γ, θ	0.841	0.060	0.099	-
$\alpha, \gamma, Cr_{23}C_6$	0.665	0.068	-	0.267
$\alpha, \gamma, \theta, Cr_{23}C_6$	0.634	0.050	0.082	0.234

EMsoft indexing of the bainite sample

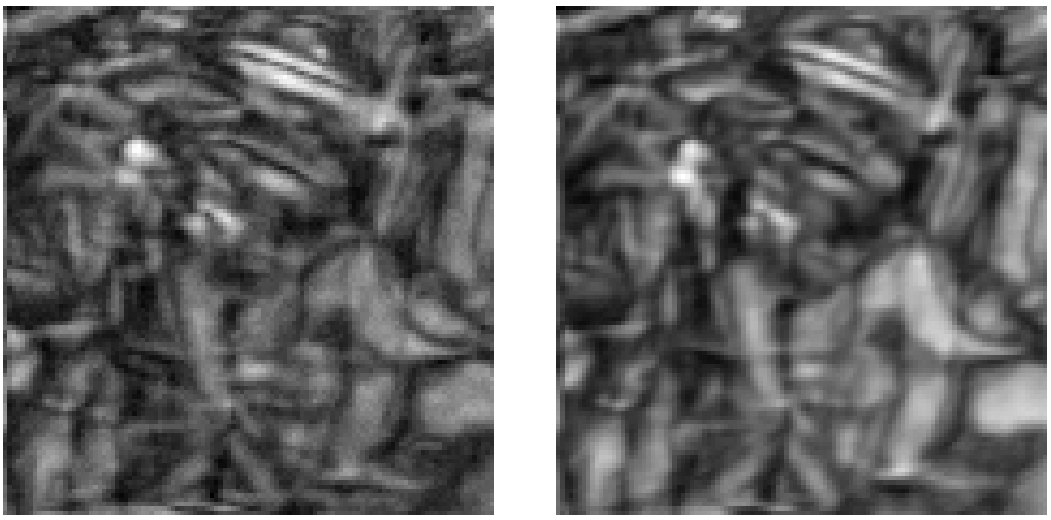

(a) Image Quality (IQ) map of the bainite sample indexed in EMsoft.

(b) Average Dot Product (ADP) map of the bainite sample indexed in EMsoft.

Figure 4.26: Alloy 1. IQ and ADP maps obtained through EMsoft describing the quality of the EBSD scan of the bainite sample.

Figure 4.26 shows Image Quality (IQ) and Average Dot Product (ADP) maps obtained by EMsoft of the bainite sample. Both of the maps describe the quality of the EBSD patterns of the scan, by being light where the patterns are good. Similar to the IQ map produced through the TSL indexing, the IQ and ADP map from EMsoft is good at presenting the needle-like structure of bainite.

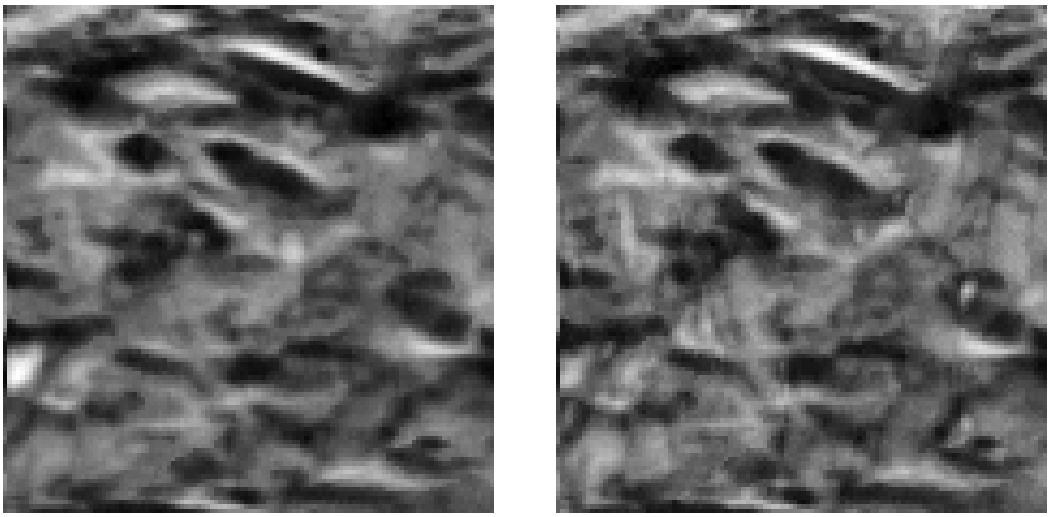

(a) Confidence Index (CI) map of the bainite sample indexed with the cementite phase in EMsoft.

(b) Confidence Index (CI) map of the bainite sample indexed with the austenite phase in EMsoft.

Figure 4.27: Alloy 1. Confidence Index (CI) maps from the indexing with the θ, γ, α and α' phase done of the bainite sample in EMsoft.

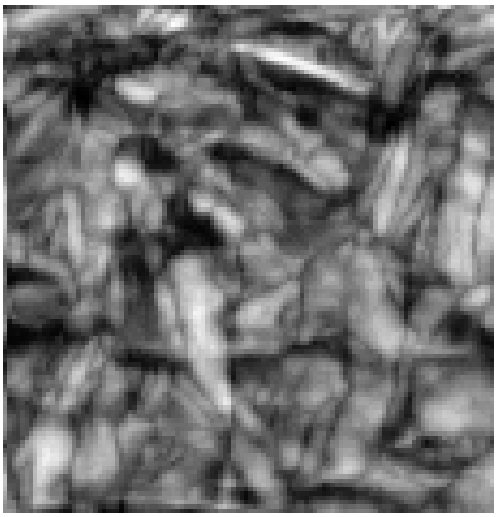

(c) Confidence Index (CI) map of the bainite sample indexed with the ferrite phase in EMsoft.

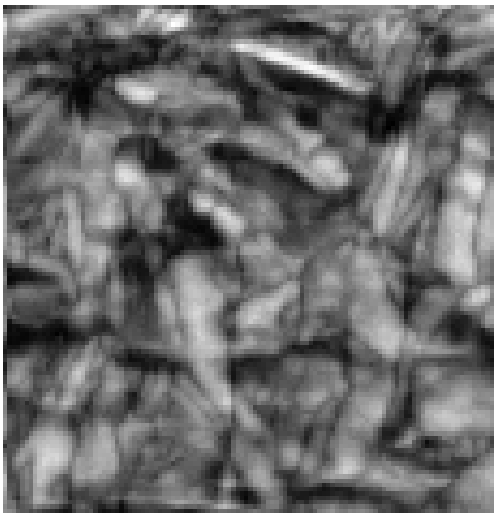

(d) Confidence Index (CI) map of the bainite sample indexed with the martensite (1.3 wt% C) phase in EMsoft.

Figure 4.27: Alloy 1. Confidence Index (CI) maps from the indexing with the θ, γ, α and α' phase done of the bainite sample in EMsoft. (cont.)

Figure 4.27 presents the Confidence Index (CI) maps of the different indexings done of the bainite sample with the θ, γ, α and α' phase through EMsoft. These maps are bright where the software finds pixels where the simulated kikuchi patterns for each indexing phase matches best with the experimental patterns of the sample. In contrast to the CI maps of the pearlite and martensite sample of this alloy, the CI maps of the bainite sample does not give a clear image of any distinct areas of cementite or austenite, but one can see that the ferrite and martensite phase, which are very similar, matches the experimental patterns best on average with being light and showing more details.

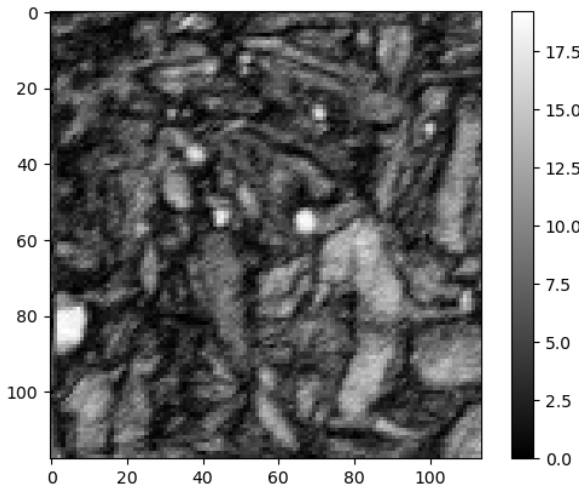

(a) Orientation Smilarity map of the bainite sample indexed with the cementite phase in EMsoft. The indexing has an OSM mean value of 5.74.

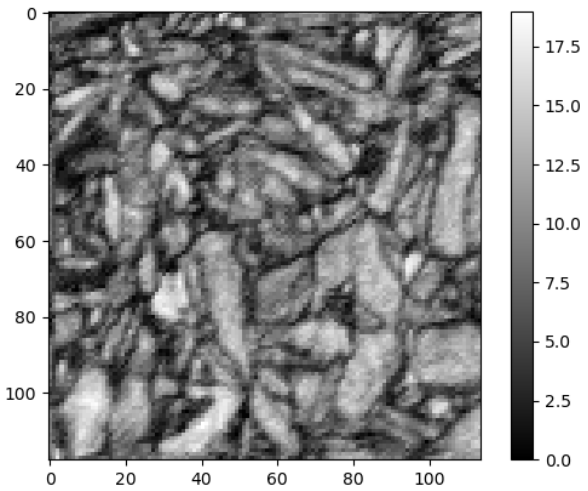

(b) Orientation Smilarity map of the bainite sample indexed with the austenite phase in EMsoft. The indexing has an OSM mean value of 8.44.

Figure 4.28: Alloy 1. Orientation Similarity (OS) maps from the indexing with the θ, γ, α and α' phase done of the bainite sample in EMsoft.

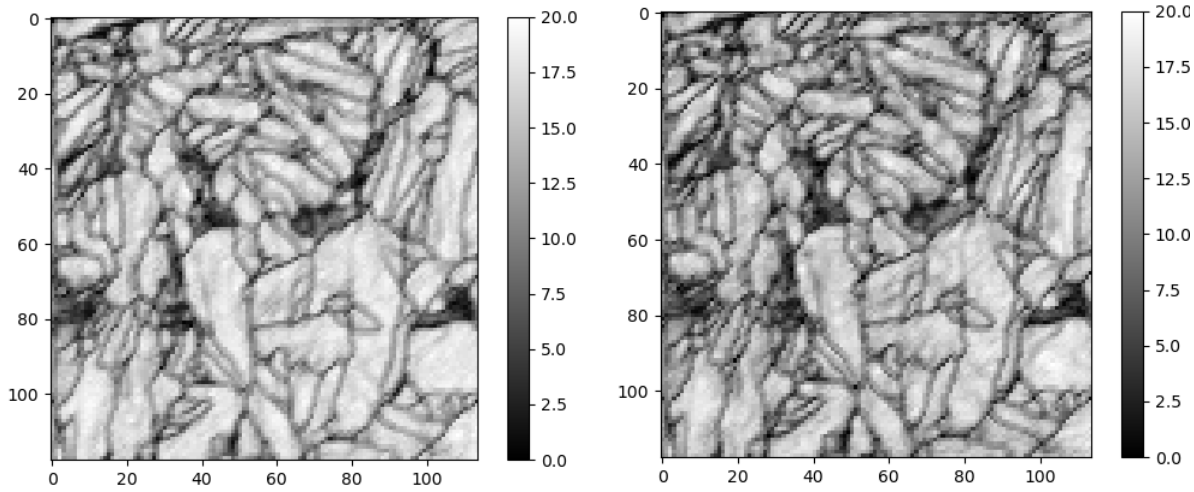

(c) Orientation Smilarity map of the bainite sample indexed with the ferrite phase in EMsoft. The indexing has an OSM mean value of 13.41.

(d) Orientation Smilarity map of the bainite sample indexed with the martensite (1.3 wt% C) phase in EMsoft. The indexing has an OSM mean value of 12.10.

Figure 4.28: Alloy 1. Orientation Similarity (OS) maps from the indexing with the θ, γ, α and α' phase done of the bainite sample in EMsoft. (cont.)

Figure 4.28 shows Orientation Similarity (OS) maps of the bainite sample indexed with the cementite, austenite, ferrite and martensite (1.3 wt% C) phase. In contrast to the TSL indexing, the indexing with EMsoft manages to deliver maps with better accuracy on details, and there is less obvious mis-indexed pixels. Figure 4.28a shows some particles indexed as cementite (light areas with size up to 1 μm), which in the TSL indexing in Figure 4.23b could be interpreted as mis-indexing because of typical poor kikuchi patterns at grain boundary. In the indexing with EMsoft, however, this is clearly cementite particles because of the delivered high intensity (light areas in OS maps).

Table 4.6: Alloy 1. The OSM max and mean values from the indexing done of the bainite sample with EMsoft.

Indexing phase	θ	γ	α	α' **(1.3 %)**	α**' (1.16%)**
OSM max value	19.25	19.00	20.00	20.00	19.25
OSM mean value	5.74	8.44	13.41	12.10	12.14

Table 4.6 shows the max and mean OSM intensity values for the different indexings done of the bainite sample through EMsoft. A fifth phase is included in this table, showing the indexing done of a martensite phase with reduced carbon content than the first used. Why this is done and the maps presenting the indexing can be found in Appendix A. The highest OSM mean intensity value was obtained for the indexing done with ferrite with a value of 13.41.

4.5 Indexing the EBSD scans of Alloy 2: 34CrNiMo6

In contrast to Alloy 1, the scans done of alloy 2 were not indexed with the chromium carbide phase in TSL, and only one indexing of each sample is presented.

4.5.1 Ferrite sample

The EBSD scan of the ferrite sample of alloy 2 was done with magnification 400x, working distance 26.0 mm and step size 0.2 μm. The acquisition and calibration settings were as follows:

Acquisition settings
Frame rate: 140 fps
Resolution: 160x160 px
Exposure time: 7092 μs
Gain: 1

Calibration settings
Frame rate: 140 fps
Resolution: 160x160 px
Exposure time: 7092 μs
Gain: 1

TSL indexing of the ferrite sample

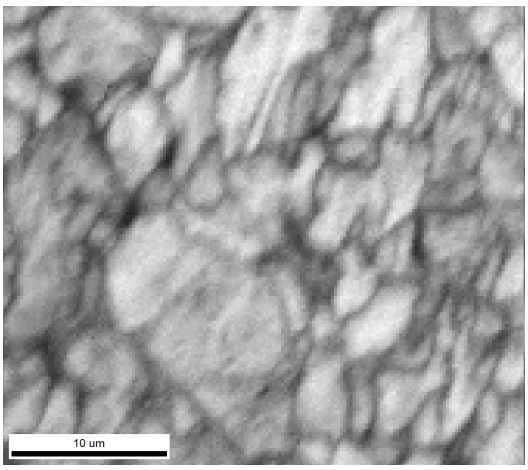

Figure 4.29: Alloy 2. Image Quality (IQ) map from the indexing of the ferrite sample, obtained through TSL.

Figure 4.29 shows the Image Quality (IQ) of the ferrite sample produced through the indexing in TSL. The map is overall light and shows an EBSD scan with good patterns. Only the grain boundaries seems to be darker than the matrix, which is to be expected.

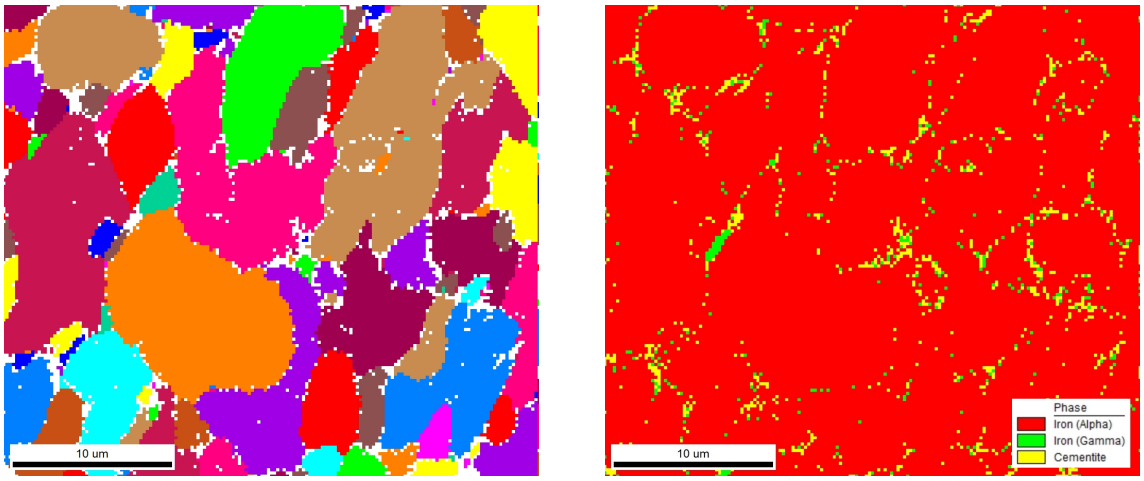

(a) Grain map of the ferrite sample indexed with the γ, α and θ phase.

(b) Phase map of the ferrite sample indexed with the γ (green), α (red) and θ (yellow) phase.

Figure 4.30: Alloy 2. Grain and phase maps of the ferrite sample indexed with the γ, α and θ phase.

Figure 4.30 shows the grain and phase maps of the ferrite sample indexed with the γ, α and θ phase. In contrast to the indexing of all the samples of Alloy 1, no distinct areas of cementite can be seen. The cementite and some of the austenite indexed areas are mainly on the grain boundaries which corresponds to the white areas in the grain map in Figure 4.30a. White areas in grain maps often show pixels with poor pattern quality, and are areas prone to mis-indexing of phases. There is a tiny needle-like grain indexed as austenite along one grain boundary middle left in the image where more than a few pixels have indexed with the same phase, which confirms that the austenite phase is present there.

The biggest ferrite grain found in the scan have a width up to 15 μm, while the smallest ferrite grains have sizes of about 2μm.

The phase fractions from the phase map are presented in Table 4.7.

Table 4.7: Alloy 2. Phase fractions obtained through the indexing in TSL of the ferrite sample. α = ferrite, γ = austenite, θ = cementite.

Indexing phases	**Fraction α**	**Fraction γ**	**Fraction θ**
α, γ, θ	0.946	0.016	0.038

EMsoft indexing of the ferrite sample

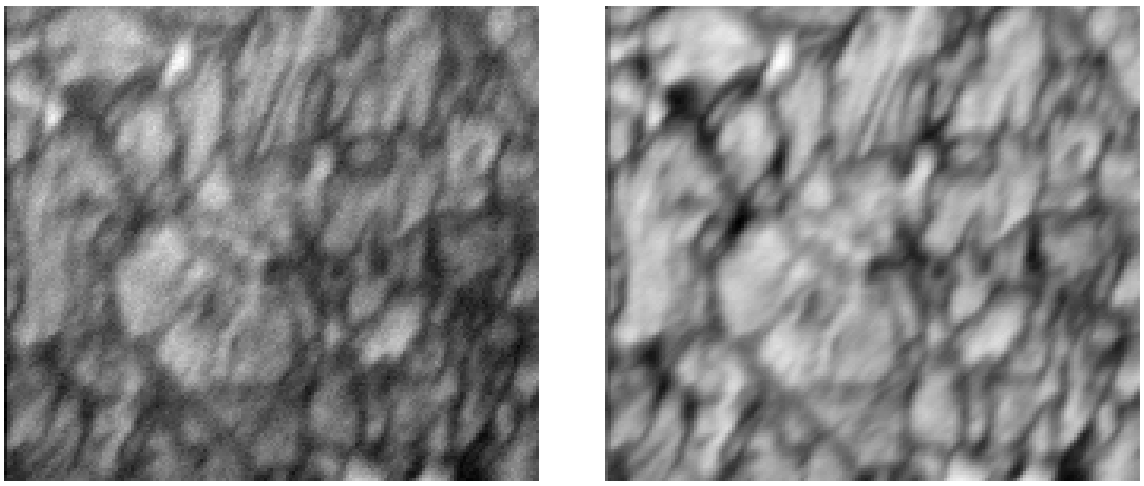

(a) Image Quality (IQ) map of the ferrite sample produced through the indexing with EMsoft.

(b) Average Dot Product (ADP) map of the ferrite sample produced through the indexing with EMsoft.

Figure 4.31: Alloy 2. IQ and ADP maps of the ferrite sample indexed with EMsoft.

Figure 4.31 shows Image Quality (IQ) and Average Dot Product (ADP) maps of the ferrite sample obtained through the indexing with EMsoft. Both of the maps are relatively bright, which represents an EBSD scan with good and easily readable kikuchi patterns.

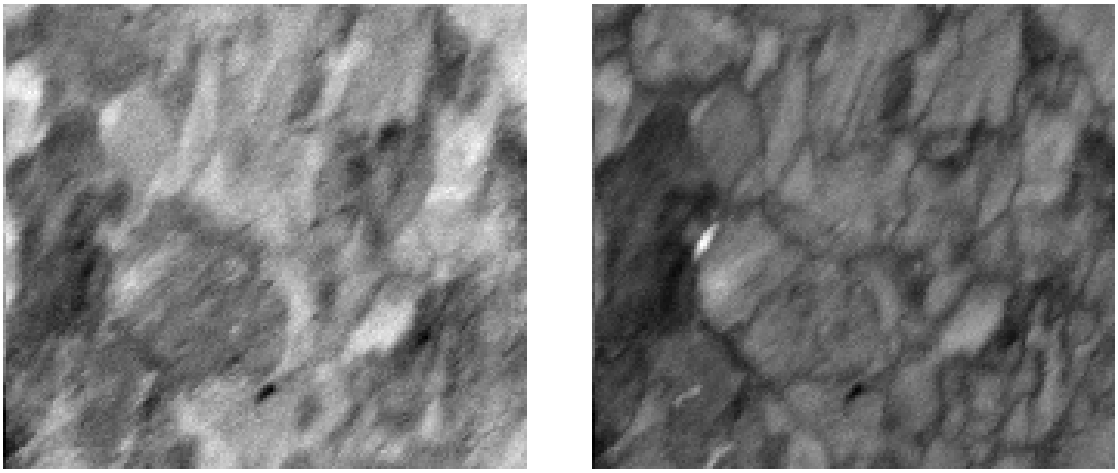

(a) Confidence Index (CI) Map of the ferrite sample indexed with the cementite (θ) phase.

(b) Confidence Index (CI) Map of the ferrite sample indexed with the austenite (γ) phase.

Figure 4.32: Alloy 2. CI maps obtained through the EMsoft indexing of the ferrite sample using the θ, γ, α and α' phase.

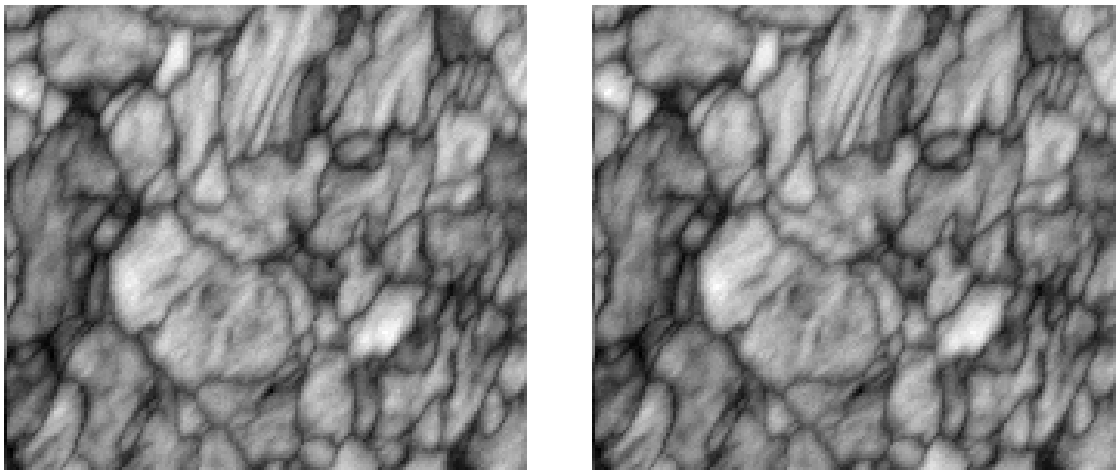

(c) Confidence Index (CI) Map of the ferrite sample indexed with the ferrite (α) phase.

(d) Confidence Index (CI) Map of the ferrite sample indexed with the martensite (α')(0.36 wt%C) phase.

Figure 4.32: Alloy 2. CI maps obtained through the EMsoft indexing of the ferrite sample using the θ, γ, α and α' phase. (cont.)

Figure 4.32 shows Confidence Index (CI) maps of the ferrite sample indexed with cementite (θ), austenite (γ), ferrite (α) and martensite (α')(0.36 wt% C) phase. The ferrite sample is mainly indexed best as ferrite or martensite, with no prominent good match with cementite or austenite. However, the tiny grain indexed as austenite in TSL in Figure 4.30b can also be found in the indexing with austenite in EMsoft in Figure 4.32b.

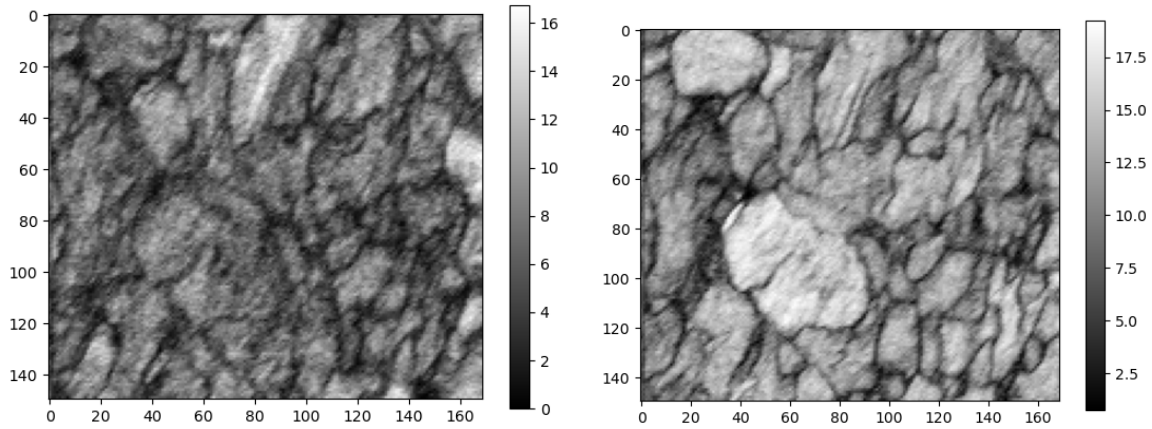

(a) Orientation Similarity (OS) Map of the ferrite sample indexed with the cementite (θ) phase. The indexing has an OSM mean value of 6.86.

(b) Orientation Similarity (OS) Map of the ferrite sample indexed with the austenite (γ) phase. The indexing has an OSM mean value of 10.78.

Figure 4.33: Alloy 2. Orientation Similarity (OS) maps obtained through the EMsoft indexing of the ferrite sample using the θ, γ, α and α'(0.36 wt%C) phase.

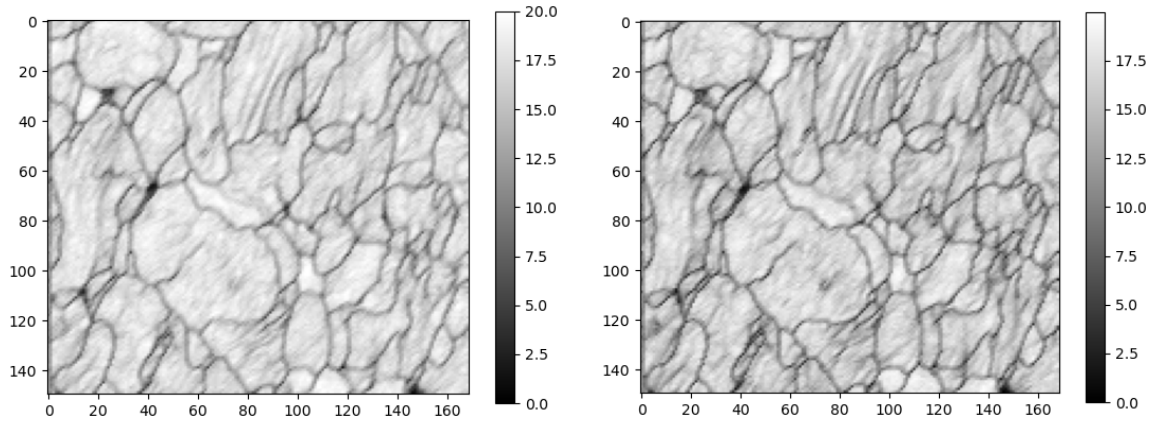

(c) Orientation Similarity (OS) Map of the ferrite sample indexed with the ferrite (α) phase. The indexing has an OSM mean value of 16.10.

(d) Orientation Similarity (OS) Map of the ferrite sample indexed with the martensite (α')(0.36 wt%C) phase. The indexing has an OSM mean value of 14.97.

Figure 4.33: Alloy 2. Orientation Similarity (OS) maps obtained through the EMsoft indexing of the ferrite sample using the θ, γ, α and α'(0.36 wt%C) phase. (cont.)

Figure 4.33 shows Orientation Similarity (OS) maps of the ferrite sample indexed with the cementite (θ), austenite (γ), ferrite (α) and martensite (α')(0.36 wt%C) phase. The maps show a relatively poor match between the experimental patterns and the simulated patterns of both cementite and austenite, but a good match with both ferrite and martensite.

Table 4.8 shows the max and mean OSM intensity values of the different indexing in EMsoft. The result shows that the overall best match of the ferrite sample scan is with the ferrite phase with a mean OSM value of 16.10. The martensite phase has a lower mean OSM value at 14.97. Both of these indexings found some areas with the maximum possible intensity value at 20.00.

Table 4.8: Alloy 2. The OSM max and mean values from the indexing done of the ferrite sample with EMsoft.

Indexing phase	θ	γ	α	α' **(0.36 %)**
OSM max value	16.75	19.25	20.00	20.00
OSM mean value	6.86	10.78	16.10	14.97

4.5.2 Martensite sample

An EBSD scan of the martensite sample was performed with magnification 1000x, working distance 26.0 mm and step size 0.1 μm. The acquisition and calibration settings were as follows:

Acquisition settings
Frame rate: 70 fps
Resolution: 240x240 px
Exposure time: 14235 μs
Gain: 1

Calibration settings
Frame rate: 140 fps
Resolution: 160x160 px
Exposure time: 7092 μs
Gain: 1

TSL indexing of the martensite sample

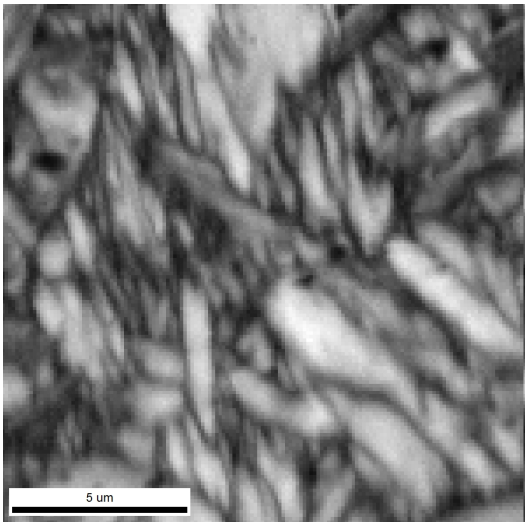

Figure 4.34: Alloy 2. Image Quality (IQ) map from the indexing of the martensite sample, obtained through TSL.

Figure 4.34 shows an IQ map of the martensite sample obtained through indexing with TSL. The IQ map describes the quality of the patterns collected by the EBSD scan. The map is dark where the patterns are poor and hard to index, and light where they are good. The map also is good to show the needle like structure of martensite, and needles with widths ranging from 0.5 to 2 μm can be seen.

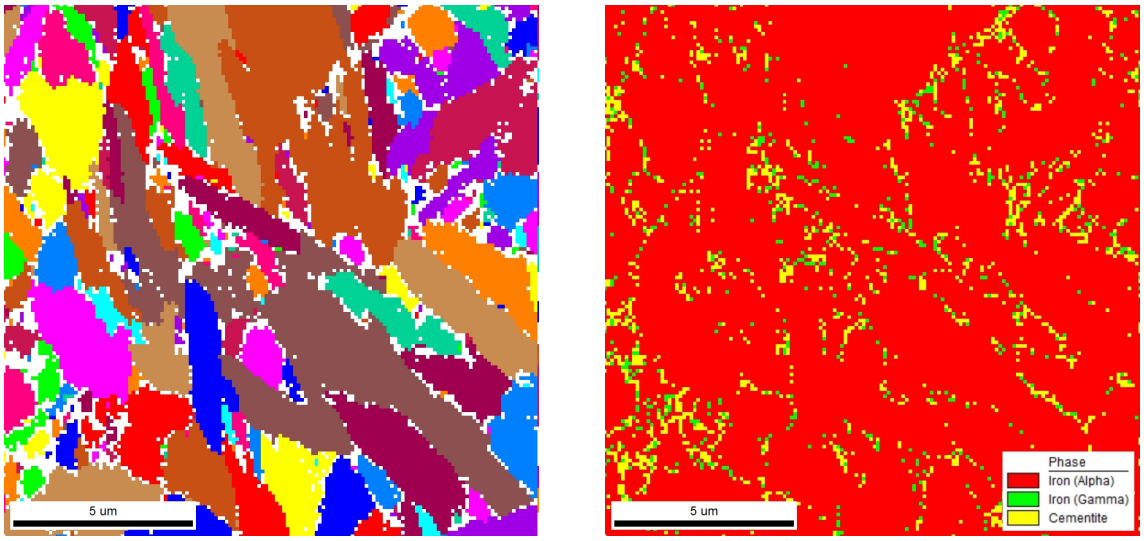

(a) Grain map of the martensite sample indexed with the γ, α and θ phase.

(b) Phase map of the martensite sample indexed with the γ (green), α (red) and θ (yellow) phase.

Figure 4.35: Alloy 2. Grain and phase maps of the martensite sample indexed with the γ, α and θ phase.

Figure 4.35 shows the grain and phase maps presenting the indexing with the austenite, ferrite and cementite phase of the martensite sample done in TSL. In this scan, all cementite indexed seen in the Auto Phase map in Figure 4.35b corresponds to the white areas in the grain map in Figure 4.35a presenting patterns that are hard to read. The indexing also shows a result of many stand-alone pixels, which often is to be considered as mis-indexing. The same could be said of the pixels indexed as austenite.

The phase fractions from the phase map is presented in Table 4.9.

Table 4.9: Alloy 2. Phase fractions obtained from the phase map through the indexing in TSL of the martensite sample. α = ferrite, γ = austenite, θ = cementite.

Indexing phases	**Fraction α**	**Fraction γ**	**Fraction θ**
α, γ, θ	0.911	0.026	0.063

EMsoft indexing of the martensite sample

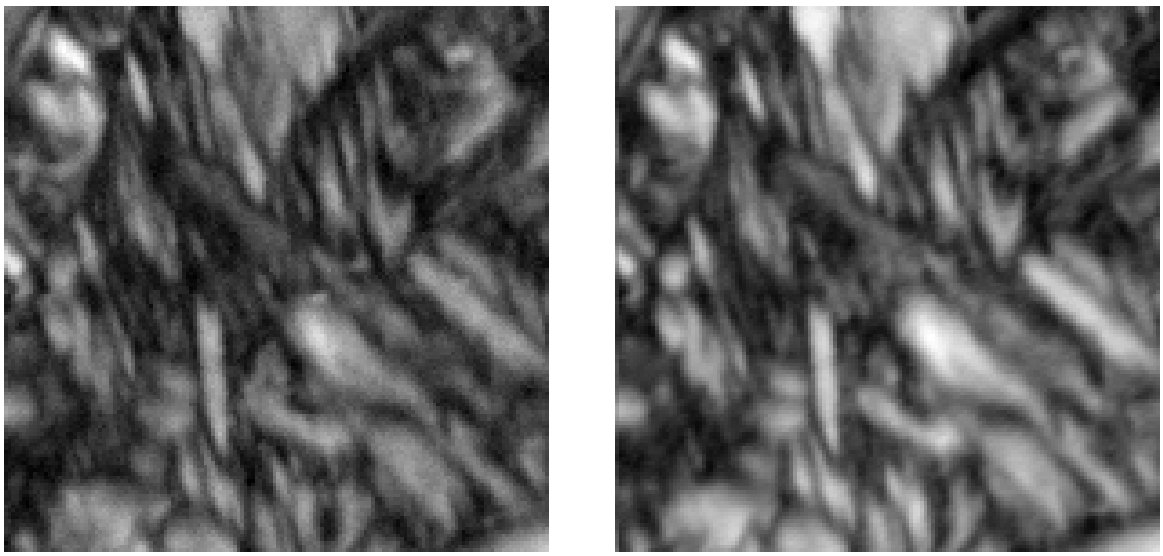

(a) Image Quality (IQ) map of the martensite sample indexed in EMsoft.

(b) Average Dot Product (ADP) map of the martensite sample indexed in EMsoft.

Figure 4.36: Alloy 2. IQ and ADP map obtained through EMsoft describing the quality of the EBSD scan of the martensite sample.

Figure 4.36 shows Image Quality (IQ) and Average Dot Product (APD) maps of the EMsoft indexing of the martensite sample. Both of the maps present quite a lot of dark areas, which means that the patterns of the EBSD scan can be hard to read and index.

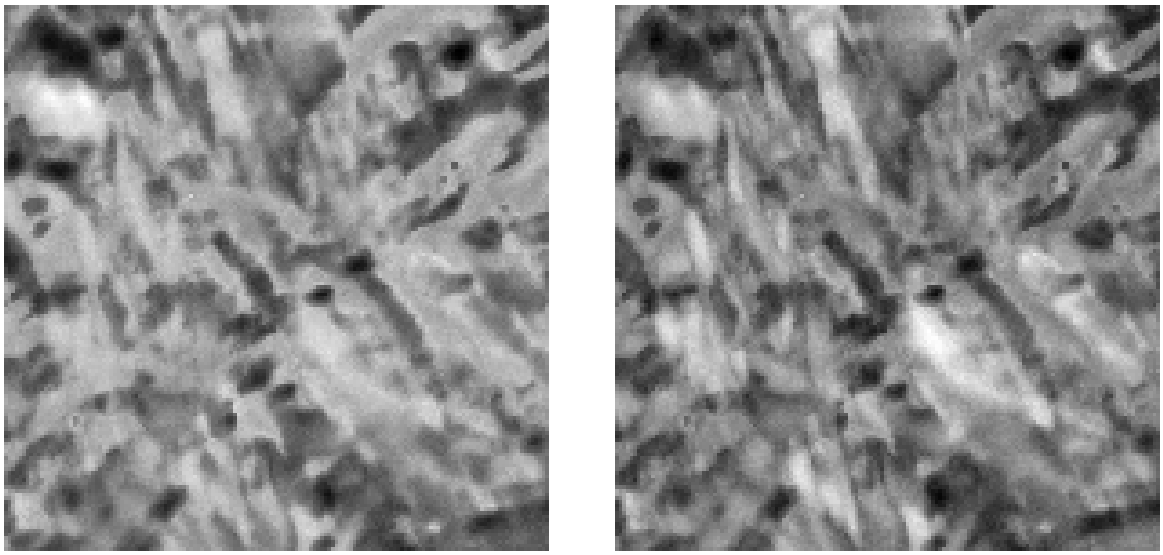

(a) Confidence Index (CI) map of the martensite sample indexed with the cementite phase in EMsoft.

(b) Confidence Index (CI) map of the martensite sample indexed with the austenite phase in EMsoft.

Figure 4.37: Alloy 2. Confidence Index (CI) maps from the indexing with the θ, γ, α and α' phase done of the martensite sample in EMsoft.

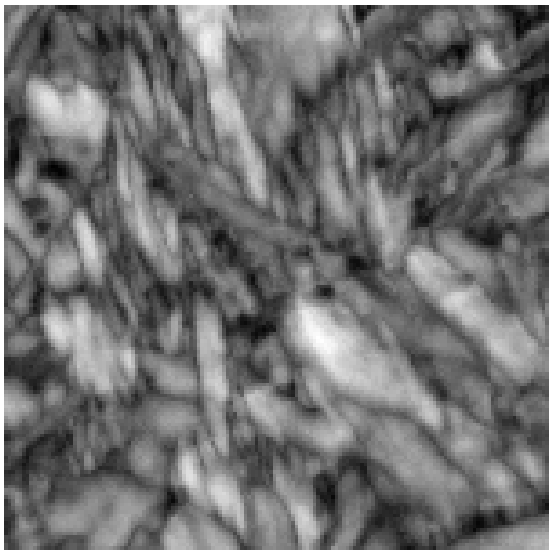

(c) Confidence Index (CI) map of the martensite sample indexed with the ferrite phase in EMsoft.

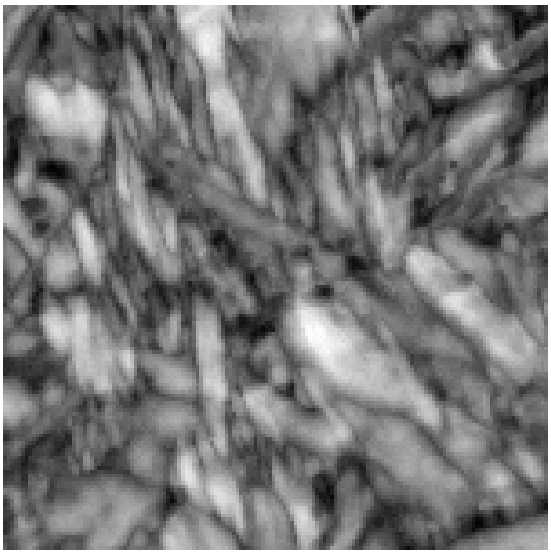

(d) Confidence Index (CI) map of the martensite sample indexed with the martensite (0.36 wt% C) phase in EMsoft.

Figure 4.37: Alloy 2. Confidence Index (CI) maps from the indexing with the θ, γ, α and α' phase done of the martensite sample in EMsoft. (cont.)

Figure 4.37 shows the Confidence Index (CI) maps of the martensite sample indexed with the θ, γ, α and α' phase, and as for the ferrite sample no distinct areas of cementite or austenite can be found. Again, maps of better detail is obtained when the scan is indexed with ferrite and martensite.

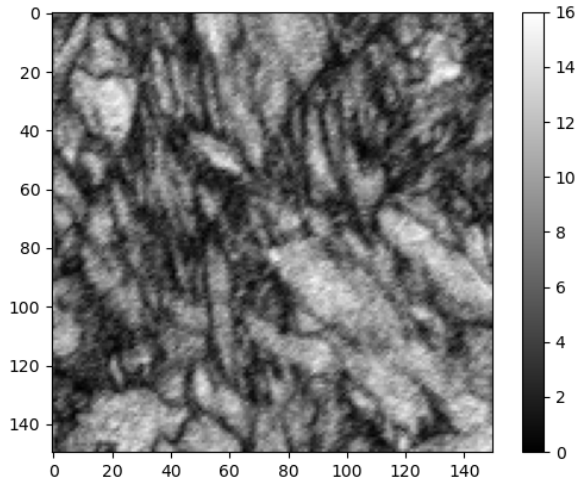

(a) Orientation Similarity map of the martensite sample indexed with the cementite phase in EMsoft. The indexing has an OSM mean value of 6.62.

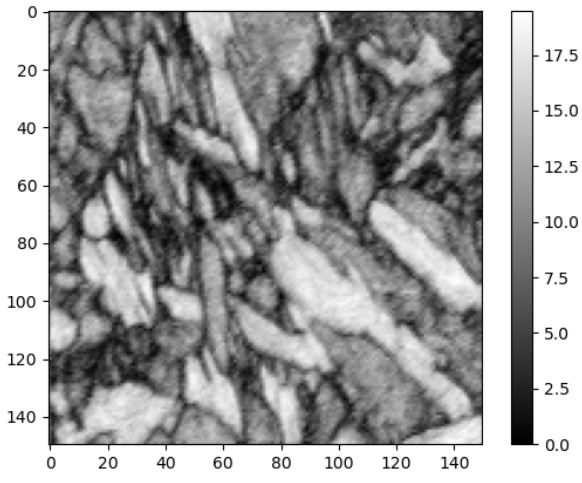

(b) Orientation Smilarity map of the martensite sample indexed with the austenite phase in EMsoft. The indexing has an OSM mean value of 9.76.

Figure 4.38: Alloy 2. Orientation Similarity (OS) maps from the indexing with the θ, γ, α and α' phase done of the martensite sample in EMsoft.

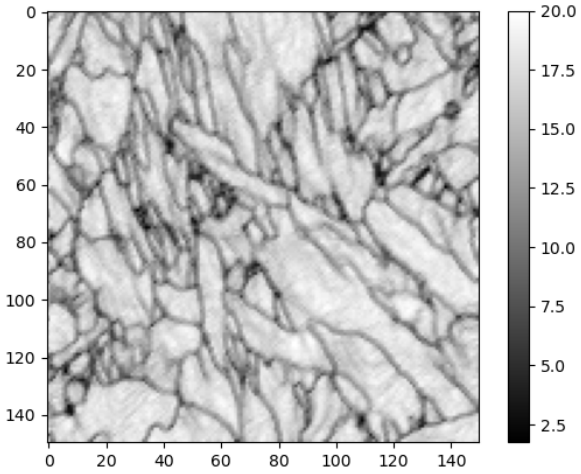

(c) Orientation Smilarity map of the martensite sample indexed with the ferrite phase in EMsoft. The indexing has an OSM mean value of 15.11.

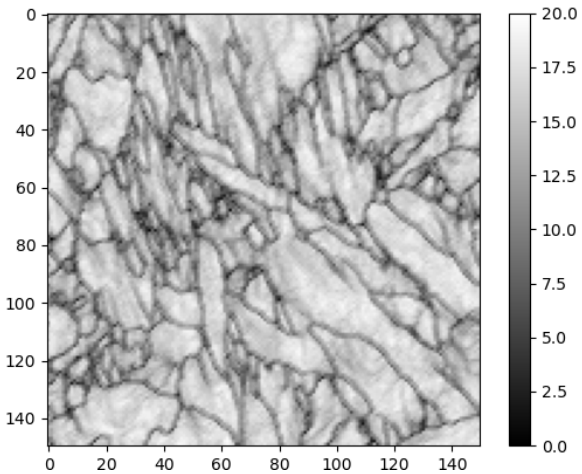

(d) Orientation Smilarity map of the martensite sample indexed with the martensite (0.36 wt% C) phase in EMsoft. The indexing has an OSM mean value of 14.02.

Figure 4.38: Alloy 2. Orientation Similarity (OS) maps from the indexing with the θ, γ, α and α' phase done of the martensite sample in EMsoft. (cont.)

Figure 4.38 shows the Orientation Similarity (OS) maps from the indexing of the martensite sample with the θ, γ, α and α' phase. They are all presented with a scalebar of the intensity color, and brighter color means that in these areas there are several adjacent pixels with the same orientation, an indication of a good match between experimental and simulated patterns. The mean and max OSM intensity values for the different indexings are presented in Table 4.10, and the highest mean value is obtained by the ferrite indexing with a value of 15.11. The indexing with the martensite phase gives a mean OSM value of 14.02.

Table 4.10: Alloy 2. The OSM max and mean values from the indexing done of the martensite sample with EMsoft.

Indexing phase	θ	γ	α	α' **(0.36 %)**
OSM max value	16.00	19.50	20.00	20.00
OSM mean value	6.62	9.76	15.11	14.02

4.5.3 Bainite sample

An EBSD scan of the bainite sample is presented below. The scan was done with magnification 1000x, working distance 26.0 mm and step size 0.1 μm. The acquisition and calibration settings were as follows:

Acquisition settings
Frame rate: 70 fps
Resolution: 240x240 px
Exposure time: 14235 μs
Gain: 4

Calibration settings
Frame rate: 140 fps
Resolution: 160x160 px
Exposure time: 7092 μs
Gain: 4

TSL indexing of the bainite sample

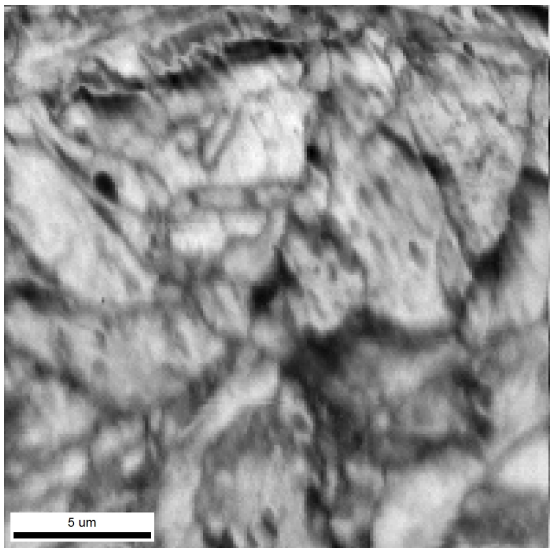

Figure 4.39: Alloy 2. Image Quality (IQ) map of the bainite sample indexed with TSL.

Figure 4.39 shows the Image Quality (IQ) map of the bainite sample indexed with TSL. The map is overall light in color, showing an EBSD scan with good kikuchi patterns.

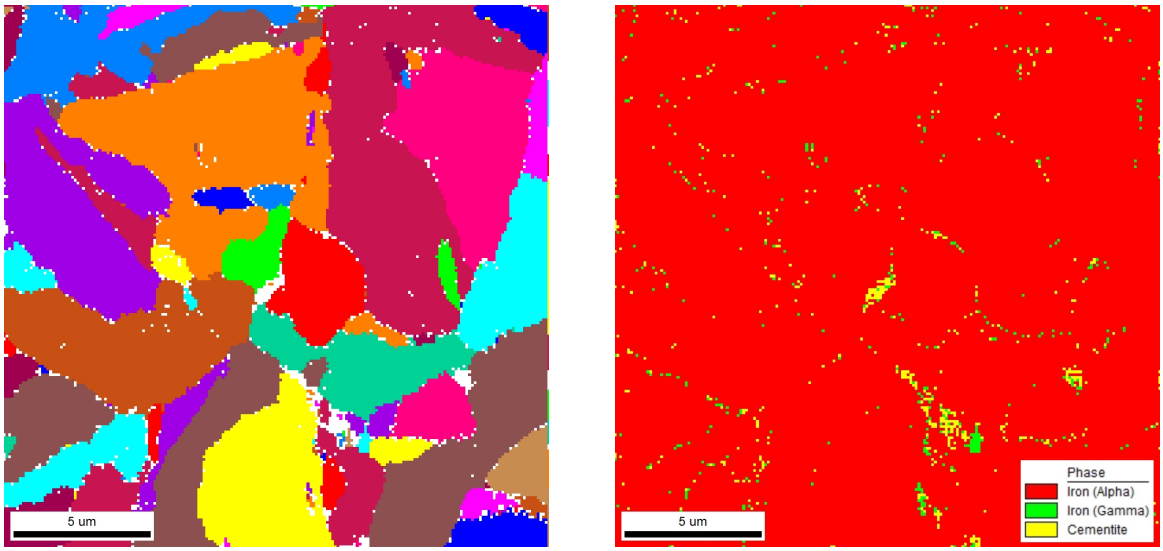

(a) Grain map of the bainite sample indexed with the α, γ and θ phase.

(b) Phase map of the bainite sample indexed with the α, γ and θ phase. Red = ferrite, green = austenite, yellow = cementite.

Figure 4.40: Alloy 2. TSL indexing of the bainite sample using the α, γ and θ phase.

The grain and phase maps in Figure 4.40 presents the indexing of the bainite sample with the α, γ and θ phase through TSL. The grain map shows little of white areas which, again, is proof of an EBSD scan with good kikuchi patterns. The bigger areas indexed as cementite in the phase map corresponds to the white areas in the grain map, and could be considered as mis-indexed pixels. A few tiny areas of austenite is indexed in the phase map (lower right), but these also corresponds to grains found in the grain map and may be considered as being correctly indexed.

The phase fractions obtained from the phase map is presented in Table 4.11.

Table 4.11: Alloy 2. Phase fractions obtained from the phase map produced through the indexing in TSL of the bainite sample. α = ferrite, γ = austenite, θ = cementite.

Indexing phases	**Fraction α**	**Fraction γ**	**Fraction θ**
α, γ, θ	0.976	0.009	0.014

EMsoft indexing of the bainite sample

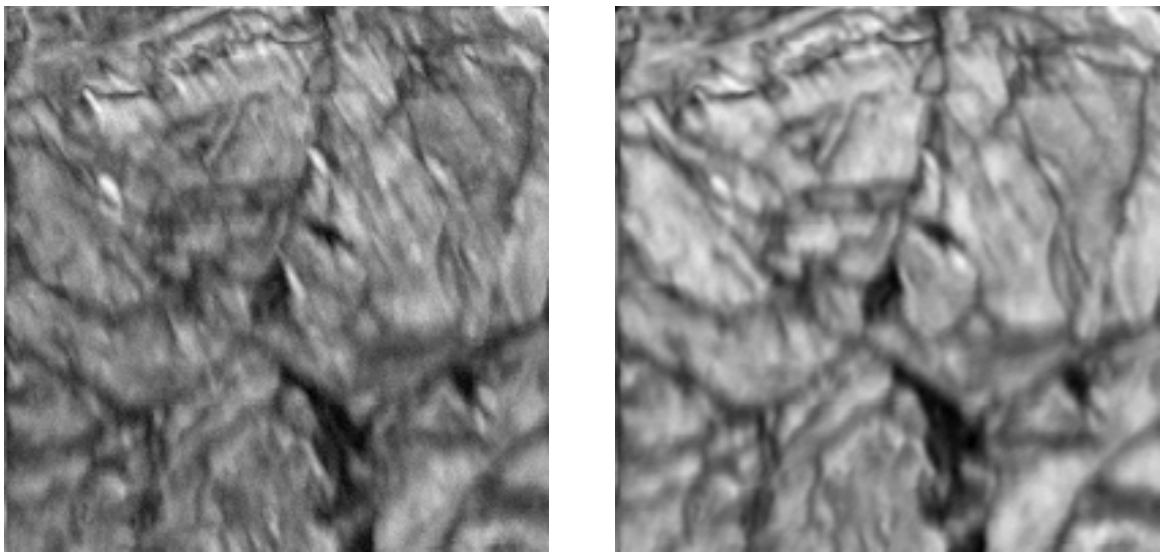

(a) Image Quality (IQ) map of the bainite sample indexed in EMsoft.

(b) Average Dot Product (ADP) map of the bainite sample indexed in EMsoft.

Figure 4.41: Alloy 2. IQ and ADP maps obtained through EMsoft describing the quality of the EBSD scan of the bainite sample.

Figure 4.41 shows the Image Quality (IQ) and Average Dot Product (ADP) map of the bainite sample obtained through the indexing with EMsoft. Since both of the maps are bright, they show that the EBSD scan has good patterns. The maps are dark at grain boundaries, and therefore also shows the structure of the sample surface.

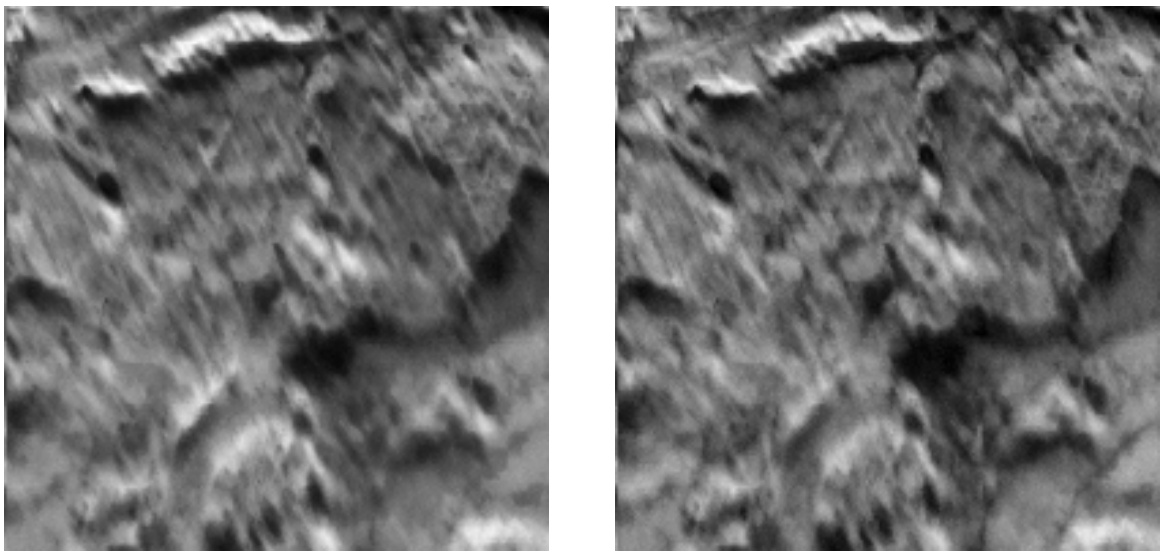

(a) Confidence Index (CI) map of the bainite sample indexed with the cementite phase in EMsoft.

(b) Confidence Index (CI) map of the bainite sample indexed with the austenite phase in EMsoft.

Figure 4.42: Alloy 2. Confidence Index (CI) maps from the indexing with the θ, γ, α and α'(0.36 wt% C) phase done of the bainite sample in EMsoft.

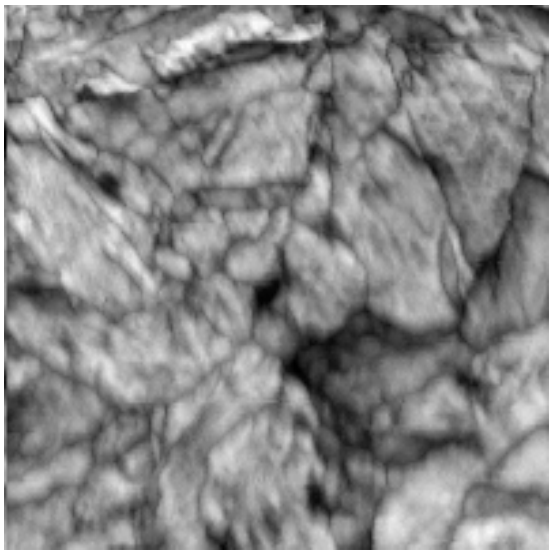

(c) Confidence Index (CI) map of the bainite sample indexed with the ferrite phase in EMsoft.

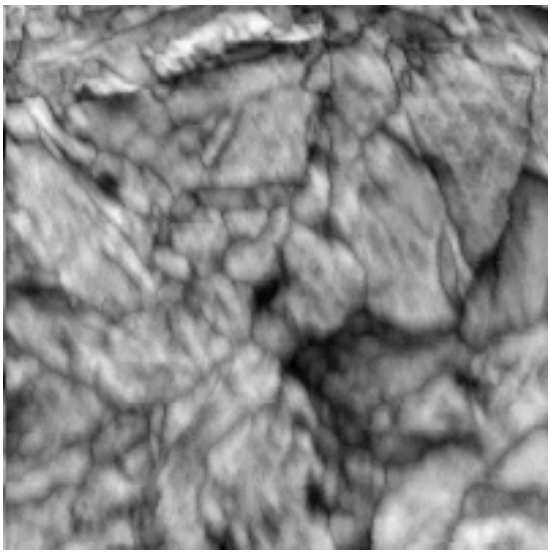

(d) Confidence Index (CI) map of the bainite sample indexed with the martensite (0.36 wt% C) phase in EMsoft.

Figure 4.42: Alloy 2. Confidence Index (CI) maps from the indexing with the θ, γ, α and α'(0.36 wt% C) phase done of the bainite sample in EMsoft. (cont.)

Figure 4.42 shows Confidence Index (CI) maps of the bainite sample indexed with the θ, γ, α and α' phase in EMsoft. As for the martensite sample, the maps produced from the cementite and austenite indexing does not find any distinct areas that match well with any of the phases, and again, the indexing with ferrite and martensite gives very similar results of a relatively good match.

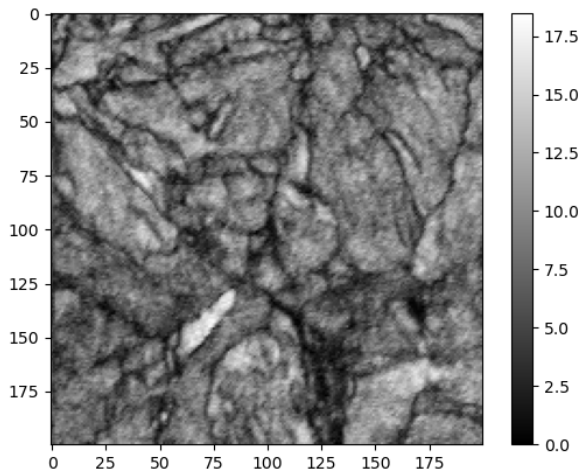

(a) Orientation Smilarity map of the bainite sample indexed with the cementite phase in EMsoft. The indexing has an OSM mean value of 7.94.

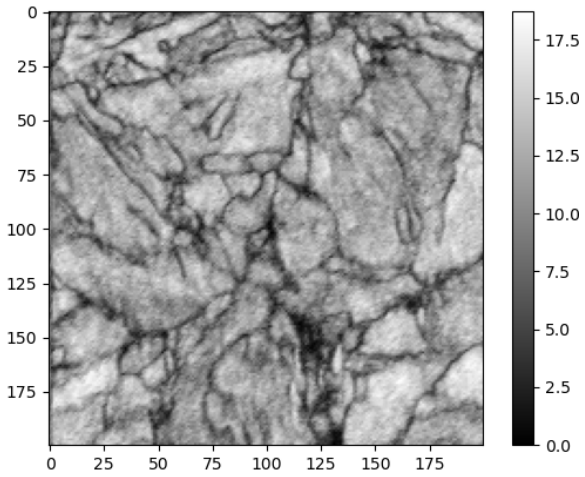

(b) Orientation Smilarity map of the bainite sample indexed with the austenite phase in EMsoft. The indexing has an OSM mean value of 11.10.

Figure 4.43: Alloy 2. Orientation Similarity (OS) maps from the indexing with the θ, γ, α and α'(0.36 wt% C) phase done of the bainite sample in EMsoft.

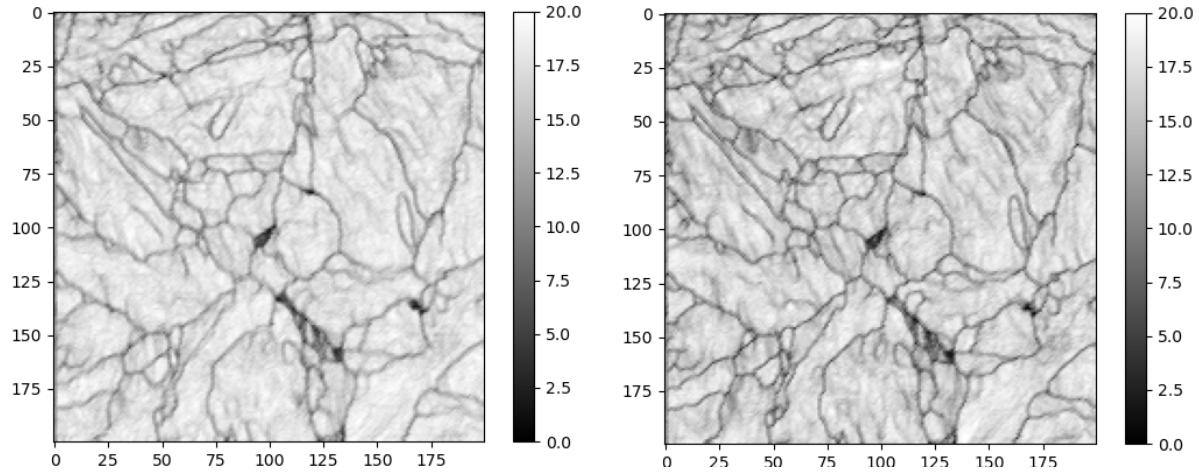

(c) Orientation Smilarity map of the bainite sample indexed with the ferrite phase in EMsoft. The indexing has an OSM mean value of 16.54.

(d) Orientation Smilarity map of the bainite sample indexed with the martensite (0.36 wt% C) phase in EMsoft. The indexing has an OSM mean value of 15.54.

Figure 4.43: Alloy 2. Orientation Similarity (OS) maps from the indexing with the θ, γ, α and α'(0.36 wt% C) phase done of the bainite sample in EMsoft. (cont.)

Figure 4.43 Shows Orientation Similarity (OS) maps of the indexing with the θ, γ, α and α'(0.36 wt% C) phase through EMsoft of the bainite sample. The colorbar is added to each map to compare the intensities in the different areas in the maps. Light areas represents pixels that have neighbors with similar grain orientation, and large light areas are a good sign of an indexing being correct. The max and mean OSM intensity values are presented in Table 4.12, and the ferrite phase indexing has the highest mean OSM value of 16.54, and the martensite phase indexing has a mean OSM value of 15.54.

Table 4.12: Alloy 2. The OSM max and mean values from the indexing done of the bainite sample with EMsoft.

Indexing phase	θ	γ	α	α' **(0.36 %)**
OSM max value	18.50	18.75	20.00	20.00
OSM mean value	7.94	11.10	16.54	15.54

4.6 TEM analysis

TEM analysis was done of the bainite and martensite sample of both alloys to show differences in the microstructures that could differentiate the two microstructures. Below are bright field images of all samples and some scanning precession electron diffraction (SPED) images and phase map of the bainite samples.

4.6.1 Alloy 1: 103Cr3/103C3

Martensite sample

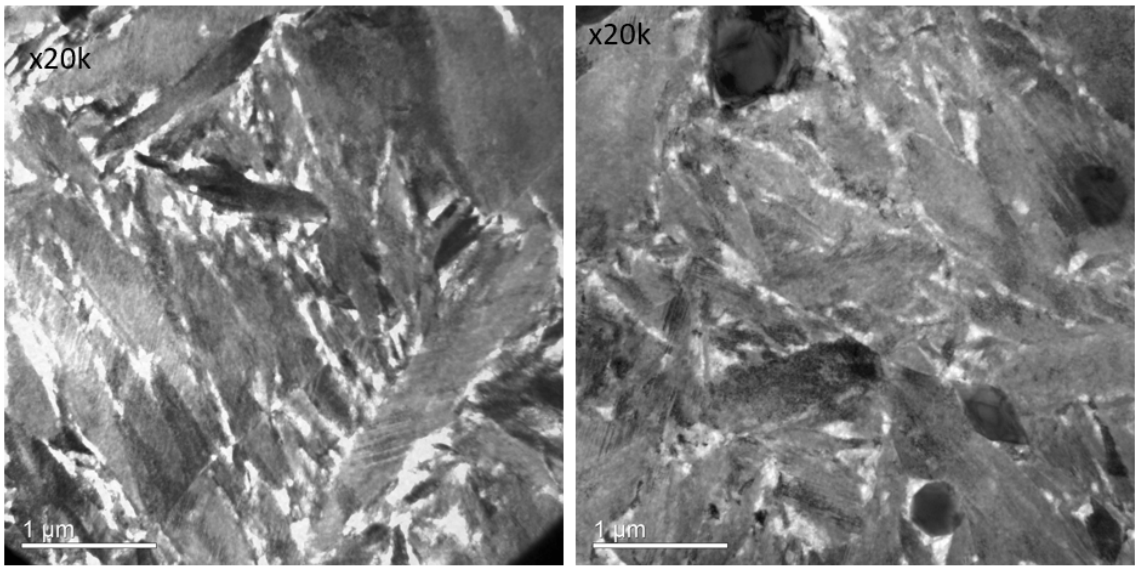

Figure 4.44: Alloy 1. Bright Field image of the martensite sample. The dark round particles in the right image are cementite.

Figure 4.44 shows Bright field images of two areas in the martensite sample. The right image shows the same round dark cementite particles as encountered in OM and SEM analysis. No carbides can be found (small dark needles) in the images, in contrast to the bainite sample of the same alloy. Bright areas indicates holes where the electron beam shines through, presumably made by uneven electropolishing of the sample.

Bainite sample

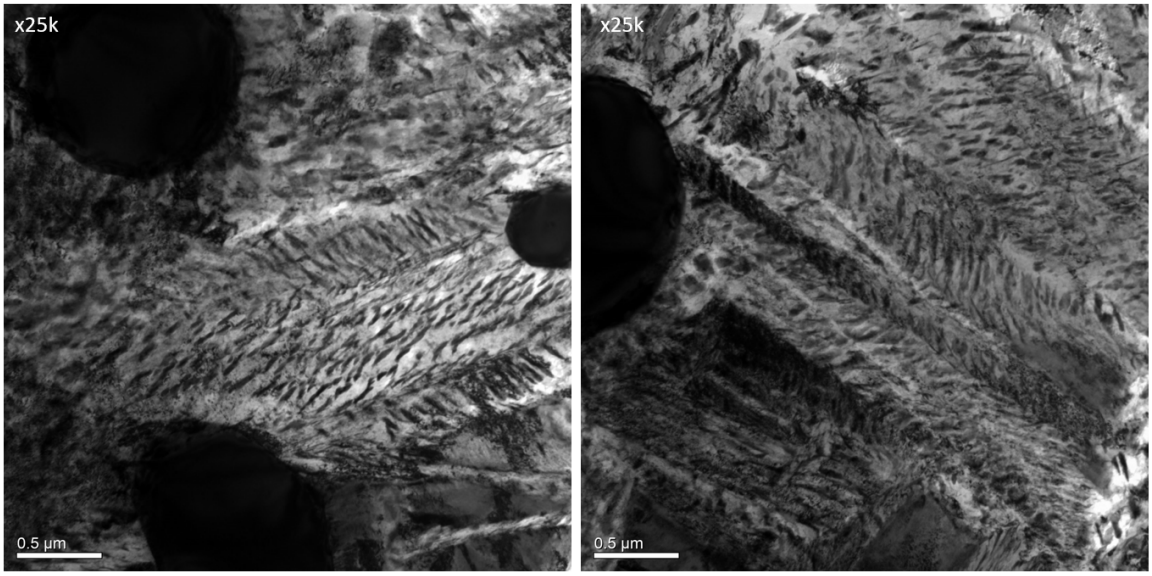

Figure 4.45: Alloy 1. Bright Field image of the bainite sample. The small black needles inside the ferrite sheaves are carbides. The larger black round particles are cementite.

Figure 4.45 shows bright field images of the bainite sample. The large black particles are presumably cementite particles with size up to about 1 μm. The tiny dark needles are carbides inside the light-colored bainitic ferrite sheaves. Different sheaves can be seen where these carbides change direction.

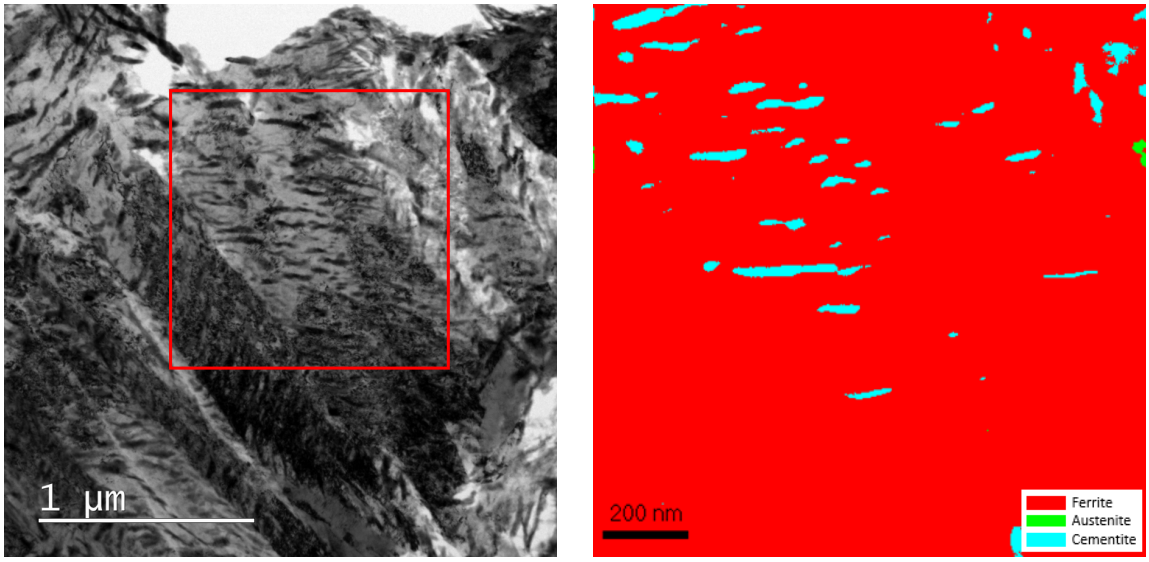

(a) Bright field image showing the area of interest for the SPED scan.

(b) Phase map obtained from the SPED scan indexed with ferrite (red), austenite (green) and cementite (blue).

Figure 4.46: Alloy 1. The images shows region of interest and phase maps from the SPED scan done of the bainite sample.

Figure 4.46 shows the result from a SPED scan done of the bainite sample. The map shows the bainitic ferrite sheaves indexed as ferrite and the tiny needle-like carbides inside the sheaves indexed as cementite. The carbide needles have a thickness of about 20 nm. Not all the black needles in figure 4.46a are indexed correctly in Figure 4.46b, but it shows their presence.

4.6.2 Alloy 2: 34CrNiMo6

Martensite sample

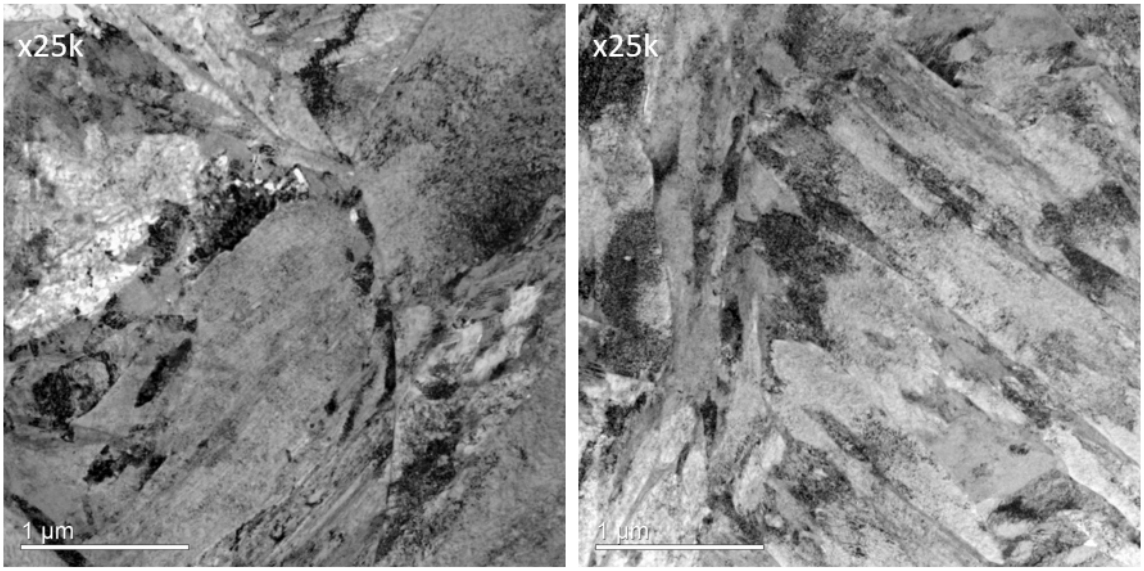

Figure 4.47: Alloy 2. Bright Field image of the martensite sample.

Figure 4.47 shows bright field images of the martensite sample. In contrast to the bainite structure, no needle-formed carbides were found in the sample.

Bainite sample

With less carbon content than Alloy 1 a lower amount of carbides in the bainite structure was expected.

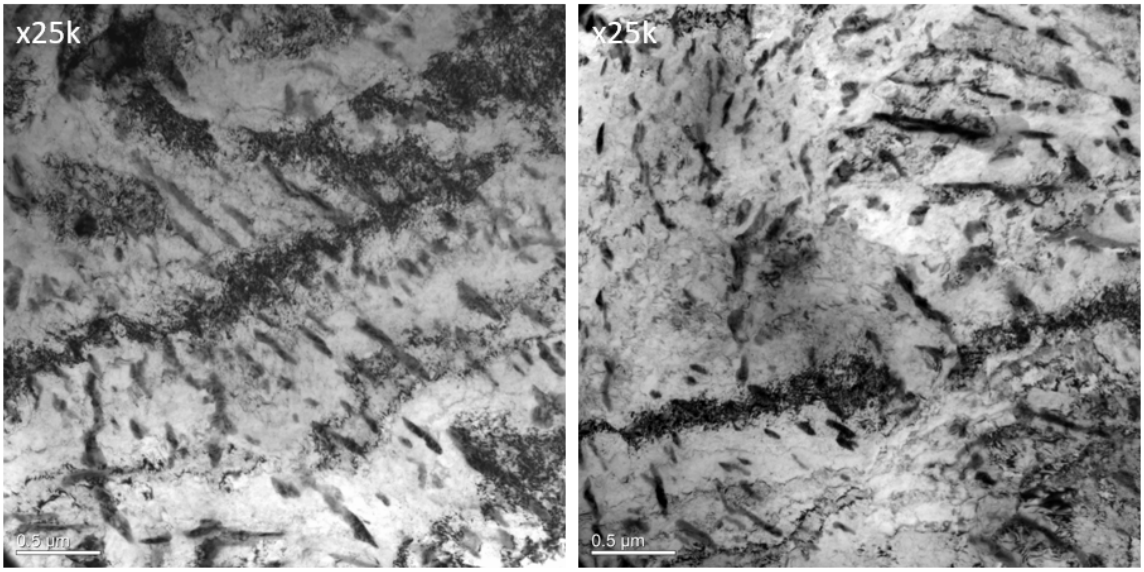

Figure 4.48: Alloy 2. Bright Field image of the bainite sample. The small black needles inside the bainitic ferrite sheaves are carbides.

Figure 4.48 shows bright field images of the bainite sample. The black needle-formed particles are carbides found inside the bainitic ferrite sheaves. They were found in a lower amount than for Alloy 1, but their presence still proved the bainitic structure.

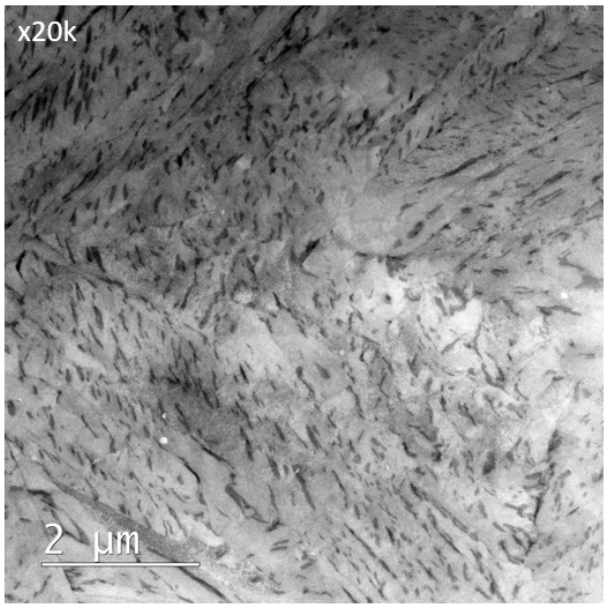

Figure 4.49: Alloy 2. SPED image of the bainite sample. The small black needles inside the ferrite sheaves are carbides.

Figure 4.49 shows a SPED image of the bainite sample, were a better overview of the carbides are presented. The carbides inside one bainitic ferrite sheaf has the same orientation. The carbides varied more in size than for Alloy 1, but seems to have thickness around 30-40 nm.

5 Discussion

5.1 Prior Microstructure

5.1.1 Alloy 1: 103Cr3/103C3

The first alloy was tested to contain about 1.3 wt% C after a chemical analysis done by SINTEF Norlab, and so the composition was confirmed to be hypereutectoid (containing 0.76-2.14 wt% C). For this type of composition, proeutectoid cementite forms along austenite grain boundaries as the temperature is lowered through the two-phase region of γ and θ/Fe_3C. In Figure 4.1 the original structure of the steel was polished and etched for an optical light microscopy (OM) analysis. Here the martensitic structure obtained a brown color while cementite remained un-etched and can be seen as the light particles in the image (Vander Voort, 2001). Continuing with the analysis in SEM, the same cementite particles could be found with a magnification larger than 1000x.

5.1.2 Alloy 2: 34CrNiMo6

The second alloy was delivered along with the chemical composition from the producer, and after an analysis of the polished and etched sample surface in OM, the structure could be confirmed to be non-martensitic because the steel was not tinted brown by the etch. With a carbon content of 0.36 wt% C, this alloy was hypoeutectoid, and in contrast to Alloy 1 this structure was assumed to be without cementite particles and have a matrix of ferritic structure. During the SEM analysis, no particles other than impurities could be found, which agrees well with the theory of no proeutectoid cementite forming during cooling of a steel alloy of hypoeutectoid composition.

5.2 Hardness testing

The hardness of the martensite sample of each alloy was tested with the purpose of comparing these results with what could be expected from the each alloy knowing the carbon content and using the graph presented in Figure 2.11 showing Vickers hardness against carbon wt%.

5.2.1 Alloy 1: 103Cr3/103C3

The hardness testing of the martensite sample gave an average vickers hardness of 994,1 HV. Figure 2.11 does not cover higher carbon content than 1.25 wt%, but the hardness for a steel alloy of 1.3 wt% C could be expected to range from 900-1100 HV. The hardness of the martensite structure in a steel alloy with carbon content above 0.8 wt% is not expected to be uniform and can not be precisely decided to have a specific value. This is because an increase in carbon content lowers the M_F temperature, and for an alloy with 1.3 wt% C the M_F is expected to be far below 20 °C tempered water used to quench the sample. Since M_S was not reached, not all

the austenite were transformed into martensite and areas of retained austenite appear throughout the martensite sample. The hardness of austenite is lower than martensite, and therefore the HV values across the sample fluctuated depending on the varying austenite amounts. The samples of this alloy also had relatively great amounts of cementite, which also holds a lower hardness than martensite, even though this phase in known to be hard and brittle. Still the hardness results prove that the matrix was of martensitic structure since no other steel phases have hardness with such high values for the given carbon content.

5.2.2 Alloy 2: 34CrNiMo6

This alloy had a carbon content of 0.36 wt% C and the hardness of the martensite sample was through Figure 2.11 expected to be around 650-700 HV. The results of the 16 indents gave a mean hardness value of 662.7 HV. In comparison to Alloy 1 where both cementite particles and areas of retained austenite were present, this sample was more or less of only martensitic structure. This resulted in a hardness value with less deviation, and the experimental value fitted well with what was expected from theory.

5.3 EDS analysis of Alloy 1

Particles of unknown structure and chemical composition could be seen across the surface of the entire sample of all of the samples of Alloy 1, and therefore an EDS scan was done of the pearlite sample. The results presented in Figure 4.7 revealed that areas with higher amounts of carbon and chromium could be found, and that the amount of iron was less in these areas than in the matrix. These areas was then assumed to be cementite, chromium carbide or a chromium rich cementite. It was reasonable to think that the appearance of carbide-forming elements as chromium could be found close to cementite particles since they use the carbon from the cementite areas to form carbides. The chemical analysis delivered from SINTEF Norlab showed the alloy to contain 0.74 wt% Cr, which is a relatively low value. During tempering of martensite formation of chromium carbides are not to be expected before the chromium amount exceeds 4 wt% (Bhadeshia and Honeycombe, 2017). Cr in known to form carbides that is more thermodynamically stable than cementite, but to do so the concentration would need to be sufficient and the steel must have reached a temperature of 500-600 °C.

The alloy with 1.3 wt%C classified to have a hypereutectoid composition, and the occurrence of cementite grains at the austenite grain boundary is not uncommon. All samples of this alloy, regardless of the heat treatment, obtained the same darker areas in the SEM analysis. It was safe to say that all information collected from the OM, EDS and EBSD analysis could be used to conclude that the areas in discussion was of cementite structure and not chromium carbide.

5.4 EBSD indexing

All samples of each alloy were prepared and polished the same way, but the EBSD scan patterns still differed in quality from sample to sample. For both the alloys the EBSD scans of the martensite sample gave the patterns of poorest quality, which could be seen by the IQ maps produced through both the TSL and EMsoft indexing presented for each EBSD scan. The transformation from austenite to martensite phase is a deformation transformation which result in the martensite structure containing more internal strain than other structures. This strain increases

with the carbon concentration in the alloy since the carbon in solid solution is placed in interstitial sites in the lattice. The internal stress caused by the deformation transformation causes kikuchi lines with less contrast and sharpness in some areas of the scan (Wilkinson and Dingley, 1991; Stojakovic, 2012).

Reduced quality of the kikuchi patterns of the EBSD scans opens up for error during the indexing, and the results from this work shows that the TSL indexing software has more problems with using the pixels of poorer pattern quality than the EMsoft software. For the indexing with TSL, the grain maps presents areas of too poor quality as white areas, which simply can be explained as pixels that did not show enough similarity to the adjacent pixels to form a grain in the map. The TSL phase map still uses every pixel in the scan and indexes them as one of the indexing phases, even though the pixel might not show any kikuchi lines at all. Since EMsoft produces a library of pattern images for each indexing phase which focus just as much on the background of the pattern as the kikuchi lines, the pixels that show some change in intensity but not a fully functional pattern can also be used in some extent during the indexing with EMsoft.

5.4.1 Alloy 1: 103Cr3/103C3

Throughout all of the samples of Alloy 1 cementite particles with size ranging from 1-4 μm could be seen, and because of that the theoretically fraction of cementite and ferrite/martensite/ bainite was calculated so they could be compared to the phase fractions obtained from the TSL indexing of the EBSD scans.

Calculated phase distribution for equilibrium phases at room temperature was obtained by using Equation 5.1 and 5.2. Martensite and bainite are not equilibrium phases and therefore the equations could not be used without expecting possible deviations between the theoretically and experimentally values. Eutectic concentration of 0.76 wt% C is used.

$$f_\alpha = \frac{C_\theta - C_0}{C_\theta - C_\alpha} = \frac{6.7 - 1.3}{6.7 - 0.76} = 0.909 = 90.9wt\% \tag{5.1}$$

$$f_\theta = \frac{C_0 - C_\alpha}{C_\theta - C_\alpha} = \frac{1.3 - 0.76}{6.7 - 0.76} = 0.091 = 9.1wt\% \tag{5.2}$$

All samples of this alloy was indexed with chromium carbide ($Cr_{23}C_6$) because the EDS scan of the pearlite sample found areas enriched with carbon and chromium. The indexing with TSL however gave messy results with grains being broken up in the map because of every other pixel being indexed as ferrite or chromium carbide. As mentioned, appearance of Cr in these areas could not be excluded completely, but with the chromium amount in the alloy being relatively low the conclusion fell on these areas consisting mainly of cementite. The maps from the two indexings where chromium carbide was included could not be used when studying the phase fractions of ferrite obtained from the phase maps, but the cementite values for all rounds of indexing could be proven to show more or less the same values, both with or without the chromium carbide phase included in the indexing. It also revealed that the austenite fractions for all indexings showed similar values as long as cementite was included. Even if the maps gave a messy result as long as chromium carbide was included, the phase fractions could be compared to show values for both austenite and cementite without too much deviation.

TSL indexing of the pearlite sample

The phase fraction of ferrite obtained through TSL for the pearlite sample indexed with ferrite, austenite and cementite matches well with the theoretical expected value of ferrite. Here the experimental fraction of ferrite was $f_{\alpha,e} = 0.918$ and the theoretical value was calculated to be $f_{\alpha,t} = 0.909$. The fraction of austenite was almost neglectable with only a value of $f_{\gamma,e} = 0.002$, and the experimental fraction of cementite at $f_{\theta,e} = 0.080$ was not far off the theoretical calculated value of $f_{\theta,t} = 0.091$. The maps of this indexing showed little possible mis-indexed pixels, and the fraction of cementite was mainly collected from the particles. It is reasonable to think that the cementite also indexed along the grain boundaries of this scan makes sense since cementite is known to precipitate at former austenite grain boundaries during cooling for a hypereutectoid composition, but by comparing the phase map to the grain map, these areas corresponded to white pixels in the grain map which represent pixels of poor kikuchi patterns. For the few pixels indexed as austenite in this scan, only mis-indexing was the reasonable conclusion. This was because most of these austenite indexings were for stand-alone pixels.

Table 5.1: Phase fractions obtained through the different rounds of indexing in TSL of the pearlite sample. α = ferrite, γ = austenite, θ = cementite, $Cr_{23}C_6$ = chromium carbide.

Pearlite sample - TSL indexing				
Indexing phases	**Fraction α**	**Fraction γ**	**Fraction θ**	**Fraction $Cr_{23}C_6$**
α, γ, θ	0.918	0.002	0.080	-
α, γ, $Cr_{23}C_6$	0.479	0.023	-	0.498
α, γ, θ, $Cr_{23}C_6$	0.453	0.002	0.077	0.468

Table 5.1 shows the phase fractions of all indexings done of the pearlite scan. As mentioned in the beginning of the section, the fractions of chromium carbide greatly reduces the fractions of ferrite indexed, but for the first and third indexing in Table 5.1 fractions of both austenite and cementite are more or less unchanged. Comparing the different indexings rounds like this proved the first indexing to be genuine and trustworthy.

TSL indexing of the martensite sample

As mentioned before, the martensite EBSD scan obtained poorer patterns than the pearlite sample, and from the maps obtained through TSL there is more pixels with kikuchi lines not good enough for indexing that end up being mis-indexed in the phase map. In contrast to the pearlite sample, in the indexing with ferrite, austenite and cementite *areas* of austenite was indexed and not only stand-alone pixels. These areas could be found in the grain maps as whole grains with other adjacent pixels showing the same orientation. This was a confirmation of the austenite phase being indexed correctly. Because this alloy had carbon content as high as 1.3 %, the M_F temperature was assumed to be way lower than the temperature of the water used for the quenching of the steel (about 20°C). Because the M_F was not reached by the quenching, retained austenite throughout the sample was to be expected.

The EBSD scan of the martensite sample was done with magnification 1000x while pearlite was done with 400x, and still the grains of the martensite structure were relative small in the scan. Small grains means more grain boundary, and in most grain maps the grain boundary is typical areas where patterns merge together and the resulting pattern is difficult to index. This combined with the effect the internal strain had on the patterns of the martensite structure, the grain and phase maps showed a more messy result than the pearlite sample.

Table 5.2: Phase fractions obtained through the different rounds of indexing in TSL of the martensite sample. α = ferrite, γ = austenite, θ = cementite, $Cr_{23}C_6$ = chromium carbide.

Martensite sample - TSL indexing				
Indexing phases	**Fraction α**	**Fraction γ**	**Fraction θ**	**Fraction $Cr_{23}C_6$**
α, γ, θ	0.673	0.131	0.196	-
α, γ, $Cr_{23}C_6$	0.527	0.199	-	0.274
α, γ, θ, $Cr_{23}C_6$	0.462	0.138	0.176	0.225

Combining what we know of low M_F temperature and reduced quality of the kikuchi patterns from the EBSD scan, the relatively big deviations between the experimental phase fractions $f_{\alpha,e} = 0.673$ and $f_{\theta,e} = 0.196$ and the theoretical values of $f_{\alpha,t} = 0.909$ and $f_{\theta,t} = 0.091$ could be explained to some extent. Of course, because of the reduced pattern quality, the amount of mis-indexed pixels was increased (stand-alone pixels indexed as austenite or cementite in the ferrite matrix), which resulted in the ferrite fraction being reduced.

TSL indexing of the bainite sample

The EBSD indexing of the bainite sample showed less austenite and cementite than the martensite sample, but more austenite than the ferrite sample. Similarly as for the martensite sample, the scan of the bainite sample showed some white areas in the grain map, which messily was indexed as cementite or austenite in the phase map as for the martensite scan. There was therefore also bigger chance of mis-indexing and too high phase fractions of cementite and austenite than for the pearlite scan. There were however areas of both cementite and austenite in the phase map that definitely were not mis-indexing, since we could find these areas as grains with the same orientation in the grain maps. Cementite particles in the bainite samples was explained the same way as for the pearlite and martensite sample; proeutectoid cementite formed on former austenite grain boundaries because of the hypereutectoid composition. The austenite areas in the maps were on the other hand harder to explain. As mentioned, most of the austenite indexed pixels were mis-indexings, but there was some areas that could not be assumed to be indexed wrongly. A possible explanation could be that segregation of alloying elements as Mn and Cr could be found at grain boundaries during the rapid cooling and retarded the bainite transformation, preventing some of the austenite to transform before the air cooling, resulting in areas of retained austenite (Goulas et al., 2016).

Table 5.3: Phase fractions obtained through the different rounds of indexing in TSL of the bainite sample. α = ferrite, γ = austenite, θ = cementite, $Cr_{23}C_6$ = chromium carbide.

Bainite sample - TSL indexing				
Indexing phases	**Fraction α**	**Fraction γ**	**Fraction θ**	**Fraction $Cr_{23}C_6$**
α, γ, θ	0.841	0.060	0.099	-
α, γ, $Cr_{23}C_6$	0.665	0.068	-	0.267
α, γ, θ, $Cr_{23}C_6$	0.634	0.050	0.082	0.234

When the mis-indexing was accounted for, the phase fractions for the scan with ferrite, austenite and cementite (Table 5.3) with $f_{\alpha,e} = 0.841$, $f_{\gamma,e} = 0.060$ and $f_{\theta,e} = 0.099$ were not so far off the theoretical values $f_{\alpha,t} = 0.909$ and $f_{\theta,t} = 0.091$ calculated in Equation 5.1 and 5.2. As for the pearlite and martensite scan, the first and third indexing done of the bainite sample could be used to show that the phase fractions of austenite and cementite remained somewhat the same, proving that the indexing of these areas was not a result of mis-indexed pixels.

EMsoft indexing of all the samples of Alloy 1

The indexing with the EMsoft software gave results and maps showing much of the same information as TSL, but the biggest difference in the analysis done with TSL and EMsoft in this work was the *grade* of match that EMsoft delivered. While TSL gave a typical match or no match answer, each indexing done with EMsoft gave a percentage of match with a phase in each pixel. That meant that some pixels could match with some probability with all the phases tried in the indexing, while in contrast TSL always only chose one phase for each pixel. This showed how EMsoft took use of all the patterns, even those of poor quality and included them in the analysis. Even though the match would be poor because of the quality of the pattern, EMsoft gave different values for each phase showing which of the phases matched better.

Several maps was obtained through the indexing with EMsoft, and the Confidence Index (CI) and Orientation Similarity (OS) maps where chosen to present the results in this work. The CI maps was included to best observe areas of the EBSD scan that matched well with the simulated pattern library of each phase. These maps was compared to the phase maps obtained through TSL, to see if the two softwares gave the same result - which they very much did. These maps also showed how the mis-indexing that is a bit of a nuisance in TSL, no longer was a problem in EMsoft. The CI maps from the indexing with EMsoft found distinct particles of cementite and areas of retained austenite in the martensite and bainite sample which agreed with the indexing done with TSL.

The OS maps was used as the factor deciding if the indexing with one phase in EMsoft was better than the other. Each map was presented with an intensity scale bar, showing brighter areas with a high intensity value, and darker with lower values. The grain boundaries always appeared darker because the intensity was calculated from the similarity of the orientation in one pixel compared to its neighbors. Little similarity would result in a low intensity value, which then was presented as dark in the map. These maps also would be overall brighter for a phase giving a good match with the pattern (ferrite phase with the pearlite sample) than a phase not giving a good match (cementite phase with the pearlite sample).

Table 5.4: Summary of the OSM max and mean intensity values from the EMsoft indexing of the samples of Alloy 1: 103Cr3/103C3.

ALLOY 1	**PEARLITE**				
Indexing phase	θ	γ	α	α' **(1.3 %)**	α**' (1.16%)**
OSM max value	20.00	19.75	20.00	20.00	20.00
OSM mean value	12.73	14.69	18.52	18.13	18.18
	BAINITE				
Indexing phase	θ	γ	α	α' **(1.3 %)**	α**' (1.16%)**
OSM max value	19.25	19.00	20.00	20.00	19.25
OSM mean value	5.74	8.44	13.41	12.10	12.14
	MARTENSITE				
Indexing phase	θ	γ	α	α' **(1.3 %)**	α**' (1.16%)**
OSM max value	20.0	19.50	20.00	19.75	20.00
OSM mean value	5.86	9.29	12.77	11.51	11.53

The OSM mean and max values are summed up for all the samples in Table 5.4. Each EBSD scan of Alloy 1 was indexed with five phases; ferrite, austenite, cementite and a martensite phase for 1.3 wt% C and one for 1.16 wt% C. The highest possible intensity value was at 20.00, and the indexing shows that all phases except austenite found some areas with OSM intensity at max. The values of the three samples could not be compared since this was dependent on the pattern quality of each of the scans, but the values for the different phases for each sample scan was compared. All indexings showed in the end that the intensity mean OSM value was highest for the ferrite phase for all the samples, meaning best match.

The indexing with the martensite 1.3 wt% C phase for the pearlite, bainite and martensite sample had a mean value of 2,1%, 9,8% and 9,9% lower than the ferrite indexing of each sample, respectively. The table also showed that the OSM mean values for the two martensite phases differed very little, but that the martensite phase with less amount of carbon accounted for matched slight better for all samples (OSM mean values 1,8%, 9,5% and 9,7% lower than the OSM mean value from the ferrite indexing of the pearlite, bainite and martensite sample, respectively). If this was because it actually was a better match with the experimental patterns or it just was a better match because it was closer to the lattice parameters of ferrite is hard to prove or decide. Overall, the indexing with EMsoft shows that the bainite and martensite structures are no closer being differentiated with the method used in this work with the experimental data obtained.

5.4.2 Alloy 2: 34CrNiMo6

In difference to Alloy 1, Alloy 2 showed no distinct particles of cementite throughout the sample. For a hypoeutectoid steel with 0.36 wt% C, cementite particles at former austenite grain boundaries are not expected, and the indexing of the samples of Alloy 2 showed that.

TSL indexing of the samples of Alloy 2

As for Alloy 1, the theoretically expected phase fractions of ferrite and cementite were calculated for carbon content of 0.36 wt% using Equation 5.3 and 5.4.

$$f_\alpha = \frac{C_\theta - C_0}{C_\theta - C_\alpha} = \frac{6.7 - 0.36}{6.7 - 0.022} = 0.949 = 94.9wt\% \tag{5.3}$$

$$f_\theta = \frac{C_0 - C_\alpha}{C_\theta - C_\alpha} = \frac{0.36 - 0.022}{6.7 - 0.022} = 0.051 = 5.1wt\% \tag{5.4}$$

For this alloy the chromium carbide phase was excluded from the indexing, and only one round with ferrite, austenite and cementite is presented. The phase fractions of ferrite, austenite and cementite obtained from the phase maps produced of the indexing with TSL are presented in Table 5.5. Again, these fractions were expected to deviate some from the expected theoretical fractures because of mis-indexing that always will happen without refining and averaging the EBSD scan further, but either way the result of the TSL indexing of all the samples gave fractions of ferrite that was very close to what the theory predicted.

Table 5.5: Phase fractions obtained through the different rounds of indexing in TSL of all the samples of Alloy 2. α = ferrite, γ = austenite, θ = cementite, $Cr_{23}C_6$ = chromium carbide.

Ferrite sample - TSL indexing			
Indexing phases	**Fraction α**	**Fraction γ**	**Fraction θ**
α, γ, θ	0.946	0.016	0.038

Martensite sample - TSL indexing			
Indexing phases	**Fraction α**	**Fraction γ**	**Fraction θ**
α, γ, θ	0.911	0.026	0.063

Bainite sample - TSL indexing			
Indexing phases	**Fraction α**	**Fraction γ**	**Fraction θ**
α, γ, θ	0.976	0.009	0.014

The ferrite fractions $f_{\alpha,e,ferrite} = 0.946$, $f_{\alpha,e,martensite} = 0.911$ and $f_{\alpha,e,bainite} = 0.976$ were all very close to the theoretical value of $f_{\alpha,t} = 0.949$. The fractions of cementite in the ferrite and martensite samples with $f_{\theta,e,ferrite} = 0.038$ and $f_{\theta,e,martensite} = 0.063$ were not deviating much from the theoretical value of $f_{\theta,t} = 0.051$, but the cementite fraction from the bainite sample deviated some. The low amount of cementite indexed in the bainite scan could also be dependent on the size of the EBSD scan area. Here, for all samples, quite small areas were scanned to rather obtain a good resolution of the scan. Choosing to do so could have resulted in choosing an area of the sample surface with less average cementite amount than the matrix, and a bigger scan might have revealed a higher amount.

In contrast to Alloy 1, the carbon content of this alloy was low enough to obtain a M_F temperature calculated to be around 190°C (Equation 2.2) which the sample quenched to martensite easily reached in water at 20°C. Because of the relatively high M_F temperature, all the austenite was expected to transform into martensite, leaving no areas of retained austenite. This could also be observed from the indexing of the martensite sample, where almost all pixels indexed as austenite were stand-alone pixels. All cementite indexed was found along grain boundaries, areas that also revealed poor kikuchi patterns in the grain maps (white areas) and were prone to mis-indexing.

EMsoft indexing of the samples of Alloy 2

Since there was no prominent particles of cementite or other structures much different from the ferrite/martensite BCC/BCT structure, the maps produced of all the samples through EMsoft gave less contrasts between grains and areas than Alloy 1. The maps obtained through the indexing with cementite and austenite phase for all the EBSD scans found little to none areas matching well to the simulated patterns for the two phases.

Table 5.6: Summary of the OSM max and mean intensity values from the EMsoft indexing of the samples of Alloy 2: 34CrNiMo6.

ALLOY 2	**FERRITE**			
Indexing phase	θ	γ	α	α' **(0.36 %)**
OSM max value	16.75	19.25	20.00	20.00
OSM mean value	6.86	10.78	16.10	14.97
	BAINITE			
Indexing phase	θ	γ	α	α' **(0.36 %)**
OSM max value	18.50	18.75	20.00	20.00
OSM mean value	7.94	11.10	16.54	15.54
	MARTENSITE			
Indexing phase	θ	γ	α	α' **(0.36 %)**
OSM max value	16.0	19.50	20.00	20.00
OSM mean value	6.62	9.76	15.11	14.02

Table 5.6 shows the max and mean OSM intensity values collected from the OS maps produced from the indexing with EMsoft. The table shows how the OSM max intensity for both cementite and austenite never reached max value at 20.00, and that cementite in particular obtained a relatively low OSM max value for all the samples. Again the ferrite and martensite indexing gave very similar results, and the OS maps for the two for each sample were very hard to differentiate by studying the images. The OSM mean values for the ferrite indexing was for all samples the highest value, with the OSM mean values for the martensite indexing for the ferrite, bainite and martensite sample being 7,0%, 6,1% and 7,2% lower than the indexing with ferrite, respectively.

For this alloy the lattice parameters for the BCT martensite structure was more similar to the ferrite BCC structure than for Alloy 1. Compared to the martensite indexings of Alloy 1, the OSM mean values of the martensite indexing of the martensite and bainite sample was closer to the ferrite indexing of those samples for this alloy, which again emphasized the hypothesis of the martensite phase indexing any of the samples better when the lattice parameters was closest to the ferrite lattice parameters. No indexing with other phases matched better than ferrite.

5.4.3 Advantages and disadvantages using the two indexing softwares

The conventional TSL software is a simple, user friendly software that delivers perfectly usable results after, in worst case, a few hours. The user can freely try different phases from the software's structure library in a quantitatively test on a more or less unknown sample and get results that reveals the phases present in the sample. Of course, this relies on the phases being available in the library. The martensite structure in steel can not be found in such a library because of the lattice parameter's dependency on the carbon content of the alloy, and TSL could therefore not be used with the purpose of differentiating bainitic and martensitic structures using EBSD indexing.

Using EMsoft for indexing EBSD patterns, the indexing phases could not be chosen without knowing what to expect in the sample, especially for the martensite structure where different structure files were needed to be produced for the two alloys. To do that the carbon content of the alloy was needed. In this work the EMsoft indexing was always done after the TSL indexing, both to know what phases to expect in the sample, but also to gather the pattern center coordinates (x*, y*, and z*) from the 5 reference patterns chosen during the EBSD scan in SEM which were obtainable through TSL. Before being able to start indexing the EBSD scan with a phase in EMsoft, three programs was needed to be run to collect all data and produce input files for the indexing program. Depending on the computer's RAM and number of threads in the processor, these programs could take several hours to finish. The indexing program for the simplest phases (cubic, few atoms in the cell unit) as ferrite and austenite took in this work around 4 hours to finish of a scan with image size between 100x100 and 200x200 pixels, but for the most complex phase, in this work cementite, the longest scan took over 48 hours to run.

The results from the EMsoft indexing showed indexed maps with much higher detail than those obtained through TSL, and as mentioned before, even for pixels with poor pattern quality EMsoft managed to index these pixels with a probability of match with all the phases used in the indexings. Where TSL could not be used for differentiating bainite and martensite in any way, EMsoft ran indexings with martensite and ferrite phase separately, delivering values (OSM max and mean values in this work) that revealed which of the indexing phases that matched best with the experimental patterns.

In this work little averaging and refining of the EBSD patterns and the indexings was done, and because of that TSL delivered phase maps where mis-indexing of pixels was impossible to avoid. Because TSL in the phase maps wanted to index every pixel as one of the indexing phases chosen, even though the EBSD pattern there could be unreadable, stand alone pixels were more or less indexed randomly. In EMsoft, mis-indexing were not a problem since each phase was indexed separately, preventing the software to have to choose one phase or another. The result of indexings with EMsoft was separate maps for each phase used in the indexings of the same scan, where areas in the maps with highest intensity represented areas that matched well with the given phase. The software, instead of giving a yes or no match with a phase in a given pixel, gave a probability or a grade of match with the indexing phase. Comparing the maps for the different phases of the same scan, one could detect what phase matched the pixel best by looking at that value.

5.5 TEM analysis

The TEM analysis of the martensite and bainite samples of both the alloys was done to conclude that the correct structures were obtained during the heat treatment in the experimental work.

From the theory of the hardening procedures of formation of martensite and bainite, it is known that carbon in the austenite during direct hardening to martensite has no time to diffuse out of the forming martensite and is locked into interstitial sites in the new lattice. During transformation from austenite to bainite, carbon in the forming bainitic ferrite sheaves have time to diffuse some into the surrounding austenite. For the lower bainite structure, also tiny needle-formed carbides were to be expected inside the sheaves of ferrite.

For the alloys used in this work the carbon content was sufficient to expect carbide particles inside the ferrite sheaves in the bainitic structure. The particles were found as elongated carbide particles, and inside one sheaf the carbides all had the same orientation - a direct confirmation of having obtained a bainitic structure (Goulas et al., 2019). Along with the hardness test results for both martensite samples, this TEM analysis confirmed having obtained the martensitic structure during the heat treatment by not finding any carbides in the structures of the two martensite samples.

6 Conclusion

- The hardness values for the martensite samples of both alloys matched well with the expected values gathered from the graph showing Vickers and Rockwell C hardness for varying carbon content in steels in Figure 2.11. Only the hardness of the martensite phase matched well with the high experimental values obtained of the two samples.
- The TEM analysis showed needle-formed carbides in the structures of the bainite samples of the two alloys, and no carbides in the martensite samples. This was added to present the easiest method for distinguishing the two structures.
- The pearlite/ferrite samples from both alloys was much included in the analysis to prove the indexing with both softwares worked as it should, providing two reliable indexing softwares. Both samples was well indexed, and TSL and EMsoft gave no contradictory results.
- To begin with, this work was based on choosing a steel alloy with high carbon content to enhance the differences in the martensitic and bainitic lattice parameters so they more easily gave different results during the indexing with EMsoft. The large amount of carbon in Alloy 1 resulted in cementite particles precipitating on the grain boundaries of the prior austenite grains, areas of retained austenite appearing because of a low M_F temperature and a large amount of diffuse EBSD kikuchi bands. The poor kikuchi patterns were caused by internal strain caused by the carbon in solid solution. This made it difficult to obtain good EBSD scans of the martensite structure.
- TSL and EMsoft were both used to index the same EBSD scans to show similarities, and making sure that EMsoft managed to index the different phases with the same results as TSL. This showed to work very well, and EMsoft was validated to index the samples without error.
- From the values collected from the orientation similarity maps from the indexing with EMsoft, the software was to able to differentiate the martensitic and the bainitic structure. Preferably the martensite structure files produced in EMsoft should have matched better with the martensite EBSD scans than the ferrite structure file. The indexings run of all six samples studied in this work showed that the ferrite phase matched best for the ferritic, pearlitic, bainitic and martensitic microstructure.
- The use of EMsoft was much more time consuming and less user friendly than the TSL software that did much of the work for the user. That said, the EMsoft software delivered maps of higher detail than TSL, and could deliver a value telling the user which phase matched the scan best on average (in this work the OSM mean values were used). Most importantly the software could deliver different results for the bainite and martensite structure, even though they yet could not be used to differentiate the two.

7 Further work

The procedure tested in this work is open to further work, and an overview of some areas worth investigating is presented below.

- During the experimental work, problems with the SEM computer was met, presumably because of old equipment or little available memory for the NORDIF software to run the process. The desired EBSD scan quality could therefore not be achieved. Further work for obtaining EBSD scans of better quality by choosing higher resolution, preferably 480x480 px, choosing an averaging value of 4 or higher, and having a low step size of 0.1 μm or lower would be ideal to give the best possible starting point for the indexing.
- The EMsoft software were in this work used without much exploration, and only one setting for the indexings were tested. The software showed great potential for a more thorough analysis, and several parameters could have been changed to obtain different results that could have delivered a different outcome.
- The indexings done with EMsoft could have been further refined using the EMsoft program `EMFitOrientation`, and *neighbor pattern averaging* could have been done with the python program KikuchiPy.
- KikuchiPy is still under under constant development for more features for extracting information from the files produced in EMsoft and presenting them systematically and clearly for the user, and for further refining the files produced in EMsoft for better results. The use of the varieties of opportunities this python program delivers would be greatly recommended to try out.

Bibliography

Andrews, K.W. (1956). The calculation of transformation temperatures and austenite-ferrite equilibria in steels. *JISI*, 184:414.

Barnard, J.S., Johnstone, D.N., and Midgley, P.A. (2017). High-resolution scanning precession electron diffraction: Alignment and spatial resolution. *Ultramicroscopy*, 174:79–88.

Bendersky, L. and Gayle, F. (2001). Electron diffraction using transmission electron microscopy. *Journal of Research of the National Institute of Standards and Technology*, 106(6):997.

Bhadeshia, H.K.D.H. (2015). *Bainite in Steels*. CRC Press. URL `https://www.ebook.de/de/product/24526108/h_k_d_h_bhadeshia_bainite_in_steels.html`.

Bhadeshia, H.K.D.H. and Honeycombe, R.W.K. (2017). *Steels : microstructure and properties.* Butterworth-Heinemann, Amsterdam, 4th edition harshad bhadeshia and robert honeycombe. edition.

Bruker (2015). Periodic table of elements and x-ray energies. URL `https://www.bruker.com/fileadmin/user_upload/8-PDF-Docs/X-rayDiffraction_ElementalAnalysis/HH-XRF/Misc/Periodic_Table_and_X-ray_Energies.pdf`.

Buseck, P., Cowley, J., and Eyring, L. (1989). *High-Resolution Transmission Electron Microscopy: And Associated Techniques*. Oxford University Press.

Callahan, P.G. and De Graef, M. (2013). Dynamical electron backscatter diffraction patterns. part i: Pattern simulations. *Microscopy and Microanalysis*, 19(5):1255–1265.

Callister, W.D. and Rethwisch, D.G. (2015). *Materials Science and Engineering*. Wiley, 9 edition.

Chen, Y.H., Park, S.U., Wei, D., Newstadt, G., Jackson, M.A., Simmons, J.P., De Graef, M., and Hero, A.O. (2015). A dictionary approach to electron backscatter diffraction indexing. *Microscopy and Microanalysis*, 21(3):739–752.

De Graef, M. (2019). Program: Emgetosm. URL `https://github.com/EMsoft-org/EMsoft/wiki`.

Fruchart, D., Chaudouet, P., Fruchart, R., Rouault, A., and Senateur, J. (1984). Etudes structurales de compose´s de type ce´mentite: Effet de l'hydroge`ne sur fe3c suivi par diffraction neutronique. spectrome´trie mo¨ssbauer sur FeCo2b et co3b dope´s au57fe. *Journal of Solid State Chemistry*, 51(2):246–252.

Goldstein, J.I., Newbury, D.E., Joy, D.C., Lyman, C.E., and Echlin, P. (2002). *Scanning Electron Microscopy and X-Ray Microanalysis*. Springer Science+Business Media.

Goulas, C., Mecozzi, M.G., and Sietsma, J. (2016). Bainite formation in medium-carbon low-silicon spring steels accounting for chemical segregation. *Metallurgical and Materials Transactions A*, 47(6):3077–3087.

Goulas, C., Kumar, A., Mecozzi, M.G., Castro-Cerda, F.M., Herbig, M., Petrov, R.H., and Sietsma, J. (2019). Atomic-scale investigations of isothermally formed bainite microstructures in 51crv4 spring steel. *Materials Characterization*, 152:67–75.

Jackson, M.A., Pascal, E., and De Graef, M. (2019). Dictionary indexing of electron backscatter diffraction patterns: a hands-on tutorial. *Integrating Materials and Manufacturing Innovation*, 8(2):226–246. URL `https://doi.org/10.1007/s40192-019-00137-4`.

Kittel, C. (2004). *Introduction to Solid State Physics*. John Wiley & Sons Inc.

Kohl, H. and Reimer, L. (2008). *Transmission Electron Microscopy*. Springer New York.

Krauss, G. (1978). Martensitic transformation, structure and properties in hardenable steels. *Metallurgical Society AIME,*, pages 229–248.

Krauss, G. (2015). *Steels: Processing, Structure, and Performance*. ASM International, Materials Park, Ohio, 2. edition edition.

Lobodyuk, V., , and and, Y.M. (2017). On the issue of the nature of tetragonality of a martensite. *METALLOFIZIKA I NOVEISHIE TEKHNOLOGII*, 39(9):1281–1298.

Lobodyuk, V.A., Meshkov, Y.Y., and Pereloma, E.V. (2019). On tetragonality of the martensite crystal lattice in steels. *Metallurgical and Materials Transactions A*, 50(1):97–103. URL `https://doi.org/10.1007/s11661-018-4999-z`.

Lu, Y., Yu, H., and Sisson, R.D. (2017). The effect of carbon content on the c/a ratio of as-quenched martensite in fe-c alloys. *Materials Science and Engineering: A*, 700:592–597. URL `http://www.sciencedirect.com/science/article/pii/S0921509317307128`.

Marder, A.R. (1967). The morphology of martensite in iron-carbon alloys. *Trans. ASM*, 60:651–660.

Marquardt, K., Graef, M.D., Singh, S., Marquardt, H., Rosenthal, A., and Koizuimi, S. (2017). Quantitative electron backscatter diffraction (EBSD) data analyses using the dictionary indexing (DI) approach: Overcoming indexing difficulties on geological materials. *American Mineralogist*, 102(9):1843–1855.

Ånes, H. and Bergh, T. (2020). kikuchipy/kikuchipy: Kikuchipy v0.1.2.

Ram, F. and De Graef, M. (2018). Phase differentiation by electron backscatter diffraction using the dictionary indexing approach. *Acta Materialia*, 144:352–364. URL `http://www.sciencedirect.com/science/article/pii/S1359645417309369`.

Rauch, E. and Véron, M. (2014). Automated crystal orientation and phase mapping in TEM. *Materials Characterization*, 98:1–9.

Roşca, D. (2010). New uniform grids on the sphere. *Astronomy and Astrophysics*, 520:A63.

Ryde, L. (2006). Application of ebsd to analysis of microstructures in commercial steels. *Materials Science and Technology*, 22(11):1297–1306. URL https://doi.org/10.1179/174328406X130948.

Schwenk, M. (2014). Transformation hardening in steel. In R.B. Hetnarski, editor, *Encyclopedia of Thermal Stresses*, pages 6140–6153. Springer Netherlands, Dordrecht. URL https://doi.org/10.1007/978-94-007-2739-7_464.

Singh, J. (2019). Moseley's law. *Concept of Physics*. URL https://www.concepts-of-physics.com/modern/media/moseleys-law.pdf.

Spence, J.C.H. (2013). *High-resolution electron microscopy*. OUP Oxford.

Stojakovic, D. (2012). Electron backscatter diffraction in materials characterization. *Processing and application of ceramics*, 6(1):1–13.

Vander Voort, G.F. (2001). Etching isothermally treated steels. *Heat Treating Progress*, 1(2):25–32.

Wang, R., Wang, C., Zhang, H., Tao, J., and Bai, X., editors (2018). *Progress in Nanoscale Characterization and Manipulation*. Springer Singapore.

Wilkinson, A.J. and Dingley, D.J. (1991). Quantitative deformation studies using electron back scatter patterns. *Acta Metallurgica et Materialia*, 39(12):3047–3055.

Wyckoff, R.W.G. (1964). *Crystal structures*. Krieger.

Yang, H.S. and Bhadeshia, H.K.D.H. (2007). Uncertainties in dilatometric determination of martensite start temperature. *Materials Science and Technology*, 23(5):556–560. URL https://doi.org/10.1179/174328407X176857.

Appendices

Appendix A

Calculated carbon content in the martensite structure

The 103Cr3/103C3 alloy is a hypereutectoid carbon steel with carbon content of 1.3 wt% C. Because of this, during the hardening procedure of producing the martensite structure, cementite forms on grain boundaries and can precipitate inside matrix grains. Because the cementite phase being so rich in carbon, the carbon content in the martensite structure will be reduced with the increasing amount of cementite.

The martensite sample of alloy 103Cr3/103C3 was heat treated at 860 °C and if the temperature was assumed to be about 850 °C when it reached the water used for quenching, the amount of cementite can be calculated as follows:

$$f_\theta = \frac{1.3 - 1.18}{6.7 - 1.18} = 0.0217 \tag{A.1}$$

The amount of C in cementite (θ):

$$0.0217 \cdot 6.7 \text{ wt\%} \approx 0.145 \text{ wt\%}$$

Amount of C in the remaining austenite (γ) before the transformation to martensite structure:

$$1.3 - 0.145 = 1.155 \text{ wt\% C} \approx 1.16 \text{ wt\% C.}$$

For indexing of martensite in EMsoft, the lattice parameters a and c must be determined. This is calculated from the carbon content in the structure. Using 1.16 wt% C, Equation 2.3 and the parameter $a = 0.2851$nm from Lobodyuk et al. (2017), the c parameter can be calculated:

$$c = a(1 - 0.045 w_c) = 0.2851(1 + 0.045 \cdot 1.16) = 0.3000nm \tag{A.2}$$

A.1 EMsoft indexing with the 1.16 wt% C martensite phase

A new martensite structure file was produced for indexing in EMsoft using the parameters calculated above. The pearlite, martensite and bainite EBSD scan was then indexed with a 1.16 wt% C martensite phase, and the CI and OSM maps are presented below.

Figure A.1, A.2 and A.3 shows the Confidence Index (CI) and Orientation similarity map of the pearlite, martensite and bainite sample indexed with the martensite (1.16 wt% C) phase through EMsoft. These maps are light where the software is positive that the simulated and the experimental patterns have a good match, and dark when they do not match well.

A.1.1 Pearlite sample

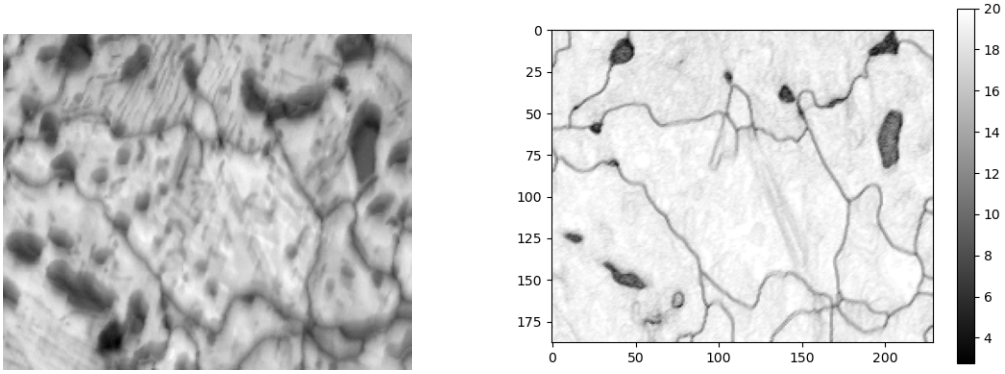

(a) Confidence Index Map of the pearlite sample indexed with the martensite (α')(1.16 wt% C) phase.

(b) Orientation Similarity Map of the pearlite sample indexed with the martensite (α')(1.16 wt% C) phase.

Figure A.1: Alloy 1. CI and OSM maps from the EMsoft indexing of the pearlite sample using the α'(1.16 wt% C) phase

A.1.2 Martensite sample

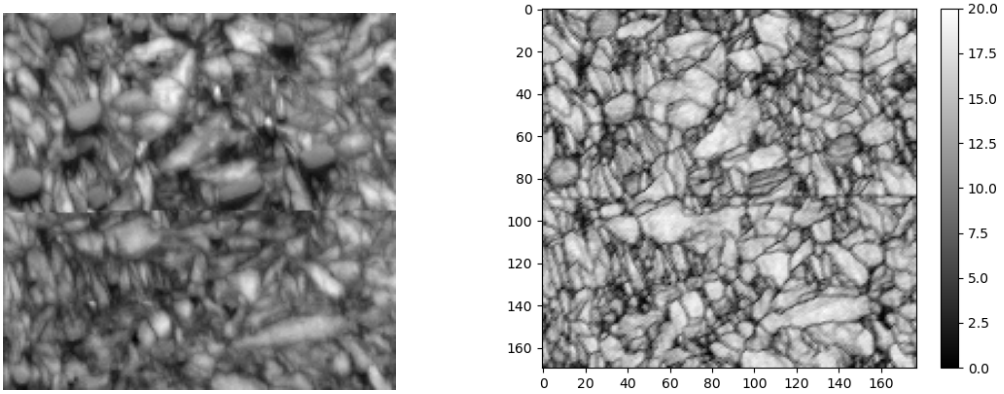

(a) Confidence Index Map of the martensite sample indexed with the martensite (α')(1.16 wt% C) phase.

(b) Orientation Similarity Map of the martensite sample indexed with the martensite (α')(1.16 wt% C) phase.

Figure A.2: Alloy 1. CI and OSM maps from the EMsoft indexing of the martensite sample using the α'(1.16 wt% C) phase

A.1.3 Bainite sample

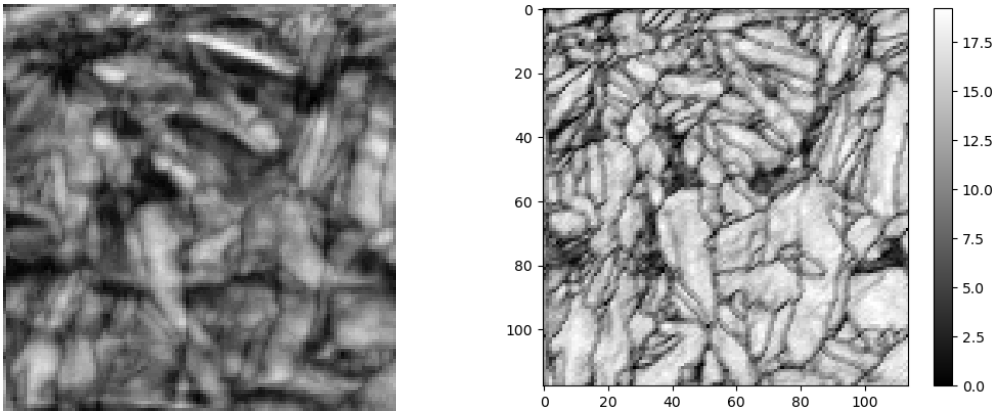

(a) Confidence Index Map of the bainite sample indexed with the martensite (α')(1.16 wt% C) phase.

(b) Orientation Similarity Map of the bainite sample indexed with the martensite (α')(1.16 wt% C) phase.

Figure A.3: Alloy 1. CI and OSM maps from the EMsoft indexing of the bainite sample using the α'(1.16 wt% C) phase

Appendix B

EMsoft input .nml files

The following .nml files shows input values used for running the Monte Carlo simulation, for making the master pattern file, for running the Dictionary Indexing program for each phase, for refining the indexing for each phase, and for merging the different maps together.

Input file for the program "EMMCOpenCL"

```
 &MCCLdata
! only bse1, full or Ivol simulation
 mode = 'full' ! 'bse1' or 'full', 'Ivol',
! name of the crystal structure file
 xtalname = 'ferrite/ferrite.xtal',
! for full mode: sample tilt angle from horizontal [degrees]
 sig = 70.0,
! for bse1 mode: start angle
 sigstart = 0.0,
! for bse1 mode: end angle
 sigend = 30.0,
! for bse1 mode: sig step size
 sigstep = 2.0,
! sample tilt angle around RD axis [degrees]
 omega = 0.0,
! number of pixels along x-direction of square projection [odd number!]
 numsx = 501,
! number of incident electrons per thread
 num_el = 10,
! GPU platform ID selector
 platid = 1,
! GPU device ID selector
 devid = 1,
! number of work items (depends on GPU card; leave unchanged)
 globalworkgrpsz = 150,
! total number of incident electrons and multiplier (to get more than 2^(31)-1 electrons)
 totnum_el = 2000000000,
 multiplier = 1,
! incident beam energy [keV]
 EkeV = 20.D0,
! minimum energy to consider [keV]
 Ehistmin = 5.D0,
! energy binsize [keV]
 Ebinsize = 1.0D0,
! maximum depth to consider for exit depth statistics [nm]
 depthmax = 100.D0,
! depth step size [nm]
 depthstep = 1.0D0,
! should the user be notified by email or Slack that the program has completed its run?
 Notify = 'Email',
```

```
! output data file name; pathname is relative to the EMdatapathname path !!!
 dataname = 'crystal_data/ferrite/ferrite_mc_mp_20kv.h5'
 /
```

The crystal structure of ferrite is used as an input (`xtalname = 'ferrite/ferrite.xtal'`). The voltage range is chosen from 20keV to 5keV (`EkeV = 20.D0` and `Ehistmin = 5.D0`). The program produces a .h5 file containing information of each energy bin from 5 to 20 keV for the chosen structure.

Input file for the program "EMEBSDmaster"

```
 &EBSDmastervars
! smallest d-spacing to take into account [nm]
 dmin = 0.05,
! number of pixels along x-direction of the square master pattern  (2*npx+1 = total number)
! in Legendre mode (see below), this number will be the maximum band width for
! the spherical harmonic transform
 npx = 500,
! number of OpenMP threads (0 to use the maximum available)
 nthreads = 0,
! name of the energy statistics file produced by EMMCOpenCL program; relative to
  EMdatapathname;
! this file will also contain the output data of the master program
 energyfile = 'crystal_data/ferrite/ferrite_mc_mp_20kv.h5',
! BetheParameters file name
 BetheParametersFile = 'BetheParameters.nml',
! do you wish to receive a notification (Email or Slack) when the program completes ?
 Notify = 'Email',
! name of EMMCOpenCL output file to be used to copy the MC data from for this
! master pattern run;
! This can be used to perform multiple master pattern runs starting from the same
! MC data set without having to rerun the MC computation.  Leave this variable set to
! 'undefined' if not needed.
 copyfromenergyfile = 'undefined',
! if copyfromenergyfile is not 'undefined', then:
!   - for EMsoft developers who have the EMsoft_SDK installed, the following parameter
!     will be ignored;
!   - all other users will need to provide the full path to the h5copy program here
 h5copypath = 'undefined',
! restart computation ?
 restart = .FALSE.,
! create output file with uniform master patterns set to 1.0 (used to study background only)
 uniform = .FALSE.,
 /
```

The information from the EMMCOpenCL program stored in a .h5-file (`energyfile = 'crystal_data/ferrite/ferrite_mc_mp_20kv.h5'`) is used as an input, and from this information the program produces master patterns for the different energy bins. These patterns are stored in the same .h5-file.

Input file for the program "EMEBSDDI"

```
 &EBSDIndexingdata
! The line above must not be changed
!
! The values below are the default values for this program
!
!####################################################################
! INDEXING MODE
!####################################################################
!
! 'dynamic' for on the fly indexing or 'static' for pre calculated dictionary
 indexingmode = 'dynamic',
!
!####################################################################
! DICTIONARY PARAMETERS: COMMON TO 'STATIC' AND 'DYNAMIC'
!####################################################################
!
! do you want Email or Slack notification when the run has completed?
 Notify = 'Off',
! width of data set in pattern input file
 ipf_wd = 229,
! height of data set in pattern input file
 ipf_ht = 188,
! define the region of interest as x0 y0 w h;  leave all at 0 for full field of view
! region of interest has the point (x0,y0) as its upper left corner and is w x h
! patterns
 ROI = 0 0 0 0,
! X and Y sampling step sizes
 stepX = 0.1,
 stepY = 0.1,
! number of top matches to keep from the dot product results
 nnk = 50,
! the following option has been disabled starting version 4.3
! number of top matches to use for orientation averaging (<nnk)
! nnav =  20,
! number of top matches to use for Orientation Similarity Map computation (<nnk)
 nosm = 20,
! number of top matches to use for Indexing Success Map computation (<nnk)
 nism = 5,
! Indexing Success threshold angle (degrees)
 isangle = 1.5,
! to use a custom mask, enter the mask filename here; leave undefined for standard
!mask option
 maskfile = 'undefined',
! mask or not
 maskpattern = 'n',
! mask radius (in pixels, AFTER application of the binning operation)
 maskradius = 240,
! hi pass filter w parameter; 0.05 is a reasonable value
 hipassw = 0.125,
! number of regions for adaptive histogram equalization
 nregions = 4,

!####################################################################
! ONLY SPECIFY WHEN INDEXINGMODE IS 'DYNAMIC'
!####################################################################
!
! number of cubochoric points to generate list of orientations
```

```
 ncubochoric = 100,
! distance between scintillator and illumination point [microns]
 L = 9377.34,
! tilt angle of the camera (positive below horizontal, [degrees])
 thetac = 0,
! CCD pixel size on the scintillator surface [microns]
 delta = 70.0,
! number of CCD pixels along x and y
 numsx = 240,
 numsy = 240,
! pattern center coordinates in units of pixels
 xpc = 2.66,
 ypc = 59.27,
! angle between normal of sample and detector
 omega = 0.0,
! minimum and maximum energy to use for interpolation [keV]
 energymin = 10.0,
 energymax = 20.0,
! the following option has been disabled starting version 4.3
! spatial averaging method ('y' or 'n' ;can't be used with approximate energy average)
! spatialaverage = 'n',
! incident beam current [nA]
 beamcurrent = 150.0,
! beam dwell time [micro s]
 dwelltime = 100.0,
! binning mode (1, 2, 4, or 8)
 binning = 1,
! intensity scaling mode 'not' = no scaling, 'lin' = linear, 'gam' = gamma correction
 scalingmode = 'gam',
! gamma correction factor
 gammavalue = 0.33,
!
!#####################################################################
! INPUT FILE PARAMETERS: COMMON TO 'STATIC' AND 'DYNAMIC'
!#####################################################################
!
! name of datafile where the patterns are stored; path relative to EMdatapathname
 exptfile = 'NORDIF_EBSDscan/pearlite/pearlite_cropped_hs_bcorr_pattern.dat',
! input file type parameter: Binary, EMEBSD, TSLHDF, TSLup2, OxfordHDF, OxfordBinary,
! BrukerHDF, NORDIF
 inputtype = 'NORDIF',
! here we enter the HDF group names and data set names as individual strings (up to 10)
! enter the full path of a data set in individual strings for each group, in the
! correct order, and with the data set name as the last name; leave the remaining
! strings empty (they should all be empty for the Binary and TSLup2 formats)
 HDFstrings = 'Scan 1' 'EBSD' 'Data' 'patterns' '' '' '' '' '' '',
!
!#####################################################################
! OTHER FILE PARAMETERS: COMMON TO 'STATIC' AND 'DYNAMIC'
!#####################################################################
!
! temporary data storage file name ; will be stored in $HOME/.config/EMsoft/tmp
 tmpfile = 'EMEBSDDict_tmp.data',
 keeptmpfile = 'n',
! output file ; path relative to EMdatapathname
 datafile = 'crystal_data/ferrite/ferrite_dp.h5',
! ctf output file ; path relative to EMdatapathname
 ctffile = 'undefined',
```

```
! the following option has been disabled starting version 4.3
! average ctf output file ; path relative to EMdatapathname
! avctffile = 'undefined',
! ang output file ; path relative to EMdatapathname
 angfile = 'crystal_data/ferrite/ferrite_original.ang',
! euler angle input file
 eulerfile = 'undefined'

!###################################################################
! ONLY IF INDEXINGMODE IS STATIC
!###################################################################
!
 dictfile = 'undefined',
!
!###################################################################
! ONLY IF INDEXINGMODE IS DYNAMIC
!###################################################################
!
! master pattern input file; path relative to EMdatapathname
 masterfile = 'crystal_data/ferrite/ferrite_MC_MP_20kv.h5',
!
!###################################################################
! IF REFINEMENT IS NEEDED ...
!###################################################################
!
! enter the name of the nml file for the EMFitOrientation program
 refinementNMLfile = 'undefined',
!
!###################################################################
! SYSTEM PARAMETERS: COMMON TO 'STATIC' AND 'DYNAMIC'
!###################################################################
!
! number of dictionary files arranged in column for dot product on GPU
! (multiples of 16 perform better)
 numdictsingle = 1024,
! number of experimental files arranged in column for dot product on GPU
! (multiples of 16 perform better)
 numexptsingle = 1024,
! number of threads for parallel execution
 nthreads = 2,
! platform ID for OpenCL portion of program
 platid = 1,
! if you are running EMEBSDDI, EMECPDI, EMTKDDI, then define the device you wish to use
 devid = 1,
! if you are running EMEBSDDImem on multiple GPUs, enter their device ids (up to eight)
! here; leave others at zero
 multidevid = 0 0 0 0 0 0 0 0,
! how many GPU devices do you want to use?
 usenumd = 0,
 /
```

This program runs the indexing of the .dat-file collected from the NORDIF software with a single phase, and for running this program a lot of information from the pattern file is required; width and height of the scan area given in pixels (`ipf_wd` and `ipf_ht`), scan step size (`stepX` and `stepY`), distance between scintillator and illumination point (`L`), tilt angle of camera (`thetac`),

pixel size on scintillator (`delta`), resolution of scan (CCD pixels along x and y, `numsx` and `numsy`) and pattern center coordinates translated and averaged from the coordinates collected from TSL Data Collection (`xpc` and `ypc`). The software needs the NORDIF .dat-file (`exptfile = 'NORDIF_EBSDscan/pearlite/pearlite_cropped_hs_bcorr_pattern.dat'` and Monte Carlo and master pattern file for ferrite (`masterfile = 'crystal_data/ferrite/ferrite_MC_MP_20kv.h5'` as an input, and all output is stored in a .h5-file (`datafile = 'crystal_data/ferrite/ferrite_dp.h5`).

Kristin Grue Asheim

Distinguishing bainitic and martensitic microstructures using advanced characterization methods

NTNU
Kunnskap for en bedre verden